Application of an Engine Management System to a Stationary Spark Ignition Engine

by
John-Henry Corbett

Thesis presented in partial fulfilment of the requirements for the degree of Master of Engineering (Mechatronic) in the Faculty of Engineering at Stellenbosch University

Supervisor: Mr R.W. Haines

March 2017

Declaration

By submitting this thesis electronically, I declare that the entirety of the work contained therein is my own, original work, that I am the sole author thereof (save to the extent explicitly otherwise stated), that reproduction and publication thereof by Stellenbosch University will not infringe any third party rights and that I have not previously in its entirety or in part submitted it for obtaining any qualification.

Date: March 2017

Abstract

The subject of this report is the application of an engine management system to a small spark ignition engine, together with the installation of this engine to an existing small engine test bench. The purpose of this project is to further develop an existing small engine test bench to expand the testing capabilities of the Stellenbosch University Biofuel Test Facility. This was achieved by applying a fully controllable engine management system to a spark ignition engine and incorporating it into the existing small engine test bench. It allowed control over engine parameters such as ignition timing, fuel injection duration and, in turn, the air-fuel ratio. This report includes a literature review regarding spark ignition engines, engine testing and engine management systems. The main focus of the report is the application of an engine management system to a small spark ignition engine and its relevant subsystems, including the configuration and programming of the electronic control unit. The test procedures and data obtained are documented, verifying the engine's response to ignition timing and fuel injection parameter changes, as well as illustrating the management system's ability to control the engine over its operating range. In addition, this report also details the further development of an engine-indicating system employing fibre optic and piezoelectric pressure transducers to measure the in-cylinder pressure. The obtained indicating data was used to analyse the combustion process by means of a single-zone, zero-dimensional heat release model. From this model the rate of heat release together with the burn rate was obtained. The work done on the piston during various operating cycles was analysed, using both calculated and measured mean effective pressure values. It is then concluded that the developed engine management system is capable of controlling the test engine through its operating range and that the test setup as a whole is capable of producing accurate and repeatable results.

Opsomming

Die onderwerp van hierdie verslag is die toepassing van 'n enjinbeheerstelsel op ŉ klein vonkontstekingsenjin, tesame met die implementering van hierdie enjin op ŉ bestaande klein enjin toetsbank. Die doel van hierdie projek is om die bestaande klein enjintoetsbank verder te ontwikkel om die toetsvermoëns van die Stellenbosch Universiteit Biobrandstof Toetsfasiliteit uit te brei. Dit is gedoen deur die toepassing van ŉ programmeerbare enjinbeheerstelsel op 'n vonkontstekingsenjin en deur die enjin te inkorporeer in die bestaande klein enjin toetsbank. Dit bewerkstellig beheer oor enjin parameters, soos ontstekingstyd, brandstof-inspuitingperiode en gevolglik die lug-brandstof verhouding. Hierdie verslag bevat ŉ literatuurstudie insake vonkontstekingsenjins, enjin toetse en enjinbeheerstelsels. Die verslag dokumenteer die toepassing van 'n enjinbeheerstelsel op ŉ klein vonkontstekingsenjin en toepaslike substelsels, insluitende die opstelling en programmering van die elektroniese beheereenheid. Die toetsprosedures en die verkrygde data is gedokumenteer in hierdie verslag. Dit verifieer die enjin se reaksie op verandering ontstekingstyd en brandstofinspuiting parameters. Dit illustreer ook die beheerstelsel se vermoë om beheer uit te oefen oor die enjin die enjin se verrigtingreik. Hierdie verslag dokumenteer ook die besonderhede van die verdere ontwikkeling van 'n insilinderdruk metingstelsel wat gebruik maak van optiese vesel sowel as piëzo-elektriese drukopnemers. Die verkrygde data is gebruik om die verbrandingsproses te ontleed deur middel van 'n enkel-sone, nul-dimensionele, hitte-vrystelling model. Van hierdie model word die tempo van hitte-vrystelling en die verbrandingstempo verkry. Die werk wat op die suier gedoen is, word ontleed deur die gemiddelde effektiewe drukwaardes te meet. Daar word dan tot die gevolgtrekking gekom dat die ontwikkelde enjinbeheerstelsel in staat is om die toets enjin stabiel te beheer, en dat die toets opstelling in staat is om herhalende en akkurate metings te neem.

Acknowledgements

The author wishes to thank the following people:

- Mr R.W. Haines for his continuous guidance, support and motivation throughout the project.
- Mr R. Rodriguez for his assistance in the test cell and support regarding the National Instruments DAQ.
- Mr E. Grobbelaar for considering future test requirements when designing the dynamometer setup.
- Mr G. Lourens, from Sasol for his assistance in the PLC configuration.
- The staff at the Mechanical and Mechatronic Engineering workshop for their assistance and high quality workmanship.

Table of Contents

Page

List of Figures

Page

List of Tables

Page

Nomenclature

AFR	Air to fuel ratio
AFR_s	Stoichiometric air to fuel ratio
AC	Alternating current
AVSR	Anti-valve seat recession
BDC	Bottom dead centre
BMEP	Break mean effective pressure
BSFC	Break specific fuel consumption
CA	Crank angle
CI	Compression ignition
COV	Coefficient of variance
CR	Compression ratio
CV	Constant velocity
DAQ	Data acquisition
DC	Direct current
ECU	Electronic control unit
EFI	Electronic fuel injection
EGR	Exhaust gas temperature
ETA	Engine Test Automation
GDI	Gasoline direct injection
FMEP	Friction mean effective pressure
FVI	Flexible volatility index
HC	Hydrocarbon
IC	Internal combustion
$IMEP_g$	Gross indicated mean effective pressure
$IMEP_n$	Net indicated mean effective pressure
LED	Light emitting diode
MAP	Manifold absolute pressure
MEP	Mean effective pressure
MBT	Maximum brake torque
MFB	Mass fraction burned
MON	Motor octane number

MPFI	Multi point fuel injection
OEM	Original equipment manufacturer
PFI	Port fuel injection
PLC	Programmable logic controller
PRT	Platinum resistance thermometer
PV	Pressure versus volume
RON	Research octane number
SCADA	Supervisory control and data acquisition
SI	Spark ignition
TBI	Throttle body injection
TDC	Top dead centre
TPS	Throttle position sensor
UHC	Unburnt hydrocarbons
ULP	Unleaded petrol
VLI	Vapor lock index

1. Introduction

In today's society, the demand for internal combustion (IC) engines is growing and so too is the demand for higher efficiency and lower emissions (Bosch, 2013). Significant advancements have been made in recent years regarding spark ignition engines, which have resulted in improved fuel economy, lower emissions and certain power advantages (Noyori & Inoue, 2007). These advancements are only as a result of engine tests done using engine testing facilities.

The Stellenbosch University Biofuel Test Facility already had a small engine test setup utilizing an alternating current (AC) dynamometer and a single-cylinder compression ignition (CI) engine. A need was identified to incorporate this test setup with a spark ignition (SI) engine employing an engine management system that would allow full control over engine parameters such as ignition timing, fuel injection duration and, in turn, mixture concentration. The addition of an engine employing an engine management system would expand the test capability of the testing facility. The purpose of this project was to apply a fully controllable engine management system to a small capacity SI engine and incorporate it into the test facility's existing small engine test setup. The project stems from a proposal put forth by Mr R.W. Haines and forms part of a larger study, concerning the use of alternative fuels, conducted at Stellenbosch University.

The project objectives were as follows:

- Research and select an engine management system (electronic control unit, programming software package and required hardware) capable of full control over the parameters of a small SI engine.
- Integrate the engine management system to a small capacity SI engine and set up the engine on the existing small engine test bench.
- Instrument the test engine to allow performance measurements as well as engine parameters to be monitored.
- Develop control software allowing the engine management software to fully control the test engine.
- Verify that the engine management system is capable of controlling the test engine over its operating range.
- Validate the test setup to verify that repeatable and accurate results are obtained.

2. Literature Review

In order to get a good understanding of the workings of SI engines, its combustion process, management systems and testing, a literature review was undertaken. This chapter gives a summary of the relevant aspects of the literature that was studied.

2.1. Spark Ignition Engines

The following section discusses certain aspects of the SI engine that were of importance to the study, such as engine cycles, fuel metering systems and air-fuel ratio (AFR), the combustion process and emissions.

2.1.1. Overview

The four-stroke SI engine has been around since 1876 and has undergone many changes over the years. Although modern SI engines are more closely related to the light, high-speed engine developed by Karl Benz and Gottlieb Daimler, it was Nicolaus Otto who built the first of these SI engines (Heywood, 1988).

For additional engine operating principals, the reader is referred to *Internal Combustion Engine Fundamentals* by JB Heywood or *Internal Combustion Engines Applied Thermosciences* by CR Fergusson and AT Kirkpatrick.

2.1.2. Reciprocating engine cycles

All reciprocating engines follow a mechanical cycle and not a thermodynamic cycle (Stone, 1992). Gas cycle calculations treat the combustion process as an equivalent heat release process. By modelling the combustion as a heat release process, the analysis is simplified since details of the physics and chemistry of the combustion are not required (Ferguson & Kirkpatrick, 2001). These processes are represented as pressure vs volume diagrams (P-V diagrams) and are useful as the enclosed area equates to the work done by the cycle.

a) Otto-cycle

The Otto-cycle is a thermodynamic presentation of the four-stroke engine, where each thermodynamic cycle represents two mechanical cycles (four piston strokes). This cycle is also referred to as a constant-volume heat addition cycle. The Otto-cycle assumes that combustion takes place at constant volume (Ferguson & Kirkpatrick, 2001).

The working fluid in the Otto-cycle is assumed to be an ideal gas with constant specific heats. Air-standard assumptions are utilized to simplify the model. The cycle consists of four internally reversible processes (Çengel & Boles, 2007):

- 1-2 Isentropic compression
- 2-3 Constant-volume heat addition
- 3-4 Isentropic expansion
- 4-1 Constant-volume heat rejection

Figure 1 gives an illustration of the Otto-cycle in a four-stroke SI engine together with the ideal P-V diagram.

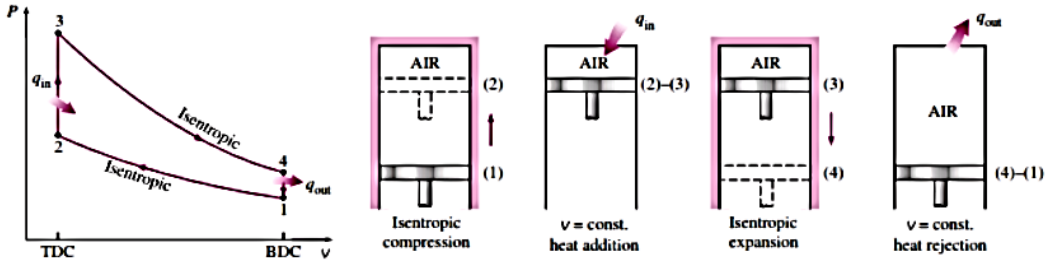

Figure 1: Otto-cycle (Çengel & Boles, 2007)

The Otto-cycle is executed in a closed system and the energy balance is expressed as:

$$(q_{in} - q_{out}) + (w_{in} - w_{out}) = \Delta u \tag{2.1}$$

No work is done during the two heat transfer processes since it takes place at constant volume. The heat transfer to and from the working fluid is expressed as:

$$q_{in} = u_3 - u_2 = c_v(T_3 - T_2) \tag{2.2}$$

And

$$q_{out} = u_4 - u_1 = c_v(T_4 - T_1) \tag{2.3}$$

The efficiency of the ideal Otto-cycle then becomes:

$$\eta_{th,Otto} = \frac{w_{net}}{q_{in}} = 1 - \left(\frac{q_{out}}{q_{in}}\right) = 1 - \frac{T_4 - T_1}{T_3 - T_2} \tag{2.4}$$

$$= 1 - \left(\frac{T_1\left(T_4/T_1 - 1\right)}{T_2\left(T_3/T_2 - 1\right)}\right)$$

Process 1-2 and 3-4 are isentropic and $v_2 = v_3$ and $v_4 = v_1$, thus:

$$\frac{T_1}{T_2} = \left(\frac{v_2}{v_1}\right)^{k-1} = \left(\frac{v_3}{v_4}\right)^{k-1} = \frac{T_4}{T_3} \tag{2.5}$$

Substituting these equations into the thermal efficiency relation and simplifying give:

$$\eta_{th,Otto} = 1 - \frac{1}{r^{k-1}} \tag{2.6}$$

where r is the compression ratio and k is the specific heat ratio c_p/c_v.

$$r = \frac{V_{max}}{V_{min}} = \frac{V_1}{V_2} = \frac{V_4}{V_3} \tag{2.7}$$

Equation 2.6 shows that under the cold-air standard assumptions, the thermal efficiency of the ideal Otto-cycle depends on the compression ratio of the engine and the specific heat ratio of the working fluid (Çengel & Boles, 2007).

b) Actual spark ignition engine cycle

Figure 2 gives an illustration of the actual four-stroke SI engine cycle together with the actual P-V diagram.

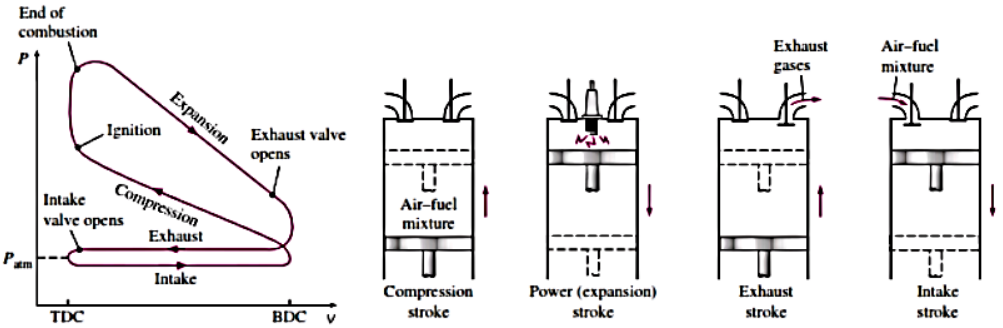

Figure 2: Actual four-stroke SI engine cycle (Çengel, 2007)

It is clear by comparing the diagrams for the ideal Otto-cycle and the actual cycle that there are deviations. These deviations are a result of the following:

Heat losses in the theoretical cycle are zero, while the actual cycle is sensitive to heat losses. As the cylinder is cooled to ensure smooth operating of the piston, a certain portion of heat is transferred from the fluid to the cylinder wall.

The ideal cycle assumes that combustion takes place at constant volume (instantaneous combustion), however combustion takes a certain time period. If ignition took place at top dead centre (TDC), combustion would occur while the piston moves. This would cause the volume to increase and the pressure to decrease, corresponding to loss in useful work. It is therefore necessary to advance the ignition timing to ensure higher in-cylinder pressures, resulting in more work done on the piston.

The ideal cycle assumes instantaneous heat removal, whereas it takes place over a period of time in the actual cycle while the exhaust valve is open. During the actual cycle heat is removed by the exhaust valve opening before the piston reaches bottom bead centre (BDC). This causes the pressure to drop close to what it would be at the beginning of the intake stroke resulting in loss of useful work.

For the ideal cycle it is assumed that the specific heats remain constant. During the actual cycle the specific heat values increase as a result of the temperature increase.

The ideal cycle does not account for dissociation in combustion. The combustion products are essentially CO_2 and H_2O, as well as other compounds such as CO, H_2 and O_2. Dissociation of these products is a reaction that takes place with heat absorption, causing the maximum temperature to be lower and a certain amount of lost-work.

The ideal cycle does not account for the pumping work done. During the actual cycle the pressure in the cylinder is slightly higher during the exhaust stroke and slightly lower during the intake stroke. This, together with frictional losses, corresponds to lost-work.

Various critical components and parameters of the SI engine will be discussed in the following sections. Starting with the engine throttle body and following the combustion process through to the engine emissions.

2.1.3. Throttle body specifications

A vital part in engine control is the proper management of airflow to the combustion chamber. A throttle body is generally used to constrict or obstruct intake airflow by making use of a throttle valve controlling airflow through the intake passage.

The choice of throttle body size is a compromise between two opposing needs: to allow sufficient airflow enabling the engine to produce maximum power, and to keep the butterfly small enough to allow progressive throttle action at small openings (Jenvey, 2015).

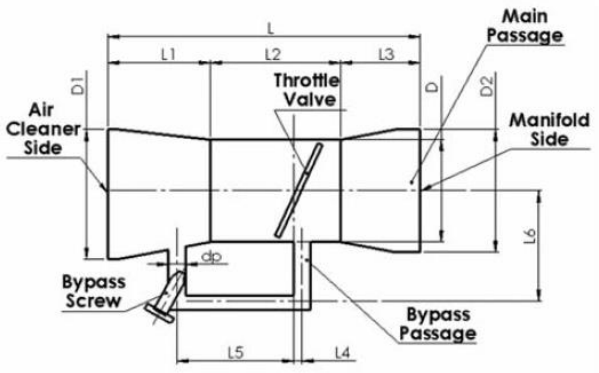

Figure 3: Throttle body assembly (Jenvey, 2015)

Figure 3 gives a representation of a basic butterfly valve throttle body illustrating critical dimensions. The major functional dimensions of the throttle body are the bore diameter (D) and the bypass diameter (d_p). The overall length (L) of the throttle body is usually fixed based on engine layout. Diameter D_1 and diameter D_2 are selected based on the air-filter fitment side and inlet manifold fitment side respectively. Since the overall length L is known, manifold side length L_3 is

determined considering the horizontal position of the butterfly valve when fully open. Length L_1 is chosen based on the air-filter mounting side and thereby length L_2 is fixed. Other lengths (L_4, L_5 and L_6) for bypass passage opening can be designed such that they do not exceed overall length L (Kumar *et al.* 2013).

a) Bore diameters

A throttle body has two main functional parameters: throttle bore diameter and bypass passage diameter. By equating the flow through the throttle body to the engine flow requirement, the throttle bore diameter can be calculated as follow:

$$D = \sqrt{\frac{4 \times V_{disp} \times {}^{N}/_{2} \times \eta_{vol}}{C_d \times \pi \times V_t}} \tag{2.8}$$

Where C_d is the coefficient of discharge though the throttle body, A_t is the area of the throttle body, η_{vol} is volumetric efficiency of the engine, V_{disp} is the displacement volume of the engine and N is the engine speed. V_t is the air velocity though the throttle body and can be calculated as follows:

$$V_t = \sqrt{\frac{2p_0}{\rho_0}\left(\frac{\gamma}{\gamma-1}\right)\left[1 - \frac{p_0}{p}\right]^{\frac{\gamma-1}{\gamma}}} \tag{2.9}$$

Where p_0 is the pressure on the intake side of the throttle body (usually atmospheric), p is the vacuum pressure at wide open throttle conditions, p_0 is air density at sea level and γ is the adiabatic constant (Kumar *et al.* 2013).

Using equation 2.8 and 2.9 a theoretical throttle bore diameter can be calculated. However, a bore diameter slightly larger than the calculated diameter should be used in practice. This will help account for the throttle plate and shaft that will provide additional restriction in the airflow path.

b) Bypass passage diameter

To calculate the bypass passage diameter for a throttle body, the mass flow rate through the bypass passage needs to be known. By estimating the mass flow rate through the bypass passage and assuming flow to be incompressible, the bypass passage diameter can be calculated as follows:

$$d_p = \frac{4\dot{m}}{\pi \times \sqrt{2p_0\rho_0\frac{\gamma}{\gamma-1}\left[\left(\frac{p}{\rho_0}\right)^{\frac{2}{\gamma}}\left(1-\frac{p}{p_0}\right)^{\frac{\gamma-1}{\gamma}}\right]}} \tag{2.10}$$

Where $\dot{m}$ is the mass flow rate through the bypass passage (estimated), A is the bypass passage area, p_0 is atmospheric pressure, p is engine vacuum pressure, ρ_0 is air density and γ is the adiabatic constant.

2.1.4. Fuel injection

The throttle of a SI engine only regulates the airflow to the combustion chamber. Since the correct AFR is critical for proper combustion, the fuel delivery system needs to accurately control the fuel supplied to the engine. The fuel delivery system responds to throttle changes, continuously supplying the engine with a combustible air-fuel mixture. This fuel regulation is usually done by a carburettor or fuel injectors, as throttle body injection (TBI) or multi-point fuel injection (MPFI). Over the last couple of decades MPFI systems have almost completely replaced carburettor and TBI systems. This is as a result of MPFI systems' inherent advantages in transient response and unburnt hydrocarbon (UHC) levels (Zhao *et al*, [S.a.]). Fuel injection is an accurate and sophisticated fuel delivery system that allows precise control over the fuel delivery (Heywood, 1988).

The engine management system calculates engine load based on manifold absolute pressure (MAP) measurements or airflow measurements. Fuel injection systems deliver fuel by spraying it into the incoming airstream based off the engine managements system. As the fuel delivery system is pressurized and delivers the fuel to the manifold under pressure, the quantity of fuel delivered can be precisely controlled. With this more positive control, fuel delivery can be adjusted to meet specific demands allowing for greater efficiency over a wider range of operating conditions (Charles, 1991).

a) Injection systems

The original purpose of fuel injection was to obtain the maximum power output from an engine. Early fuel injection systems were mechanical and made use of complex two-dimensional cams (Stone, 1992).

The fuel injection systems considered in this project are different from engine driven systems. The system delivers fuel at much lower pressures at the intake ports and is electronically controlled.

Electronically controlled fuel injection systems have major advantages over their engine-driven counterparts. The electronic systems are less complex and therefore more affordable. Fewer components are needed compared to the mechanical systems, making the control of the system much easier. These systems have a maintenance friendly design, making them more affordable to maintain (Bosch, 2013).

The port fuel injection (PFI) system delivers fuel at the engine intake ports and is the system used for this project. PFI delivers the fuel near the intake valve of the engine as shown in Figure 4. This means the intake manifold only transports air, in contrast to carburettors or single point fuel injection systems in which the intake manifold carries the air-fuel mixture. As a result, these systems offer the following advantages (Charles, 1991):

- Reduced air-fuel variability.
- Matches fuel delivery to specific operating requirements.
- Prevents stalling due to fuel-bowl wash during cornering.
- Eliminates engine run-on when the ignition is turned off.
- Greater power by avoiding venture losses, and by allowing intake runner tuning for better torque characteristics.
- Improved drivability by reducing throttle lag that occurs while the fuel travels from the throttle body to the intake port.
- Increased fuel economy by avoiding condensation of fuel on the interior walls of the intake manifold (manifold wetting).
- Simplified turbocharging applications as the turbocharger only needs to handle air.

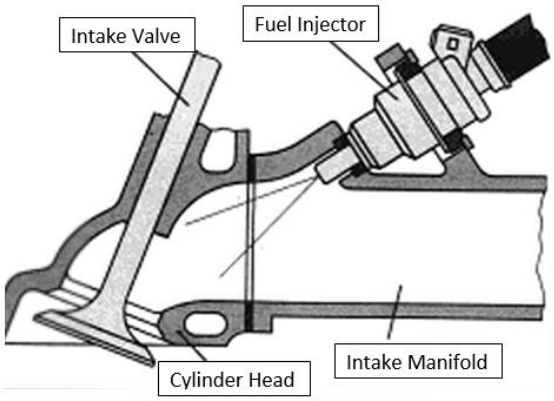

Figure 4: Port fuel injection (adapted from, Dapper, 2013)

b) Injectors

Fuel injectors play an important role in the accurate metering and atomisation of fuel in the fuel injection system. Fuel injectors are essentially electro-mechanical valves that are able to open and close in milliseconds. This quick response allows the electronic control unit optimal control over the fuel flow to the engine. Injectors are specified according to their fuel flow rate, given in grams per minute, cubic centimetres per minute or millilitres per minute.

The most important component of the fuel injection system is the fuel injector, illustrated in Figure 5, as its purpose is to deliver the atomized fuel to the cylinders for combustion (Enright, 2015). Injectors are electronically controlled by an engine management system that sends an electric signal energizing the solenoid. The resulting magnetic force then overcomes the force of a spring and hydraulic pressure, which then lifts the pintle, allowing the fuel to flow from the injector. The end of the injector is shaped into a nozzle to atomize the out-flowing fuel. The total lift on the needle is approximately 0.15 millimetres and has a reaction time of 1 millisecond (Dapper, 2013).

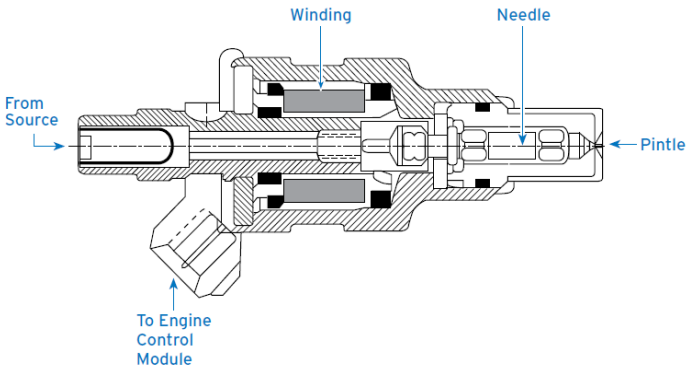

Figure 5: Fuel injector (Chevron, 2009)

The injector is supplied with fuel from a common fuel rail. The injector pulse width depends on the input signals seen by the ECU from its various engine sensors, and varies to compensate for cold engine starting and warm-up periods.

c) Injection parameters

The spray characteristics and location of the port fuel injector has a significant influence on the performance of a gasoline engine. The key influential factors are injection timing, injector placement, spray targeting accuracy, spray momentum, mean drop size and pulse to pulse variability.

Daniels *et al.* (1994) found that increasing the amount of wall wetting results in diminished engine performance, retarded transient response and an increase in HC emissions. To reduce wall wetting, the injector is located such that the injection spray is targeted towards the back of the intake valve. This reduces the amount of fuel vapour that comes into contact with the intake manifold, thereby reducing the amount of wall wetting. Targeting the injection spray at the back of the intake valve also promotes fuel vaporization, thus promoting homogeneity of the mixture in the combustion chamber. This is as a result of the high temperatures of the intake valve (Zhao *et al*. [S.a.]). If special constraints prevent the injector from targeting the intake valve, it is recommended that the injection should be placed as parallel to the intake airflow as possible and be located 60 mm to 80 mm from the intake valve. This will aid in fuel vaporization (Zhao *et al*, [S.a.]). Hushim *et al.* ([S.a.]) investigated the effect of the injector position by placing the injector at 48 and 68 degrees relative to the intake airflow. They found that placing the injector at 68 degrees provided better emissions and performance compared to the injector being placed at 48 degrees. This is in contradiction to other studies and could be a result of them purely considering the injector angle and not taking into account whether the injector is targeting the intake valve or not.

Studies done by Nogi *et al.* (1989), Yang *et al*. (1992) and Alkidas (1994) all report that HC emissions increase if injection occurs before the intake valve is closed. This was found to be the case under both high load and low load

conditions (Zhao *et al*, [S.a.]). Open-valve injection results in liquid fuel being deposited in the cylinder resulting in the increase of HC emissions. Under cold start conditions open-valve injection can possibly wet the spark plug which results in misfiring (Castaing *et al*, 2000).

Zhao *et al* ([S.a.]) states the optimal fuel preparation conditions to be: well atomised spray, a spray targeting at the back surface of the intake valve for minimal intake-wall wetting, and injection timing to occur prior to the intake stroke with the intake valve closed. This will ensure lower HC emissions and improved engine transient response.

2.1.5. Air-fuel mixtures

The majority of SI engines mix fuel and air outside the combustion chamber, however in more sophisticated, gasoline direct injection (GDI) engines mixture formation takes place inside the combustion chamber during the compression stroke (Van Basshuysen & Schäffer, 2004). As mentioned in the previous section, this project focussed on PFI where the air-fuel mixture is formed inside the intake manifold.

For combustion of typical petroleum based fuels to occur, an AFR between 12:1 and 18:1 has to be present. The stoichiometric AFR (AFR_s) depends on the composition of the fuel, but is generally between 14.2:1 and 14.7:1 (Heywood, 1988).

The chemical reaction between a general hydrocarbon fuel and air is given in equation 2.11.

$$C_aH_b + \left(a + \frac{b}{4}\right)(O_2 + 3.773N_2) \rightarrow aCO_2 + \frac{b}{2}H_2O + 3.773\left(a + \frac{b}{4}\right)N_2 \quad (2.11)$$

By setting $y = a/b$, the AFR_s can be expressed as shown in equation 2.12 (Heywood, 1988).

$$\left(\frac{A}{F}\right)_s = \left(\frac{F}{A}\right)_s^{-1} = \frac{\left(1+\frac{y}{4}\right)[32+(3.773)(28.16)]}{12.011+1.008y} = \frac{34.56(4+y)}{12.011+1.008y} \quad (2.12)$$

The measured AFR is usually related to the AFR_s as a lambda measurement (λ) or equivalence ratio ($\emptyset$) as shown in equation 2.13.

$$\lambda = \emptyset^{-1} = \frac{AFR}{AFR_S} \quad (2.13)$$

Mixture requirements vary depending on engine operating conditions. Under full load conditions the complete utilization of the induced air is needed to maximize the power for a given displacement volume. Maximum power is typically achieved at a rich mixture with a lambda value of 0.91 (Richards, 2014). Under

partial load conditions, a slightly lean AFR is advantageous as it improves the fuel conversion efficiency (Heywood, 1988). The AFR has a significant effect on engine emissions and will be discussed in section 2.1.8.

2.1.6. Combustion

Near the end of the compression stroke, the combustion process is initiated by a spark at the electrodes of the spark plug (Atkins, 2009). The spark is triggered by the ECU at a given ignition point which results in an exothermic reaction in the combustion chamber. During combustion a turbulent flame front propagates through the premixed air-fuel mixture until it reaches the combustion chamber walls and is extinguished (Richards, 2014).

The AFR of the mixture in the vicinity of the spark plug must be between 11.7:1 and 17.6:1 to ensure reliable combustion. For the fuel mixture to ignite, the spark produced from the spark plug has to heat the air-fuel mixture to a temperature in the range of 3000 K to 6000 K (Van Basshuyen & Schäfer, 2004).

A turbulent flame front then propagates under high pressure through the combustion chamber. Figure 6 gives an illustration of in-cylinder pressure and mass fraction of fuel burned curves. This aids in understanding the propagation of the flame front (Heywood, 1988). The period after spark ignition till a mass fraction burned of 10 % is reached, is known as the flame development period. This leads to the rapid-burning period (10 % to 90 % of mass fraction burned) where the bulk of the fuel is burned. The slope of the mass fraction burned curve indicates the burn rate of the fuel and can be used as an analytical tool of the combustion process (Arcoumanis & Kamimoto, 2009).

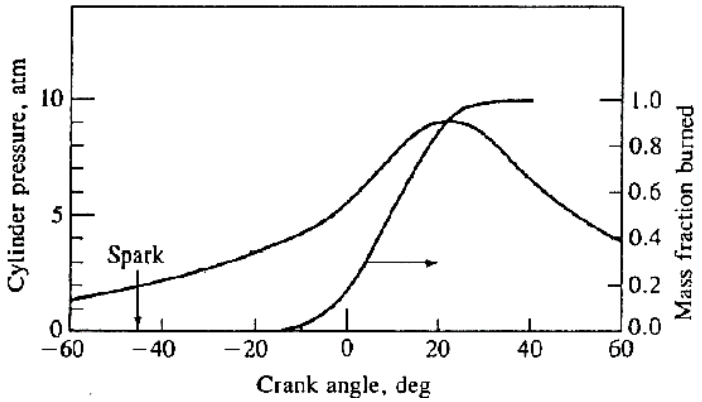

Figure 6: In-cylinder pressure and mass fraction burned curves (Heywood, 1988)

Variations in the mixture motion as well as mixture composition result in cycle-to-cycle variations in the combustion process. These cycle-to-cycle variations causes the in-cylinder pressure reading to fluctuate even under constant load and speed. Figure 7 shows a typical in-cylinder pressure versus crank angle

curves that illustrates the cycle-to-cycle variations of a PFI engine (Heywood, 1988).

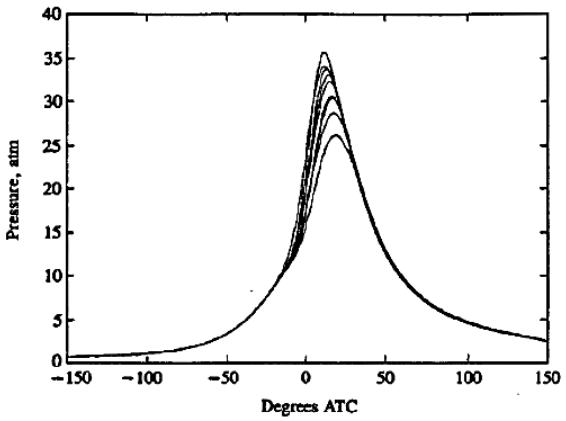

Figure 7: Cycle-to-cycle variations of in-cylinder pressure measurement of a PFI engine (Heywood, 1988)

Figure 7 also gives an indication of the in-cylinder pressure trace produced under normal combustion. During an abnormal combustion event, sharp fluctuations in the in-cylinder pressure are present as illustrated in Figure 8. This is as a result of auto-ignition and is described in section 2.1.7.

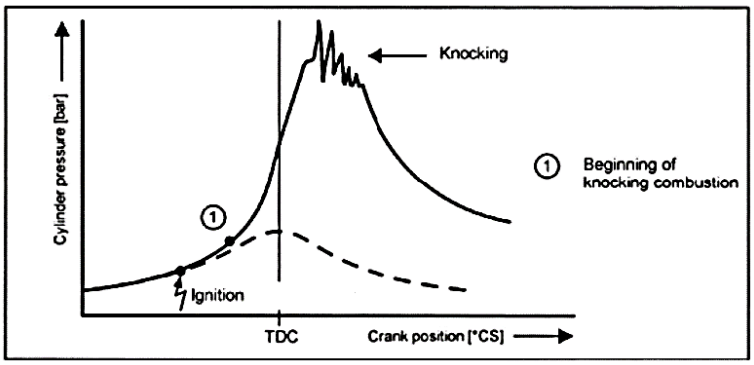

Figure 8: In-cylinder pressure curve of an abnormal combustion cycle (Van Basshuyen & Schäfer, 2004)

2.1.7. Abnormal combustion

Knock is a common term used to describe abnormal combustion in gasoline engines and is named after the characteristic noise that is generally produced under abnormal combustion conditions (Richards, 2014). It is generally accepted that engine knock is caused by auto-ignition of a portion of the end gas prior to the flame front. These auto-ignition sites are usually very close to the combustion chamber wall and the auto-ignition processes are not influenced by the propagating flame front due to the spatial separation (Worret *et al.* 2002).

Auto-ignition can be initiated under controlled conditions or it can occur in an uncontrolled way. Spark knock is an auto-ignition event that occurs at the limit of ignition advance and can be controlled by adjusting the ignition timing (Worret *et al*, 2002). Three different modes of auto-ignition have been identified, namely: deflagration, thermal explosion and developing detonation (Rogers, 2010).

During deflagration a flame front starts from local centres of auto-ignition and moves through the end-gas with sub-sonic velocities. This mode of knock is associated with no, or only light knock intensity. However, it is possible that more of these deflagration centres develop at the same time and change into other modes of auto-ignition (Eckert, 2003).

Deflagration can potentially change to a thermal explosion. This occurs when the end-gas temperature is raised by the spark initiated flame and the developing flame after auto-ignition. This results in the remaining end-gas auto-igniting nearly simultaneously. This causes homogeneous combustion that leads to high heat release and the initiation of pressure waves that generally gets associated with medium knock intensities (Eckert, 2003).

The deflagrative flame can also cause a shock wave that results in detonation. The deflagrative flame follows the shock wave leading to compression and heating in the end-gas and is associated with a high knock intensity (Eckert, 2003).

Abnormal combustion is a damaging phenomenon that can be initiated in a managed way or occur in an uncontrolled way (Eckert, 2003). If knock occurs over extended periods of time it can lead to, breakage of piston rings, cylinder head erosion, piston crown and top land erosion and piston melting (Rogers, 2010).

2.1.8. Emissions

During combustion, fuel mixed with air is ignited resulting in a release of energy and certain by-products of combustion or emissions. These emissions make up the exhaust gases of the SI engine of which the main components are carbon dioxide (CO_2), water (H_2O), carbon monoxide (CO), unburnt and partially burnt hydrocarbons (HC) and nitrogen oxides (NO_x). NO and NO_2 form the largest part of the nitrogen oxide emissions, but smaller quantities of NO_3, N_2O, N_2O_3, N_2O_4 and N_2O_5 are also present (Van Basshuyen & Schäfer, 2004).

CO_2 is produced as a result of complete combustion of the HC molecules in the fuel. The amount of CO_2 produced during combustion is directly proportional to the amount of fuel combusted, while the fuel composition has a secondary effect. Incomplete combustion of the HC molecules results in the formation of CO. The concentration of CO produced depends on the AFR as shown in Figure 9 (Richards, 2014).

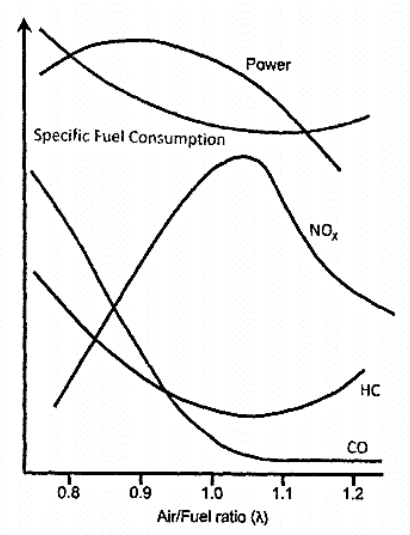

Figure 9: Influence of air-to-fuel ratio on exhaust emissions, power and specific fuel consumption (Richards, 2014).

During normal combustion, a small percentage of the fuel remains unburned, resulting in HC emissions. Various factors contribute to the presence of HC emissions in SI engines. These include: the AFR of the pre-mixed charge, air-fuel mixtures forced into crevices, fuel absorbed in oil layers and deposits, exhaust valve leakage, poor burns or misfires, and injection timing (Castaing *et al*, 2000). It is widely accepted that crevice flows are the dominant contributing factor to HC emissions. The crevice flow mechanism is caused by a portion of the air-fuel mixture that enters the crevices that are too small for flame propagation. The largest contributor to the crevice volume is the area created by the piston and piston rings in relation to cylinder wall. Other crevice areas are represented by the threads around the spark plug, the area around the spark plug electrode, the space between the heads of the intake and exhaust valves and the cylinder head, as well as the head gasket cut out (Bohacs, 2001). The air-fuel mixture is forced into the crevices under high pressure and re-enters the combustion chamber where it mixes with the hot in-cylinder gasses after combustion (Drake *et al*, 1995).

The formation of NO_x emissions is influenced by the AFR, combustion temperature, in-cylinder pressure and dwell time. From Figure 9 it can be seen that the maximum NO_x concentration occurs between lambda 1.02 and lambda 1.1 (slightly lean). The maximum formation of NO_x occurs between 2200 and 2400 K and reduces at higher temperatures (Van Basshuyen & Schäfer, 2004). NO_x formation is less at lower temperatures, but temperatures of at least 1900 K are needed for combustion to proceed rapidly enough. GDI engines therefore produce less NO_x emissions as combustion takes place at a lower temperature compared to PFI engines (Flynn *et al*, 2000). During combustion there are large differences in the temperatures of the unburnt, burning and post-burnt portions of the charge. As a result, only a small portion of the charge produces most of the NO_x (Kim *et al*, 2003).

2.2. Engine Testing

The following section gives a brief discussion of the requirements of an engine and dynamometer setup and the parameters to be measured and controlled. For basic principles on engine testing, the reader is referred to *Engine testing theory and practice* by A Martyr and M Plint.

2.2.1. Overview

An engine test facility generally consists of a test cell infrastructure that has to meet certain criteria. Typical criteria to consider include floor space, noise isolation, safety barriers that enclose the engine test setup during testing (walls, doors and protective windows), electrical supply, lighting, test cell ventilation, fire extinguishing system and access to a control room (Martyr & Plint, 1995).

The engine test setup typically consists of a test bed, test engine, dynamometer, sensors and actuators as well as control hardware and software. It is recommended that the control system incorporates a computerized alarm system capable of shutting down the engine if a test parameter exceeds predetermined limits (Martyr & Plint, 1995).

2.2.2. Measured parameters

Parameters measured during engine testing typically include engine speed, torque, fuel flow, manifold pressure, oil pressure, fuel pressure, ambient air temperature, intake air temperature, oil temperature, fuel temperature and exhaust gas temperature.

Engine torque is measured by a load cell or torque flange connected to the dynamometer, while engine speed is measured by a speed sensor connected to the back of the dynamometer. Speed sensors that are typically used are either inductive encoders or optical encoders. More information on these encoders will be given in section 2.6.2.

A fuel flow meter is used to measure the fuel consumption rate of the engine, which together with the engine torque and speed measurement allows for the calculation of the brake specific fuel consumption (BSFC). Fuel flow can either be measured cumulatively or instantaneously, with the instantaneous measurement providing the real time fuel flow rate (Ferguson & Kirkpatrick, 2004).

Thermocouples are most commonly used for measuring temperature in the engine testing environment. For space limited applications thermistors can be used, while platinum resistance thermometers (PRT) are typically used for high accuracy measurements (Lilly, 1984).

Pressure measurements can either be done using mechanical or electric methods, depending on the application. Mechanical measurements typically include

manometers or barometers whereas electronic measurements make use of pressure transducers.

2.3. Lambda Measurements

This section discusses the importance of closed-loop lambda control as well as giving an in-depth description of lambda sensors.

2.3.1. Overview

In today's modern society, major focus has been placed on emissions and the efficiency of IC engines. The most effective exhaust gas emissions control system for SI engines consists of the three-way catalytic converter, the lambda oxygen sensor and the closed-loop lambda control system. Presently there is no alternative that matches the effectiveness of this system (Bosch, [S.a]).

Most modern automobiles make use of two lambda sensors for closed-loop lambda control. These sensors are placed in contact with the exhaust gasses, one in front of the three-way catalytic converter and one thereafter.

In a closed-loop lambda control system, information regarding the oxygen content of the exhaust gas is continuously fed back into the system as an input. The lambda sensor signal provides feedback to the electronic control unit (ECU), indicating whether the AFR requires correction. The ECU adjusts the fuel metering to ensure the correct AFR is achieved for combustion (Probst, 1989).

2.3.2. Lambda sensor

The first lambda sensor was developed by Bosch in 1976. The sensor developed was a switching type lambda sensor (narrow-band lambda sensor). In 1998 Bosch developed a wide-band lambda sensor that allowed the oxygen content in the exhaust to be measured over a wider range (Classen & Shanner. 2011).

a) Narrow-band

Standard narrow-band type lambda sensors are only capable of accurately measuring a stoichiometric AFR. A richer or leaner condition results in an abrupt voltage change that is only useful for quantitative determination (Bosch auto parts, 2015). The use of narrow-band lambda sensors is therefore limited to two engine conditions: During idle and during part load conditions. This limitation promotes the use of wide-band lambda sensors.

b) Wide-band

Advanced amperometric wide-band lambda sensors are necessary for fast and reliable lambda determination across the full lambda range. The broader measuring range and high signal dynamics of wide-band lambda sensors enable continuous system control in contrast to the two position control of the narrow-band lambda sensor (Bosch, 2015) (Classen & Shanner. 2011).

The sensor element of the lambda sensor consists of a zirconium dioxide element. The zirconium element is stabilized with yttria (Y_2O_3) and this promotes sensor rigidity as well as long term stability for use in a corrosive environment. A detailed schematic of a wide-band lambda sensor is given in Figure 10.

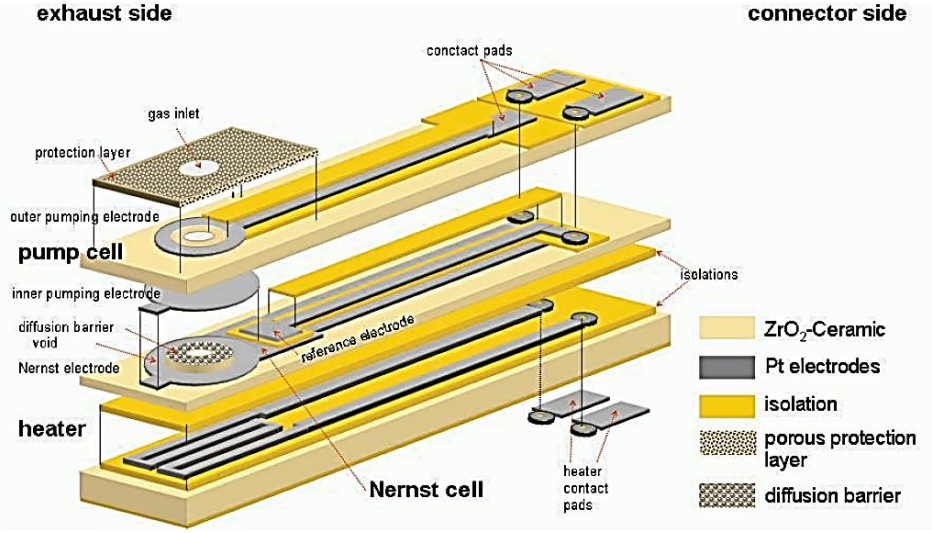

Figure 10: Wide-band lambda sensor element (Classen & Shanner. 2011)

For the lambda sensor to function, the sensor is initially heated to above 300 °C (usually kept above 700 °C). This allows for oxygen-ion conductivity to take place between the two platinum electrodes of the sensor. The lambda sensor element forms an electrochemical Nernst cell. The two electrodes of the cell are exposed to different atmospheres and a Nernst voltage is induced between the two electrodes. This induced voltage depends critically on the relative oxygen partial pressures between the two electrodes (Classen & Shanner. 2011).

Both narrow-band and wide-band lambda sensors use this Nernst cell configuration, but wide-band lambda sensors also make use of a second electrochemical cell. A controlled voltage is applied to the second cell causing oxygen to be diffused through the zirconium dioxide. The oxygen transport across this cell is limited by a porous diffusion barrier placed in front of the electrode. This generates a current across this cell that is proportional to the oxygen transport across the diffusion barrier, which in turn is proportional to the overall oxygen content in the gas. The driving voltage is controlled by closed-loop feedback and enables accurate measurements, including rich measurements (Bosch, [S.a.]) (Classen & Shanner. 2011).

2.4. Engine Management System

Internal combustion engines have come a long way since the conventional carburettor fuel systems and magneto/distributor ignition systems. These systems were all mechanical and analogue systems that required minimal or no electronic

control. Modern engines make use of a variety of sensors and actuators to control the engine parameters, all of which are controlled by the engine management system. Initially cost considerations limited engine management systems to only luxury motor vehicles, but with more stringent demands for cleaner emissions the use of these systems are now more widespread (Reif, 2015).

2.4.1. Overview

The engine management system comprises various components that enable it to have full control over the engine. At the centre of this system is the ECU. The ECU receives various input signals from sensors and switches, analyses the signal based on certain set-points and data tables (known as ECU maps) and in turn controls the corresponding actuators (Reif, 2015). These ECU maps consist of a collection of engine load and speed combinations with their corresponding fueling and ignition timing requirements (Chevron, 2009). Figure 11 gives an illustration of an engine management system for a PFI engine.

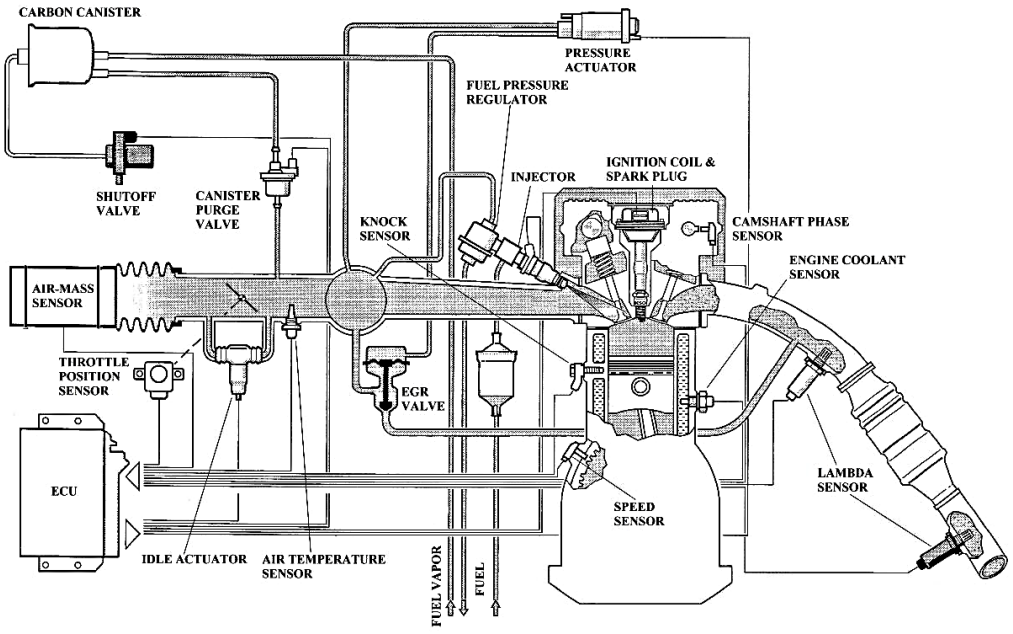

Figure 11: PFI engine management system (Bosch, 1995)

There are two main approaches to engine management, open-loop control and closed-loop control. Open-loop control regulates the engine parameters based on stored ECU map values. Closed-loop control can be seen as an adaptive or self-tuning control system that continuously optimises the engine operating points (Stone, 1992). These two control modes can also be combined to run a single system depending on the system requirements. Closed-loop control is used under steady state conditions while open-loop control is used under transient conditions as the response time of the lambda sensor is too slow.

2.4.2. Engine parameters

Engine parameters have to be monitored to enable the ECU to manage the engine. These include: crank angle, engine speed, engine load, lambda (correlates to AFR), temperatures and pressures.

For control over spark ignition timing as well as fuel injection timing and duration, the ECU requires the position of the crankshaft with reference to TDC. A crankshaft position sensor is used for this purpose as well as to indicate the engine speed. As the camshaft rotates once for every two rotations of the crank shaft, a camshaft sensor can also be used to determine the engine cycle (Bosch, 1995). The test engine used for this project was not equipped with a camshaft sensor, thus a wasted spark strategy was used (see section 4.2).

To determine the engine load, the ECU requires an air mass sensor or a MAP sensor, together with an intake air temperature sensor. These sensors are located after the throttle body in the intake system (Bosch, 1995).

As discussed in section 2.3, a lambda sensor is used to measure the oxygen content in the exhaust. The ECU receives a lambda input from the lambda sensor and, under closed-loop conditions, adjusts fuelling parameters to meet the required lambda set point.

To enable the ECU to adjust according to different operating conditions, a throttle position sensor (TPS) and engine temperature sensors are used. During acceleration the ECU provides more fuel to the engine and the fuel delivery rate is determined by monitoring the rate of change of the TPS. During engine starting and warm-up, the ECU has to provide a rich mixture to the engine, which is achieved by monitoring the engine coolant temperature and engine oil temperature (Ferguson & Kirpatrick, 2001).

2.5. Spark Ignition Engine Fuels

Early SI engines could run on any volatile flammable liquid, but it was the increased demand for more efficient and reliable engines that resulted in gasoline becoming the fuel of interest. This resulted in the interdependence of fuel and engine development. Engines are developed considering the available fuels and fuels are produced based on their application in engines (Chevron, 2009).

2.5.1. Production and properties

Petroleum is a complex mixture of organic liquids that is processed from crude oil. When crude oil is extracted it contains a mixture of hydrocarbon compounds and relatively small quantities of other materials such as oxygen, nitrogen, sulphur, salt and water. Fractional distillation separates the HCs in the crude oil into naphtha, kerosene, diesel and atmospheric bottoms. These products are then used as is or undergo further processing. The processes include cracking, reforming and alkylation (AIP, [S.a.]).

There are numerous regulations and standards that automotive fuels have to meet. These standards ensure that the fuel properties are compatible with current vehicles and meet emissions requirements (SAPIA, 2008). The properties that are regulated include: octane number, volatility, residue and exist gum, copper strip corrosion, sulphur content, total aromatics, oxygenates, oxidation stability, induction period and density.

a) Octane number

The octane number of fuel is a measure of its resistance to auto-ignition. Auto-ignition in SI engines can be clarified into two categories, namely knock and surface ignition. Both of these processes result in uncontrollable combustion and can lead to severe engine damage.

The octane number of fuel is determined by comparing its anti-knock quality to that of iso-octane and n-heptane. Iso-octane has an octane number of 100 while n-heptane has an octane number of 0. An octane number of 97 means that the fuel has the same anti-knock quality as a mixture of 97 % iso-octane and 3 % n-heptane, in a specified engine under set conditions (Chevron, 2009).

There are two test methods used for measuring the octane number of a fuel. The one test gives the research octane number (RON) and the other gives the motor octane number (MON). RON gives an indication of the fuel's anti-knock performance at lower engine speeds and acceleration conditions while MON reflects the anti-knock performance under high engine speeds and high load conditions. The fuel's sensitivity is determined by the difference between the two values and indicates the effect that changes in the operating conditions have on the fuels performance (SAPIA, 2008).

The possibility of knock occurring in an engine depends greatly on the octane rating of the fuel used and the pressure in the combustion chamber. Since each engine has a fixed compression ratio it has to be designed to work in accordance with the available fuels (SAPIA, 2008).

b) Volatility

Volatility is the tendency of a fuel to vaporise. In IC engines it is the vapour around the atomized liquid fuel droplets that burn and not the liquid itself. This makes the volatility of fuel a very important property of the fuel as a fuel that is too volatile or not volatile enough will lead to unsatisfactory combustion. The volatility of a fuel needs to be high to enable easy cold starting, but not so high that it causes vapour lock when the engine is hot. Fuels that are highly volatile run the risk of evaporating in the fuel tank. This causes unwanted environmental emissions and poses a fire risk (SAPIA, 2008).

The South African Petroleum Industry Association points out a number of aspects that influence the volatility of fuels namely: vapour pressure, distillation profile, flexible volatility index (FVI) and drivability index.

Vapour pressure is the single most important property of gasoline with regard to cold-start and warm-up drivability. The vapour pressure relates to the lighter components in the fuel. Higher vapour pressures generally result in better cold-start performance, but lower vapour pressure values aid in preventing vapour lock. A material's vapour pressure is the pressure exerted by the vapour when the vapour is in equilibrium with the liquid or solid (Chevron, 2009). The South African Petroleum Industry Association describes the measurement of the vapour pressure as a very complicated procedure. The procedure is simplified by using a parameter that refers to a standard temperature of 37.8 °C and is called the Reid vapour pressure.

The distillation profile of a fuel consists of a set of volume percentages that evaporate at specific temperatures. These temperatures are most commonly 70 °C, 100 °C, 150 °C and 180 °C (SAPIA, 2008). T50 and T90 will correspond to temperature points on the distillation profile where a percentage value of 50 and 90 respectively of liquid has evaporated. Figure 12 shows a typical distillation profile and indicate the T50 and T90 points.

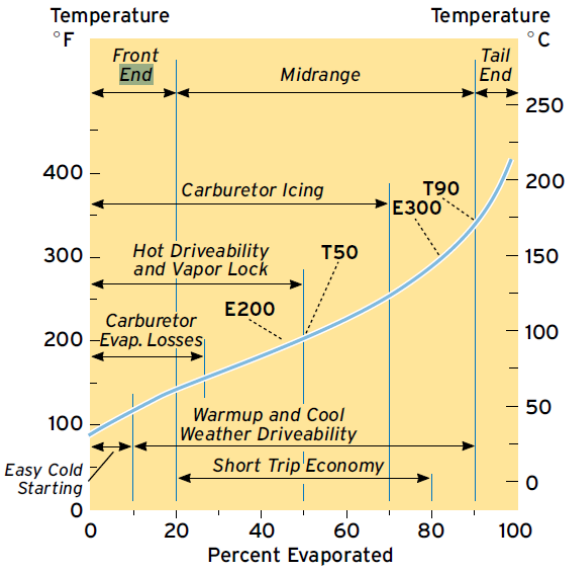

Figure 12: Correlation of distillations profiles with gasoline performance (Chevron, 2009)

The FVI is also referred to as the vapour lock index (VLI) and is an indication of a fuel's tendency to cause vapour lock. The VLI is calculated using the vapour pressure in kPa and distillation profile percentage evaporated at 70 °C. The normal range is from 800 to 1250 and varies with the season. Lower VLI values indicate greater protection against vapour lock and hot fuel handling problems (Chevron, 2009).

Vapour lock occurs when excessive gasoline vapour accumulates in the fuel system interrupting the fuel supply to the engine. Vapour lock can take place in the fuel line, fuel pump, carburettor or fuel injectors. This reduces the fuel supply to the engine, causing the air-fuel mixture to be too lean and resulting in loss of power, surging or back firing (Chevron, 2009).

In contrast to the FVI the driveability index is a measure of a fuel's performance during cold start and warm-up. A drivability index has been developed to predict the cold-start and warm-up drivability of fuels. This index uses the temperatures for the evaporated percentages of 10 %, 50 %, 90 % and ethanol content. The drivability index varies depending on the fuel grade and season. A low drivability index usually results in better cold-start and warm-up performance. Once good drivability is achieved, there is no benefit in lowering the drivability further (Chevron, 2009).

2.5.2. Petrol additives

Additives are used to change the characteristics of petrol. They are gasoline-soluble chemicals that provide characteristics not inherent in the gasoline. These additives include octane enhancing additives, oxidation inhibitors, corrosion inhibitors, oxygenates, metal deactivators (used to capture metal ions to prevent oxidation), demulsifiers (separates petrol and water), deposit control additives, dyes (used to distinguish between fuels) and anti-valve seat recession (AVSR) additives (Chevron, 2009).

2.5.3. Bio-ethanol

Bio-ethanol is produced using plant matter. The growing popularity of bio-ethanol is as a result of it being a renewable energy source, as well as having a reduced overall carbon emission compared to fossil fuels. The carbon emissions from biofuels are as a result of the carbon contained in the plant matter used to make the biofuel. The use of biofuel therefore forms a closed-loop carbon cycle. When fossil fuels are burnt they release carbon, that has been locked underground for millions of years, into the atmosphere (Milnes *et al*. 2010).

Bio-ethanol is most commonly used as a blend with petrol. Although bio-ethanol can be used in its pure form (E100), it is not suitable for standard vehicles due to its corrosive properties (WWFC, 2009). Fuel-flex vehicles are capable of running on both low and high concentration ethanol blends. To enable use of high concentration ethanol in standard engines, certain engine components need to be modified. These include components that corrode due to ethanol, certain plastics, rubbers and certain metal components (Milnes *et al*. 2010).

2.6. Pressure Indicating

The measurement of in-cylinder pressure of a reciprocating engine has been around since the dawn of the reciprocating engine. This can be seen by the early development of the steam engine, by James Watt and others, where in-cylinder

measurements were used to understand the in-cylinder processes and heat release of the engine (Rogers, 2010). Initially "indicating" exclusively referred to in-cylinder pressure measurement, but lately "indicating" refers to any angle based parameter in an engine, including intake pressure, exhaust pressure, fuel pressure, etc. (AVL, 2002).

Analysis of the in-cylinder pressure vs. the crank angle can provide quantitative information regarding the combustion characteristics of the engine. These include the amount of energy released and rate of energy release during combustion, the burn duration and the ignition delay period. These characteristics are usually presented using heat release and burn rate curves (Blair, 1999).

2.6.1. In-cylinder pressure measurement

The pressure transducer is a critical component in the pressure indicating system and there is a variety of transducer choices. The quartz crystal piezoelectric transducer is the oldest type of transducer and has to be cooled to keep the transducer at its operating range and ensure accuracy (typically below 250 °C). These sensors require a dedicated cooling system that could cause pressure pulses in the cooling stream which would be superimposed on the sensor output (AVL, 2002).

In the 1980's a synthetic material, Gallium Orthophosphate, was developed and used as a piezoelectric material in pressure transducers. As the synthetic material's stability and sensitivity is mostly unaffected by temperature, the transducers do not require a dedicated cooling system. The temperature dependency of the piezoelectric materials can be seen in Figure 13. This eliminated the possibility of the cooling system pressure pulses causing inaccuracies and also made the transducers ideally suited for use in applications where space is a problem (AVL, 2002).

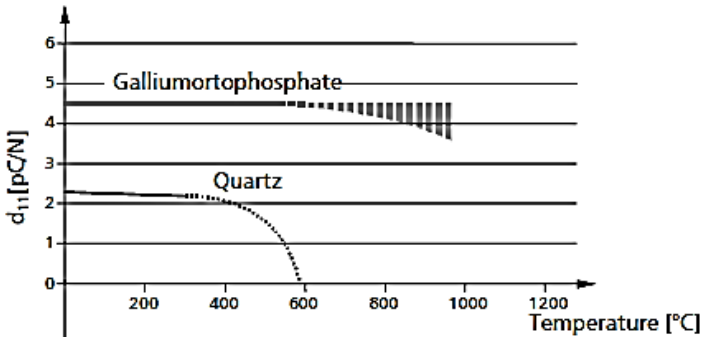

Figure 13: Temperature dependency of piezoelectric materials (AVL, 2002)

All piezoelectric transducers produce a charge signal rather that a voltage. As most data acquisition systems require an input voltage, a charge amplifier is

required to produce a voltage signal based on the charge signal it receives from the transducer.

Optical transducers are the latest to be developed and stand as an alternative for piezoelectric transducers for in-cylinder measurement. The optical sensor uses a fibre optic based technique to detect the deflection of a measuring diagram. The sensor consists of an opto-electronic module, fibre optic connecting cable and a sensor head (Rogers, 2010).

The light emanating from the light emitting diode (LED) travels through the first fibre optic cable, gets deflected by the sensor diaphragm and travels back to the photodiode through the second fibre optic cable. As the sensor diaphragm deflects, the reflected light is no longer completely aligned with the receiving end of the return optical fibre. Only a fraction of the reflected light reaches the photodiode, therefore the intensity of the reflected light is proportional to the diaphragms deflection, which in turn is proportional to the applied pressure (Optrand, 2001).

The optical transducer (made by Optrand) has numerous advantages over its piezoelectric counterparts. The small size of the transducer simplifies engine modification to accommodate the transducer, or allows it to be easily installed into a modified spark plug if modification of the engine is undesirable. The thermal tolerance of the transducer makes it ideal for use in in-cylinder pressure measurements.

Comparative prices obtained from a thesis done by J. Kotzé (2010) indicate a very reasonable price over the competing transducers. A cost saving of 80% was made over the competing transducers (AVL and Kistler).

When installing the transducer, it is important to consider pipe oscillations: a phenomenon that occurs when the transducer is recessed relative to the cylinder head ceiling. The resulting channel leading to the diaphragm of the transducer acts as an acoustic resonator causing the formation of an echo during changing pressure waves. Figure 14 illustrates how pipe oscillations and pipe length can affect the pressure reading (AVL, 2002)

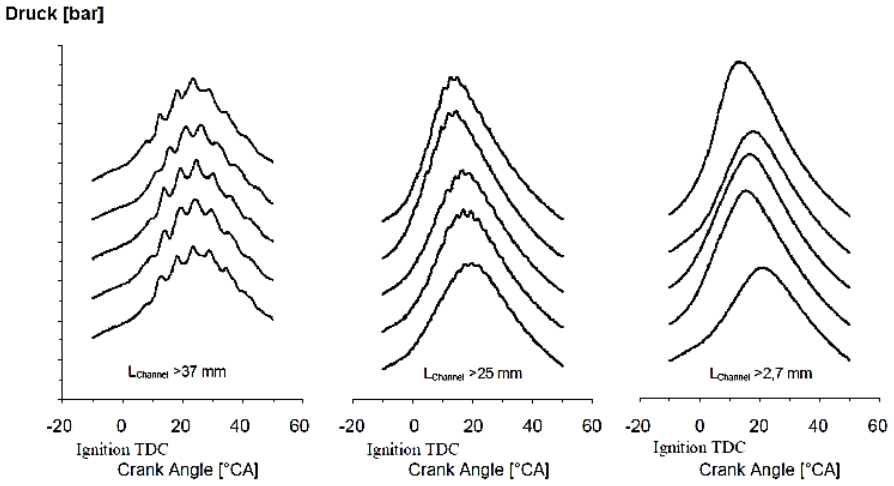

Figure 14: Effects of pipe oscillations on pressure readings (AVL, 2002)

In certain cases, pipe oscillations are unavoidable. It might be preferable to recess the transducer slightly to reduce the thermal load placed on it and prevent deposit formations in the transducer probe. AVL (2002) recommend that for these cases the diameter of the indicating channel should at least be the same as the length of the channel.

2.6.2. Crank angle measurement

The in-cylinder pressure measurement on its own does not provide adequate information to determine the characteristics or performance of the engine. The pressure trace has to be related to the engine crank angle (piston position) by means of a shaft encoder.

Encoders are classified into two main groups, namely absolute encoders and incremental encoders. Absolute encoders are rarely used in indication applications due to the sensitivity to vibrations and temperature as well as electronic noise (AVL, 2002). Incremental encoders can be subdivided into two types: inductive encoders and optical encoders, see Figure 15.

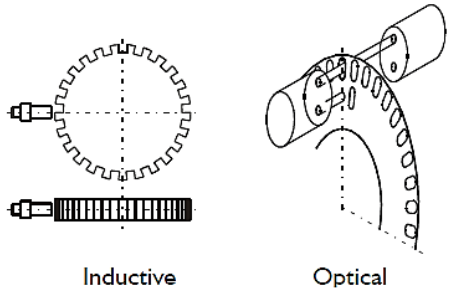

Figure 15: Inductive encoder vs optical encoder (AVL, 2002)

Optical encoders make use of a photo-transmitter (typically an LED) that emits light through a marker disk and onto a photo-receiver (photodiode). The marker disk has a precise profile that allows the light to pass through in increments. This produces an optical signal which the receiver and encoder electronics converts into an electronic pulse. This signal can then be interpreted by the data acquisition system to determine angular displacement (Rogers, 2010). The optical transducers provide good immunity to electrical noise and can offer higher resolution, but is more fragile than its inductive counterparts.

The incremental encoder can thus be seen as an analogue-to-digital converter. It is therefore important to specify a high enough sampling rate that ensures a good quality digital reproduction of the analogue data (Rogers, 2010). Common sampling thermos (i.e., Nyquist-Shannon) state that data needs to be sampled at a frequency of at least twice (2 to 10 times) as high as the highest frequency component of the sampled data to prevent aliasing of the signal. The combustion process produces a complex waveform that consist of numerous high frequency events that might be of interest (i.e., knock). Figure 16 illustrates the importance of selecting the correct sampling rate to accurately represent the combustion event.

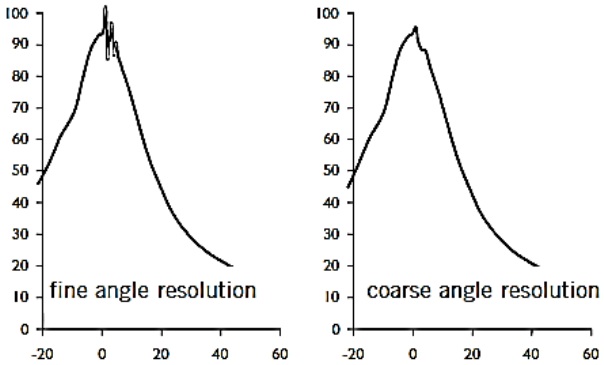

Figure 16: Influence of encoder sampling rate on signal conversion quality (AVL, 2002)

The primary knock frequency of a typical passenger vehicle ranges from 5-8 kHz. Rogers (2010) recommends that a resolution smaller than 0.2° be used for the measurements of knock and combustion noise. This correlates to the 0.1-degree sample rate recommended by AVL (2002) and Goering (1998). Table 1 as obtained from Rogers (2010), shows the recommended resolutions for specific applications.

Table 1: Measurement task and crank degree resolution (Rogers, 2010)

Task	Resolution (Crank angle degrees)
Knock	<0.2
IMEP, friction measurements	1.0
Combustion noise	<0.2
Heat release calculations	1.0
Calculation of polytropic exponent	1.0
Injection timing curve edges	0.1
Direct analysis of pressure curve	1.0
Rotational vibration analysis	<1.0

2.6.3. Pressure phasing and referencing

It is imperative that the combustion pressure trace is accurately phased with the crank angle. This ensures the accuracy of the thermodynamic calculations conducted using the pressure trace, as the crank angle is used to calculate the cylinder volume and the rate of change in volume (Blair, 1999) (Rogers, 2010). This makes the heat release calculations very sensitive to change in the phasing and it is recommended by Heywood (1988) that the phasing be accurate to within 0.2 degrees.

Various methods of phasing are available, the simplest of which is static phasing as used for the ECU tooth wheel (see section 3.5.1). This method does however not account for crankshaft twist and is inaccurate regarding pressure indicating. Dynamic phasing methods all use the pressure vs. crank angle data of an externally driven (motored) engine. However, it is not a simple case of determining where the peak pressure is and relating that to TDC. This is as a result of a phenomenon known as the thermodynamic loss angle and the peak pressure actually leads the true TDC (Figure 17). This is as a result of the piston's "slow" approach as it reaches TDC, as well as thermodynamically imperfect compression and expansion (Rogers, 2010). The thermodynamic loss angle is influenced by, among other factors, engine condition and engine speed, as lower speed lends more time for the losses to take place leading to a more profound loss angle.

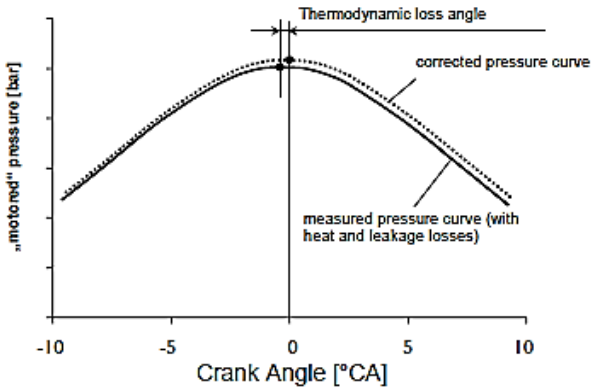

Figure 17: Thermodynamic loss angle (AVL, 2002)

The Optrand sensor used in the project measures the pressure relative to the pressure in a sealed chamber (in this case atmospheric pressure). This requires the pressure trace to be shifted as the heat release model is based on absolute pressure. The dynamic referencing and phasing is done using the polytropic relation described by:

$$PV^n = constant \tag{2.14}$$

This represents a log-log graph where the slope is described by the exponent *n*. A correctly phased and referenced pressure trace will produce straight lines, during the compression and expansion stroke on a log(P)-log(V) graph. A correctly phased and referenced graph should not cross over itself, broaden at the tip of the spike or have a curvature (Callahan *et al.* 1985). By examining the tip and base for any curvature respectively, it can be established if the correct compression ratio and reference pressure was used in the model. An illustration of a correctly phased and referenced log(P)-log(V) diagram, for a hot motoring curve, is given in Figure 18.

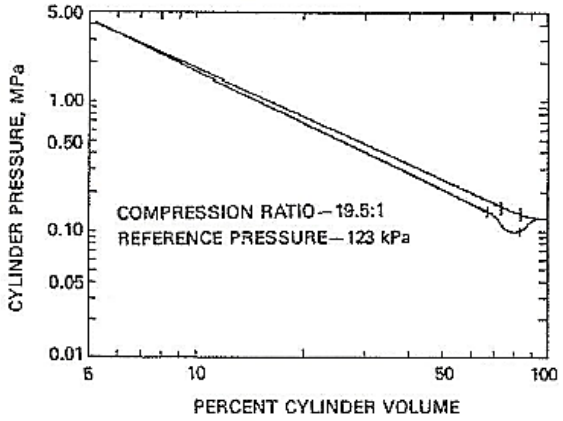

Figure 18: Log(P)-log(V) graph, motoring (Callahan *et al.* 1985)

2.6.4. Mean effective pressures

Engine torque is a valuable measurement used to give an indication of an engine's ability to do work. However, this measurement is dependent on engine capacity. A more relatable parameter is mean effective pressure (MEP) and is obtained by taking the work done per cycle by the cylinder and dividing it by the volume displaced per cycle. Equation 2.15 shows how the MEP can be expressed in terms of torque with n_R the number of crank revolutions per power stroke and V_d the cylinder volume displaced (Heywood, 1988).

$$MEP(kPa) = \frac{6.28 n_R T(N \cdot m)}{V_d(dm^3)} \tag{2.15}$$

If the torque used was measured from the engine flywheel (referred to as brake torque) the resulting MEP is known as brake mean effective pressure (BMEP).

The convention used to distinguish between various MEPs followed the terminology used by Heywood, 1988, and is as follows:

- Gross indicated mean effective pressure ($IMEP_g$), the MEP determined from the work delivered to the piston over the compression and expansion stroke.
- Net indicated mean effective pressure ($IMEP_n$), the MEP determined from the work delivered to the piston over the entire four strokes of the cycle.
- Friction mean effective pressure (FMEP), the total MEP determined from the pumping work, rubbing friction work and accessory work.
- Pumping mean effective pressure (PMEP), the MEP determined from the work done by the piston on the in-cylinder gasses during the intake and exhaust stroke.

The following relations can then be made:

$$IMEP_g = IMEP_n + PMEP \tag{2.16}$$

$$IMEP_g = BMEP + FMEP \tag{2.17}$$

2.7. Heat Release Analysis

Heat release analysis is a term used for the analysis of the in-cylinder pressure to obtain an accurate knowledge of how the combustion process propagates though the combustion chamber (Klein, 2004). By making use of the first law of thermodynamics, the in-cylinder pressure can be related to: the combustion process, the piston work produced by the gas, heat transfer to the chamber walls and mass flow in and out of crevice regions between the piston rings and cylinder lining (Heywood, 1988).

Various heat release models exist with various levels of complexity and accuracy. These models can be categorised into three main groups, namely zero-dimensional, quasi-dimensional and multi-dimensional models. Multi-dimensional models are the most complex. The zero-dimensional model is the simplest of the three as it does not take the gradient of any spatial parameters into account. This model can be subdivided into single-zone, two-zone and multi-zone models. The single-zone model approximates the entire charge as homogeneous with negligible spatial temperature gradients. The two-zone model divides the charge into two distinct thermodynamic zones, unburnt and burnt charge zones, with mass and energy transfer between them. The multi-zone model attempts to model the actual process more closely by performing mass energy balance on various zones (Klein, 2004) (Krishnan, 2004).

From in-cylinder pressure indicating data obtained in this project, a heat release profile and mass fraction burnt profile will be calculated by using a zero-dimensional, single-zone heat release model. The more accurate models are also well developed, but according to Heywood (1988) only offer slightly more accurate results, sometimes at great computational cost.

2.7.1. Heat release model

For the detailed derivation of the heat release analysis please refer to Appendix B. As derived in Appendix B.2, and confirmed by Goering (1998), the heat release can be represented by the following equation:

$$\frac{dQ_H}{d\theta} = \frac{V\frac{dP}{d\theta} + \gamma P\frac{dV}{d\theta}}{\gamma - 1} + \frac{dQ_W}{d\theta} \tag{2.18}$$

Figure 19 illustrates the basic geometry of a connecting rod and crankshaft, as well as the dimensional labels that were used in the calculations. It was assumed that the gudgeon pin offset (denoted as D) is zero.

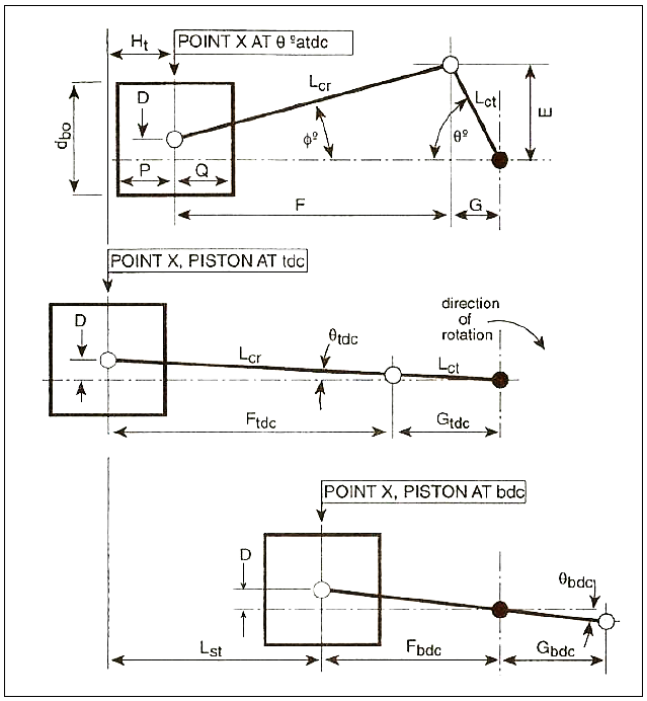

Figure 19: Connecting rod and camshaft geometry (Blair, 1999)

The piston position can then be described as follows:

$$H_t = L_{cr} + L_{ct} - \sqrt{L_{cr}^2 - (L_{ct}\sin\theta)^2} - L_{ct}\cos\theta \qquad (2.19)$$

The cylinder volume is represented by:

$$V = \frac{2A_P L_{ct}}{CR-1} + H_t A_P \qquad (2.20)$$

Where A_P represents the piston area and CR represents the compression ratio.

The mean gas temperature can be calculated by using the following relation:

$$T_i = T_{ref}\left(\frac{P_i}{P_{ref}}\right)\left(\frac{V_i}{V_{ref}}\right) \qquad (2.21)$$

The reference values used, are those obtained after the completion of the intake stroke. As the actual temperature inside the combustion chamber cannot be measured, the reference temperature will be taken as the intake temperature (measured just after the intake filter). This is not the most accurate assumption as it is expected that the charge will be heated by the hot cylinder walls and even the intake port. The port injection setup helps to offset this to some degree, as the evaporating fuel in the intake port will have an evaporative cooling effect.

With the temperature known and by using a model developed by Brunt, it is possible to calculate the specific heat ratio with the following equation (Brown, [S.a.]):

$$\gamma(T) = 1.338 - 6.0x10^{-5}T + 1.0x10^{-8}T^2 \quad (2.22)$$

2.7.2. Heat transfer through cylinder walls

Heat transfer through the cylinder walls is an additional factor that had to be taken into account and is represented by the last term in equation 2.18. Various models have been developed to approximate this and a simple yet commonly use model was developed by Eichelberg in 1936. Similar to most other models it assumes a linear relation between heat transfer and temperature difference, and models the heat transfer through the cylinder walls as a purely convective process (Goering, 1989). By assuming only convective heat transfer through the cylinder wall, it can be described by:

$$\frac{dQ_w}{d\theta} = \frac{hA_{wall}(T_w - T_i)}{60N} \quad (2.23)$$

With T_w the effective wall temperature. Eichelberg found the heat transfer calculations to be insensitive to the wall temperature and established that a wall temperature of 485 K produces satisfactory results (Goering, 1998). From this Eichelberg developed the following equation for convective heat transfer:

$$h = 0.00767S_p^{0.333}\sqrt{PT} \quad (2.24)$$

with the mean piston velocity calculated as:

$$S_p = \frac{4L_{ct}N}{60} \quad (2.25)$$

Both Annand (1963) and Woschni (1967) developed commonly used models with improvements on the model set out by Eichelberg. The heat transfer model developed by Woschni was used during this project, with the heat transfer coefficient obtained by the relation given in equation 2.26 (Klein, 2004).

$$h_c = \frac{0.013B^{-.0.2}p^{0.8}(c_1\mu_p+\left(\frac{c_2(p-p_0)T_rV_i}{p_rV_r}\right))^{0.8}}{T^{0.55}} \quad (2.26)$$

Where,

p	cylinder pressure for firing cycle	[Pa]
p_0	cylinder pressure for motored cycle	[Pa]
T	mean gas temperature	[K]
μ_p	mean piston speed	[m/s]
V_i	instantaneous volume	[m^3]
B	bore	[m]
c_1	constant	[-]
c_2	constant	[-]
T_r. V_r, P_r	reference values at selected reference condition	

The values for the parameters c_1 and c_2 were obtained experimentally by Woschni to be c_1 = 6.18 and c_2 = 0 during the gas exchange process and c_1 = 2.28 and c_2 = 3.24 x 10^{-3} during the closed part of the engine cycle (Klein, 2004).

2.7.3. Crevice losses

During compression some of the charge flows into the small region between the piston, the piston rings and the cylinder wall (crevices). Most of the charge will return to the combustion chamber during the expansion phase, but a fraction of the charge in the crevices will pass the piston rings and enter the crank case as blow-by (Heywood, 1988). Klein (2004) states that as much as 10 percent of the total charge can be trapped in crevice regions at peak pressure. Heat release models have been developed that take crevice losses into account by modelling the crevice losses as a mass transfer process in or out of the control volume (Heywood, 1988). The model developed by Gatowski models the crevices by assuming all crevices can be modelled as single aggregate constant volume and that the charge in the crevice is the same temperature as the cylinder wall and is at the same pressure as the combustion process (Klein, 2004).

Crevice losses will not be taken into account for the heat release analysis for this project as the crevice models are relatively complex and add little in the accuracy of the heat release model. A model similar to that set out by Goering (1998) will be used to create the heat release model.

2.7.4. Mass fraction burned and Vibe coefficients

With the heat release calculated for the combustion cycle, the mass fraction burned (MFB) can be determined. The MFB is assumed to be the same as the fraction of total heat released at that instant and can be calculated with the following formula:

$$B_\theta = \frac{\sum_{\theta=0}^{\theta=\theta} \delta Q_H}{\sum_{\theta=0}^{\theta=b} \delta Q_H} \tag{2.27}$$

The Vibe method was developed that allows a mathematical expression to be fitted to the mass-fraction-burned curve. Figure 20 shows an example of the Vibe method by using the following equation:

$$B_\theta = 1 - e^{-a\left(\frac{\theta-\theta_S}{b}\right)^{m+1}} \tag{2.28}$$

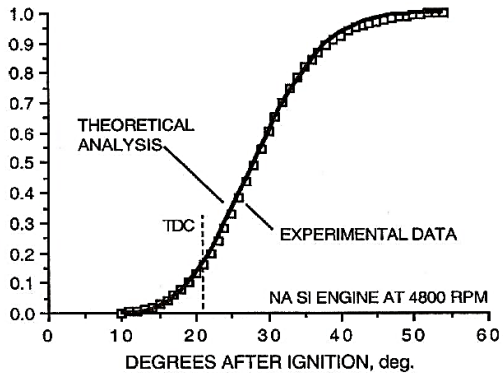

Figure 20: Example of Vibe's method (Blair, 1999)

3. Engine Management System Application

To allow full control over the engine it was required to convert the standard carburetted system to an electronically controlled fuel injected system. This was achieved by incorporating a fully programmable engine management system to a small SI engine. This allowed control over parameters such as fuel injection duration, spark ignition timing, wide-band lambda closed-loop control and various compensation conditions. Application of the engine management system required various modifications to be made to the selected test engine which are discussed in the sections that follow. The SI engine used for this project was a 2-cylinder Honda GX670 that employed a carburettor setup in its original form.

3.1. Electronic Control Unit

To enable full electronic control over the engine, an electronic control unit (ECU) was needed. A Perfect Power XMS5B stand-alone ECU was used. The XMS5B was selected based on its control capabilities, cost, use in the local motorsport

industry, recommendations and local support. The XMS5B ECU was designed to be used on engines with 4 to 8 cylinders (see section 4.2 for 2-cylinder configuration), has closed-loop control capabilities and came with the required programming software (LetRippII tuning tool). The ECU was programmed using a PC that communicated with the ECU via a universal serial bus (USB) cable. This also allowed engine parameters to be monitored while the engine was running.

Figure 21 shows the XMS5B ECU and its internal circuit. The eight injector drivers, eight ignition circuits and built in MAP sensor can clearly be identified. The ECU was also equipped with a wide-band controller, enabling closed-loop control using a wide-band lambda sensor. In addition, the ECU had provision for 8 auxiliary outputs that could be used to power relays controlling fuel pump, fans etc.

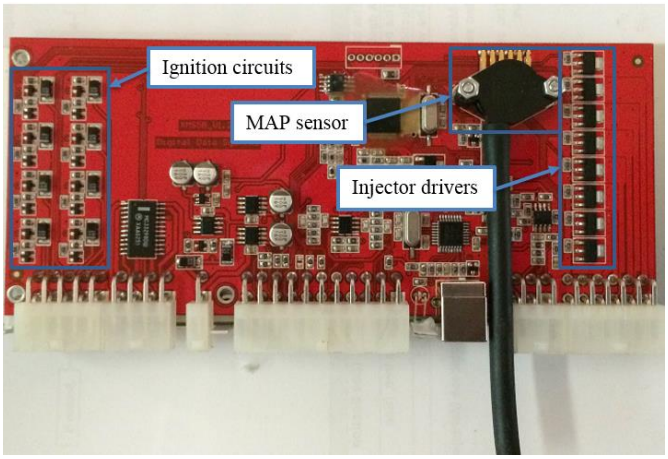

Figure 21: XMS3B ECU internal circuit

3.2. Fuel Injectors

To enable electronic control over the amount of fuel injected into each cylinder, electronic fuel injectors were used. Two small 128-gram injectors, as illustrated in Figure 22, were selected. Hose tail end connectors were implemented for a more flexible and compact design.

Figure 22: 128g Fuel injectors (Ecotrons, 2015)

3.2.1. Injector testing

An injector test bench was used to identify the spray characteristics and flow rates of the injectors under various conditions.

a) Injector test bench

The base of an existing injector test bed was used for the injector tests. A new control circuit using an Arduino *UNO* micro controller was developed and integrated into the existing control box. Together with the controller a new text based program was written to test the injectors for specified pulse durations and number of injection events.

A new fuel rail was designed and manufactured to house the small hose tail end injectors allowing them to inject into measuring flasks during injection tests. A pressure release valve was used to control the pressure inside the fuel rail and allowed tests do be done under different controlled pressures. The fuel rail was equipped with an analogue pressure gauge (to monitor the pressure while adjusting the pressure relief valve), a 0 bar to 6 bar Wika pressure transducer and a PT100 thermocouple.

b) Injector tests

White spirits were used as a substitute for petrol during the tests, as it has similar properties to that of petrol but is less hazardous. The original fuel rail and Ford ROCAM injectors were used to test the new software and control circuit, while an oscilloscope was used to measure the injection pulse time.

After it was established that the injection test bench and control circuit accurately controlled the injection pulses, the new fuel rail together with the hose tail end fuel injectors were connected to the injection test bench. The injectors were tested under different pressures as well as different injection pulse times to investigate the influence of both fuel pressure and injection time. Each test was done five times and the average result was used to compare the two injectors as shown in Table 2.

Table 2: Injector test results

Fuel Pressure (bar)	Injection time (ms)	Injector 1 flow rate (g/min)	Injector 2 flow rate (g/min)	% Difference
2.00	25	112.94	112.20	0.65
2.50	25	126.79	125.59	0.95
3.00	25	137.17	135.89	0.93
3.00	50	132.67	131.33	1.01
3.00	70	130.64	128.97	1.28

The spray patters for both injectors were captured with a 25 millisecond injection time and a fuel pressure of 3 bar and are shown in Figure 23.

Figure 23: Injector spray pattern

From the flow rate tests it can be seen that injector-1 has a slightly higher flow compared to injector-2, as well as its rated flow rate of 128 grams per minute. From Figure 23 it can be seen that injector-1 has a narrower spray angle as well as not vaporising the fuel as effectively as injector-2. To ensure that these deviations were as a result of the injector and not the test rig, additional tests were done, with the injector positions interchanged. These test produced similar results, confirming that the deviations were related to the injector and not the test bench. New injectors were ordered, but were only available towards the end of the project.

3.2.2. Injector placement

As discussed in section 2.1.4, for optimal fuel vaporisation and mixture formation the injector had to target spray on the intake valve. Due to special constraints this was not achievable. The injectors were placed on the corners of the intake manifold where it directs the airflow towards the intake valves as recommended by Zhao *et al*, [S.a.]. See Figure 24 regarding injector location. This allowed the injectors to inject parallel to the intake airflow aiding mixture formation. The injectors were targeted toward the intake wall above the intake valve, as the intake valve was seated deep in the cylinder head.

During initial testing, with the twin throttle body setup (see section 3.3), additional tests were done with the injectors repositioned further up the intake manifold. This was done as it was suspected that injection pooling might be occurring, resulting in the poor controllability and idle speed. Changing the injector placement provided no improvement in idle speed and slightly worsened the controllability of the engine. The injectors were placed back on the manifold corners as the controllability issue was found to be related to the throttle body setup, as discussed in the following section.

Figure 24: Injector placement on intake manifold

3.3. Intake Manifold

With the addition of fuel injectors, the original carburettor setup was no longer required. A new design using a throttle body had to be developed to control the airflow into the combustion chambers. The throttle body had to be placed in a similar position to that of the carburettor to maintain the same intake length as the standard setup. It was also required for the throttle body to have a connection that attached to the throttle actuator. This allowed control over the throttle position using the test setup control system.

The initial throttle body design utilized an individual throttle body setup with each cylinder having a dedicated throttle body. These throttle bodies were available off an existing setup, but it was found that they were too large for the test engine (see section 2.1.3) as throttle control was extremely limited. A small adjustment in the throttle position would result in a sudden increase in engine speed. Together with the control implications, the idle speed was also compromised as the lowest achievable idle speed was 2800 rpm, compared to the manufacturer's idle speed of 1500 rpm.

A company (Ecotrons) form the USA, specialising in small-engine EFI conversions, was consulted regarding the throttle body selection. A single 38 mm throttle body was selected based off specifications determined as described in section 2.1.3, as well as considering recommendations from the supplier, Ecotrons. Figure 25 shows the throttle body used on the test setup. The smaller overall throttle body diameter greatly improved engine control, and idle speeds below 1500 rpm were achievable. The manifold adaptor connected the single

throttle body to the existing intake manifold, as well as providing a location for MAP measurements to be taken.

Figure 25: Single throttle body assembly

3.4. Ignition

To enable electronic control of the ignition timing, the standard magneto ignition system had to be replaced with an electronically controlled ignition system. This ignition system consisted of a Perfect Power duel-channel ignition amplifier and two 12 V ignition coils, as shown in Figure 26. The ignition amplifier converted a low current signal from the ECU to a high current (30 amperes per channel) signal that drove the ignition coils. The ignition coils were charged by the ignition amplifier and discharged when the amplifier received the low current signal from the ECU. This caused the high voltage (40 kV) current formed in the ignition coil to travel through the spark plug, causing the arc that started the combustion process.

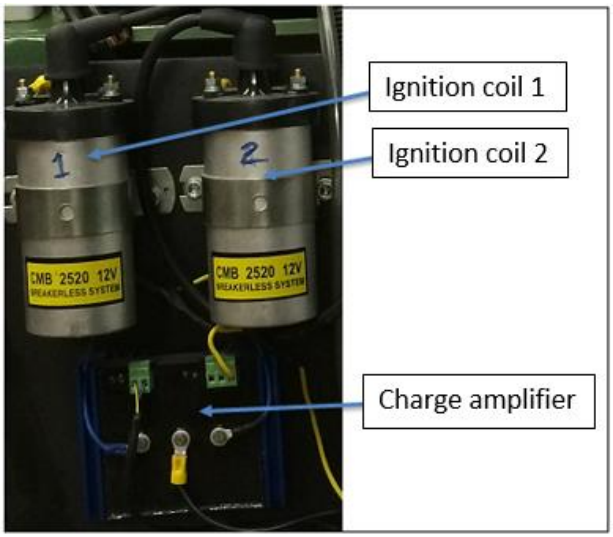

Figure 26: Electronic ignition system

3.5. Sensors

The ECU required various sensors to accurately control the electronic parameters of the engine. These included a speed sensor, throttle position sensor, oxygen sensor, pressure sensor and temperature sensors.

3.5.1. Speed sensor

The most critical sensor input for the ECU was the speed sensor, as it was used both to indicate the engine speed as well as provide a reference to TDC. The ECU used this signal to reference the ignition timing and injection timing.

A spigot and tooth wheel was designed and attached to the output shaft of the engine. Initially it was planned to use a Hall Effect sensor and a 60-2 tooth wheel. After consulting with a Perfect Power technician the design was changed to incorporate a magnetic sensor and a 36-1 tooth wheel, as can be seen in Figure 27.

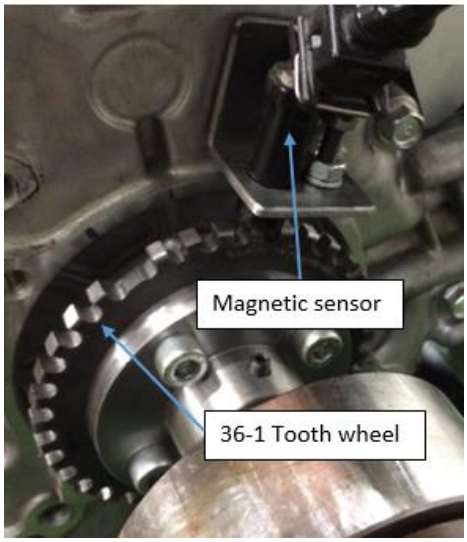

Figure 27: Tooth wheel and magnetic sensor

A magnetic sensor was used as the Perfect Power ECU and software was designed using a magnetic sensor. A Hall Effect sensor could be used, but this would require a separate voltage regulating circuit and has given communication problems in the past (Perfect Power, [S.a.]). Spatial constraints limited the diameter of the tooth wheel to 108 millimetres. A 36-1 tooth wheel design was used, resulting in very distinguishable teeth and gaps. This allowed the magnetic sensor to effectively saturate, resulting in accurate measurements.

To enable the ECU to reference TDC, the magnetic sensor had to be placed at a set position in relation to the missing tooth on the tooth wheel, as shown in Figure 28. Updated firmware in the ECU allowed the sensor to be placed up to 180 degrees after the missing tooth.

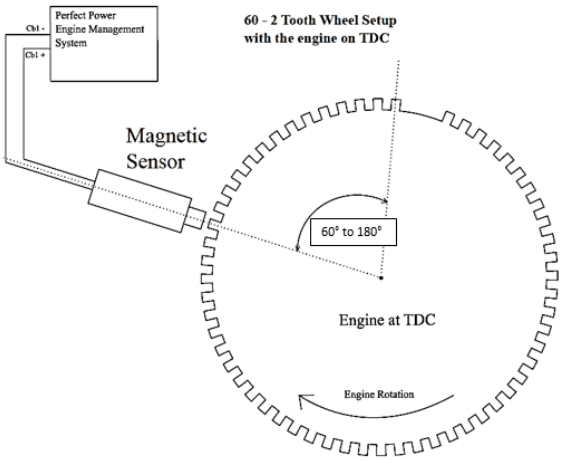

Figure 28: Magnetic sensor placement (adapted from, Perfect Power, [S.a.])

The magnetic sensor bracket was designed with a certain degree of adjustability to allow precise placement of the sensor. The bracket placement, along with the tooth wheel design, allowed the sensor to be placed precisely at 90° after the missing tooth, with the reference cylinder at TDC.

To ensure TDC was measured correctly, a dial gauge was placed in the cylinder through the spark plug hole. The piston displacement relating to certain crank angles were calculated using methods outlined in Stone (1992). Timing marks were made on the fly wheel for both cylinders, indicating TDC, 10°, 20° and 25° after TDC. These marks were initially used to ensure that the ignition reference was accurate and that the ECU adjusted the ignition timing correctly.

An oscilloscope was used to check the signal produced by the magnetic sensor while the engine was cranked with the starter motor. The magnetic sensor produced a clear sinusoidal signal with a distinguishable gap as the missing tooth passed the sensor. This resulted in a stable speed input to the ECU and was confirmed in the ECU programming software.

3.5.2. Manifold absolute pressure sensor

The XMS5B ECU came equipped with a built in MAP sensor, as illustrated in Figure 21, capable of measuring absolute pressures from 0 to 3 bar. This sensor together with an intake air temperature sensor was used by the ECU to determine the engine load.

As MAP fluctuated a lot, a dampening chamber was required to ensure stable pressure measurements. To calculate the size of the dampening chamber, the following equation was used (Byrne *et al*., 2006):

$$Transmission\ Loss = 10 \log \left[1 + \frac{1}{4}\left(m - \frac{1}{m}\right)^2 (\sin kL)^2\right] (dB) \qquad (3.1)$$

where,

$$\text{m} = \frac{\text{cross-sectional area of the dampening chamber}}{\text{cross-sectional area of the connecting ducts}}$$

$$\text{k=wave number} = \frac{2\pi f}{c}$$

L=length of dampening chamber

3.5.3. Throttle position sensor

A TPS was connected to the throttle valve shaft on the throttle body as indicated in Figure 29. The TPS was mechanically linked to the throttle plate and the sensing element had an arm that rotated with the throttle valve. The arm had a

contact point on the potentiometer which acted as a voltage divider. The potentiometer received a 5 V supply from the ECU together with a ground connection. A third pin transmitted an output voltage to the ECU, that was proportional to the rotational angle of the throttle valve.

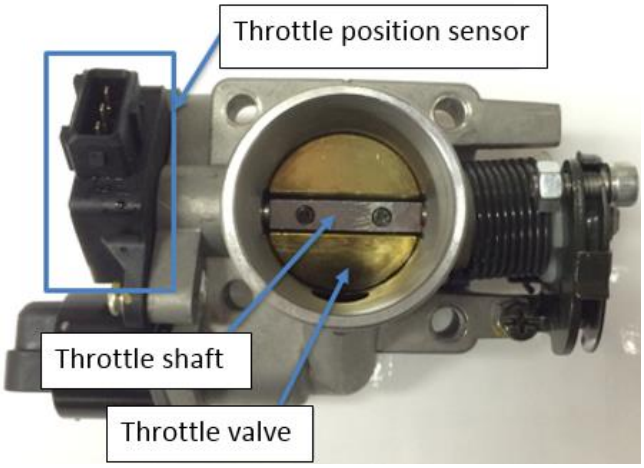

Figure 29: Throttle position sensor placement

The TPS allowed the ECU to incorporate acceleration maps as is explained in section 4.4. The sensor also made interpreting the ECU maps simpler as the map allocations could be referenced to throttle position and engine speed.

3.5.4. Temperature sensors

The ECU required certain temperature inputs that allowed it to monitor engine and ambient air conditions. These included an intake air temperature sensor and an engine temperature sensor.

The intake air temperature sensor was placed directly in front of the intake air filter, enabling measurements of the air entering the engine manifold.

Engine temperature is conventionally measured in the engine coolant after passing through the engine. As the test engine was air cooled, the engine temperature had to be measured on the engine block. A temperature sensor was placed at the back of the engine, on the engine block, as less air flowed over the engine in that region.

3.5.5. Lambda sensor

A six wire wide-band lambda sensor was required to enable the ECU to use closed-loop control during engine operation. Perfect Power recommended a Bosch LSU 4.2 (older model probe) oxygen sensor as it was the sensor used during development of the XMS5/B ECU. The sensor was placed after the exhaust

silencer as the exhaust ports for cylinder-1 and cylinder-2 merged inside the silencer. The sensor was placed at a 90-degree angle as recommended by Bosch and is shown in Figure 30.

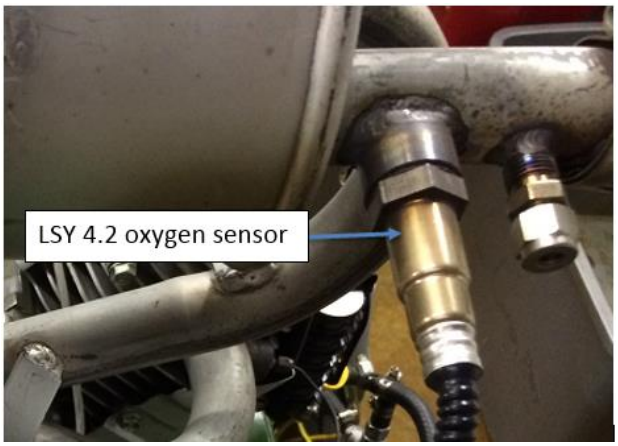

Figure 30: ECU lambda sensor placement

3.6. Wiring

A custom wiring harness had to be made to allow the ECU to communicate with the various sensors and actuators. A 12 V battery was used to supply power to the ECU, pump and ignition circuit. The circuit diagram for the ECU can be found in Appendix C.

The designed wiring harness incorporated both the existing ignition switch circuit as well as a separate relay circuit. This allowed the engine to be started by either the ignition key or the programmable logic controller (PLC).

Before the engine was started with the new engine management system, all sensors, actuators and connections were checked, together with checks for ground loops and stray voltages. This ensured good communication was achieved throughout the engine management system. The ECU, fuse and relay box and ignition circuit were placed on a steel plate and connected to the test bed, as shown in Figure 31.

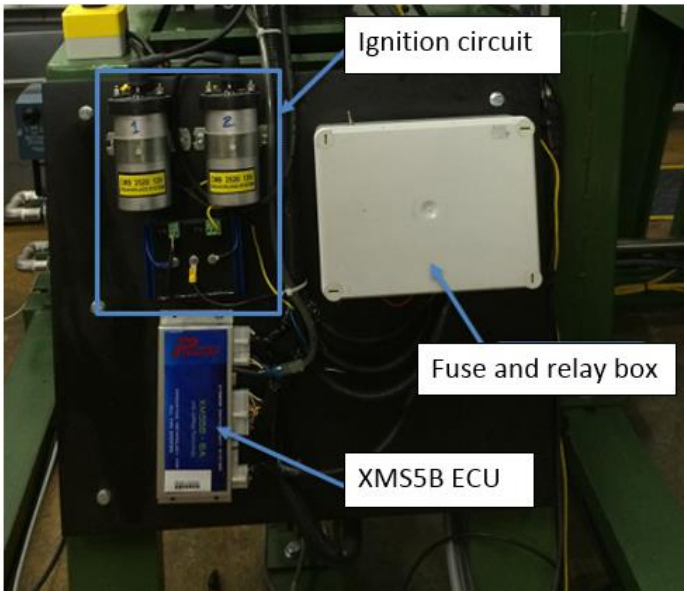

Figure 31: ECU placement

4. ECU Programming

This chapter describes the methodology followed to set up and program the ECU for the engine management system. The standardised test procedure as set in SAE J1312 (1987) was followed when generating engine performance maps and representing related data.

4.1. Overview

Configuring and programming the ECU for the small two cylinder Honda GX670 engine had a number of challenges. This was as a result of there being no base maps available for the test engine as well as the engine's 2-cylinder configuration.

The Perfect Power XMS5B ECU used to control the test engine was designed to control a 4, 6 or 8-cylinder engine. All the control parameters controlled by the ECU were referenced from a single cylinder (cylinder-1). The remaining cylinders were then phased according the firing angle which was determined by dividing 720° by the number of engine cylinders. The ECU had a fixed numerical firing order and if a particular firing order was required it has to be wired to match the ECU output.

The ECU used the engine speed, throttle position and temperature inputs to determine which map allocations to use. The programming software assigned 384 tune sites to each major map with 16 intervals on the throttle position axis (horizontal axis) and 24 intervals on the engine speed axis (vertical axis), forming a 3-dimensional map. The programmed maps can be found in Appendix D.1.

Selected maps have optional side maps with 24 tune sites each (speed dependent). These maps are used to alter the main map, which they are related to, depending on the control parameters.

The test engine ECU was initially only programmed under no load conditions. This was done to ensure easy start up and a stable idle speed, similar to that of the manufacturer's, was achievable. Thereafter the ECU was programmed for increased engine speed, but still under no load. This helped establish good throttle sensitivity as well as indicating the engine's response to changes in the ECU programming. After adequate engine control was established under no load conditions, load was incrementally applied to the engine and the ECU maps were adjusted accordingly. Details on the various maps are given in the sections that follow.

4.2. ECU Configuration

To allow the ECU to control the engine, various parameters had to be configured. This included number of cylinders, cylinder firing angle, tooth wheel placement, fuel injection limits, ignition timing limits, engine speed limit as well as certain ECU control functions.

To control the firing order and cylinder firing angle, the ECU was configured for an 8-cylinder engine. This sets the firing angle to the 90 degrees (720 degrees divided by 8) as was required for the test engine. The injector and ignition circuits were activated in the ECU as cylinder 1 and 2. The remaining cylinder circuits (3 to 8) were disabled. This was achievable as a result of the 90° firing angle of the engine matching that of a conventional 8-cylinder engine. If this was not the case, a separate tooth wheel would be required, using only two correctly placed teeth to indicate the required firing angle. The magnetic speed sensor was placed at precisely 90 degrees after TDC, as discussed in section 3.5.1, and was configured in the ECU software accordingly (ignition reference).

The ECU was configured to use only the crank shaft sensor as no cam shaft sensor was fitted to the engine. This meant both the injectors and spark plugs were fired twice during each cycle (wasted spark configuration), as the ECU had no way to distinguish the different engine cycles.

The ECU was set to limit the engine speed to 3700 rpm. This allowed the engine to run at its operating speed of 3600 rpm without interference, while preventing it from over speeding. This was achieved by temporarily applying a "hard stop" on the engine when it exceeded 3700 rpm, cutting the ignition and fuelling to the engine till engine speed dropped below 3700 rpm. This only lasted a brief moment (not specified by the ECU), allowing the engine speed to drop, before re-activating the ignition and fuelling.

Ignition advance and retard limits were set to 35 and 10 degrees respectively. This was to ensure that the ignition timing was kept within a safe range while the timing map was adjusted, and to prevent any values exceeding the limit from taking effect. This prevented the ignition timing from being advanced to an extent where engine knock occurs or retarded to an extent where the mixture is ignited while the intake valve was still open.

Certain control functions could also be enabled on the ECU depending on the requirements. These included closed-loop or open-loop control, lambda trim and injector trim. The acceleration determinant was set to activate the additional acceleration map depending on the throttle position movement.

4.3. Sensor Calibration

The ECU software required certain set points and sensors to be calibrated. The most critical of these were the engine speed range and throttle position sensor calibration, as these values were used for all the control maps (vertical and horizontal axis respectively). The speed range was set from 500 to 3700 rpm as it covered the engine operating range as well as a speed low enough to start the engine.

The TPS was initially calibrated linearly between closed and wide open throttle, but a non-linear calibration provided better throttle control. This was a result of the engine's sensitivity to change in throttle position at low loads.

The ECU engine temperature and inlet air temperature sensors were calibrated using a fluke temperature calibration well (see Appendix A). The software only required a low temperature and a high temperature calibration, then applied a linear curve to the calibrated values.

4.4. Fuel Mapping

Initially, to help estimate the fuel requirements of the test engine, injection maps of similar capacity engines were investigated. This proved challenging as all the available injection maps were for engines operating at a significantly higher speed (mostly for motorcycle applications). The low speed fuel parameters were used as an initial estimation. During initial injector map programming, an estimated conservative ignition map was used.

The ECU was kept in open-loop control mode while the fuel map was configured, as the closed-loop function required the fuel map to operate within certain lambda limits. Each map site was programmed by controlling the engine at the required speed and load, while monitoring the lambda measurement of each cylinder using an external lambda scanner and individual oxygen sensors. The injection time required for each map site was obtained by adjusting the injection value to achieve lambda measurement of 0.95. This was done for each map site within the

operating range of the engine (2400 to 3600 rpm and 0 to 45 N·m) with the ECU interpolating the values between the map sites.

4.5. Closed-Loop Control Configuration

The closed-loop control of the ECU consisted of three programming maps: the setup map, lambda target map and the long term trim map.

Perfect power provided a guideline for the initial setup of the ECU and the Bosch oxygen sensor that were used. The Bosch LSU 4.2 was chosen over the newer LSU 4.9, as the ECU was developed using the older generation sensor. The sensor setup parameters were altered based on the measurements received from an ALM-II lambda scanner to ensure the ECU operated correctly under closed-loop conditions. These sensor parameters include lambda rich and lean limits, lambda trim time and the closed-loop lambda response time. Perfect Power provided no information regarding the approach flowed during closed-loop and open-loop control, a general block diagram illustrating the control functions is given in Appendix C.

The lambda target map allowed 384 entries (similar to the fuel map and timing map) to specify the desired lambda/AFR target at each given load and speed point. This map allowed individual point map locations to be run under open-loop conditions by assigning it a value of zero. The entire map was set to a target lambda value of 1 and could easily be changed according to what was required under certain test conditions.

The long term trim map measured the average difference in the closed-loop fuel conditions and the values in the fuel map. These values were then stored in the corresponding map location. The map showed the calculated fuel adjustments required to run the engine at the set lambda target. These adjustments could be applied to the open-loop fuel map or be reset. This allowed the fuel map to be adjusted to closely match the closed-loop conditions, resulting in better open-loop operation and better closed-loop response.

4.6. Timing Mapping

Honda provided no timing information regarding the standard engine setup, apart from the 25 degrees advance at the engine operating condition (full load at 3000 rpm). Perfect Power recommended an initial conservative timing map based on the engine characteristics and its operating range. After the engine was connected to the dynamometer, a new timing map was created as follows:

With the initial estimated timing map applied, the engine was controlled at constant speed, constant throttle and at lambda 1. The ignition timing was then adjusted to obtain MBT and then retarded by 2 degrees (conservative approach). This was done for each map location. Results for a timing swing test can be found in section 6.2.2.

The resulting timing map was analysed and a smoothing function was applied to it. This was done to simplify future changes to the timing map and made it easier to compare different timing settings while testing.

With the ECU configured, various tests were done to verify that the ECU was set up correctly and that the engine responded to changes in the ECU parameters. These tests are discussed in section 6.2.

5. Engine Test Facility

In this chapter the test facility that was further developed and used during testing will be discussed. Detailed descriptions of the mechanical, electrical and software components of the facility will be given.

5.1. System Overview

The main components that were used for the test setup were a Honda GX670 SI engine, an 18 kW AC dynamometer and drive setup, an Allen Bradley PLC, an Ecotrons ALM-II lambda scanner, a National Instruments DAQ device and a AVL fuel flow meter. A diagram of the test cell and control room layout can be found in Appendix C, with the 19” cabinet containing all the control modules. Three PCs were used for engine control, ECU control and data acquisition (please see Appendix D, Honda GX670 starting procedure, for clarification on PC usage).

5.2. Engine and Dynamometer Installation

As previously stated, the engine used for the project was a Honda GX670 SI engine, that was carburetted in its original configuration. The engine was originally installed on a smaller test bench, commissioned by H.J. Lombard and connected to a water brake dynamometer. Thereafter it was instrumented with a shaft encoder and in-cylinder pressure transducer by J.L. Cuperus to enable in-cylinder engine indication. Prior to any further testing or modification to the test engine, the engine was stripped, checked and reassembled to ensure that all parts were in working order. Thereafter the engine management system was applied to the test engine as discussed in section 3 and the engine installed on the AC dynamometer test bench.

5.2.1. Test bed

To enable full controllability over the test procedures the test engine was installed on test bed designed for a previous project by E. Grobbelaar (2017). The test bed made use of an AC motor and drive system that acted as a dynamometer This dynamometer was capable of either motoring the engine or applying load to the test engine.

The test bed was initially designed for a Yanmar single cylinder diesel engine. Various modifications and additions to the test bed had to be made to enable the Honda GX670 test engine to operate on the new test bed. The engine mounting

plate required additional mounting holes and spacers to allow the Honda test engine's output shaft to align with the dynamometer. Together with these modifications to the test bench, additional mounting plates and brackets were installed to accommodate the engine management system and additional measuring equipment.

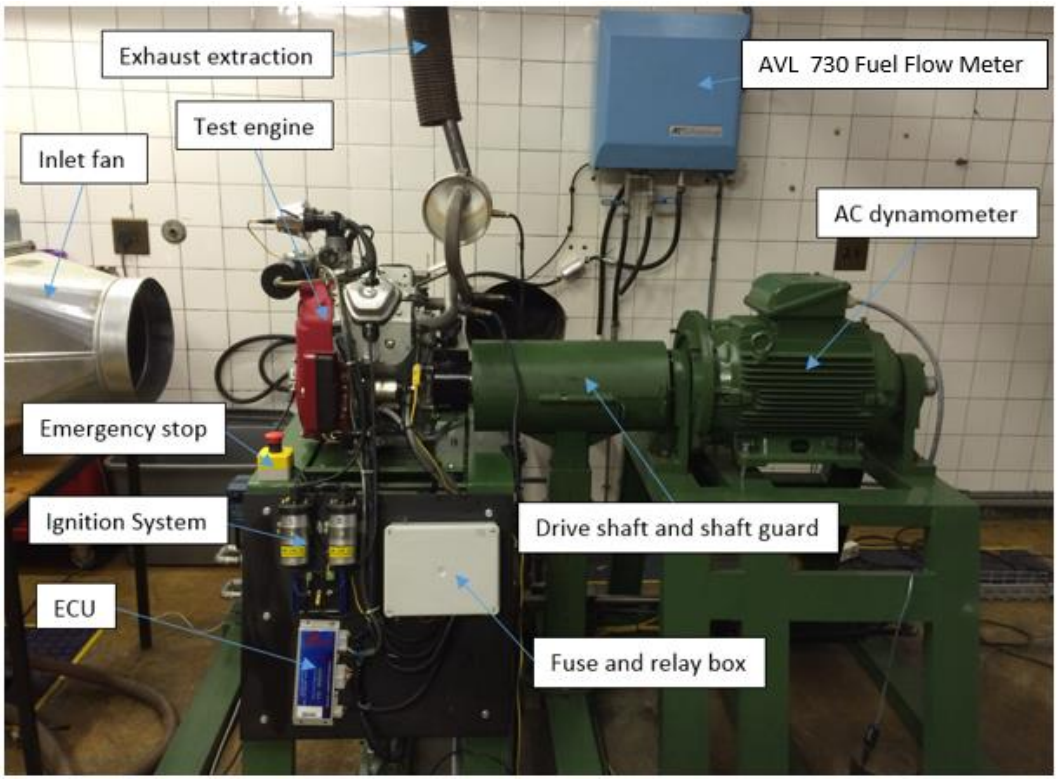

Figure 32: Engine test setup

5.2.2. Drive shaft

A new drive shaft had to be designed allowing the Honda test engine to connect to the AC dynamometer. The old drive shaft design was extended by 20 millimetres and machined from a VW polo drive shaft with the same part number as the previous design. The drive shaft was connected to the engine via a constant velocity (CV) joint and to the dynamometer by the use of a flexible coupling, as seen in Figure 33. This design was chosen over a standard drive shaft with two CV joints to minimise vibration transfer to the dynamometer, as well as minimizing torsional oscillations.

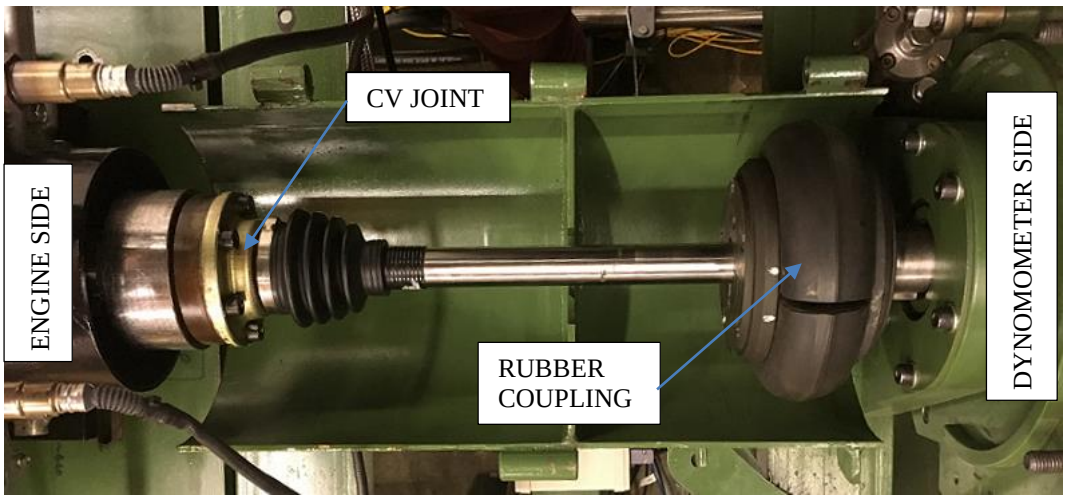

Figure 33: Drive shaft

The existing shaft guard provided sufficient protection over the newly designed drive shaft, however an additional guard had to be designed to mount to the back of the engine to cover the engine output shaft and the trigger wheel (shown in Figure 34).

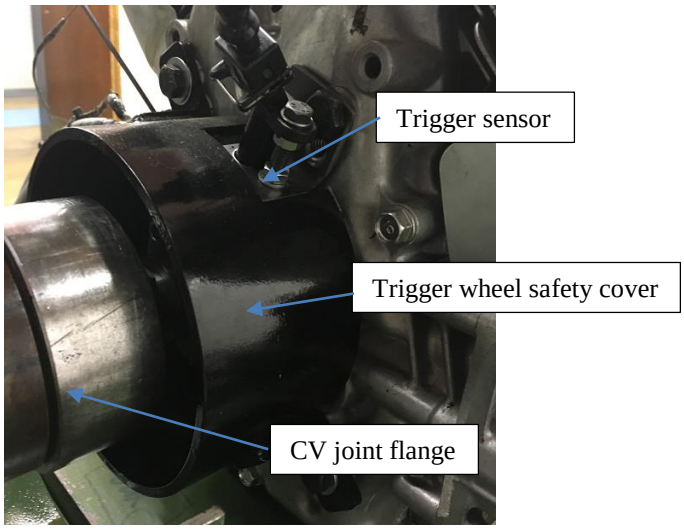

Figure 34: Trigger wheel safety cover

5.3. Fuel System

With the engine being converted from carburetted to electronic fuel injection (EFI), a new fuel delivery system had to be designed. Due to spatial constraints on the test engine, a semi-returnless fuel system was used. This allowed optimal placement of the fuel injectors, as the fuel return line was placed before the test engine.

Fuel was supplied to the engine from a measuring vessel and the fuel supply pressure to the injectors was regulated. Excess fuel was returned via closed-loop between the measuring vessel and the engine. This ensured that all the fuel passing through the measuring vessel recirculated back to the engine and not back into the vessel, allowing for accurate fuel measurements. A schematic of the fuel system can be found in Appendix C.

An AVL 730 dynamic fuel balance (Figure 35) was used for fuel flow measurements. The AVL unit made use of a highly sensitive capacitive displacement transducer connected to a thin blade spring to measure any change in the fuel mass of the vessel (AVL, 1984). The fuel flow was calculated based of the change in fuel mass over a set time period. The AVL unit was calibrated using its built-in calibrating procedure as described by the manufacturer.

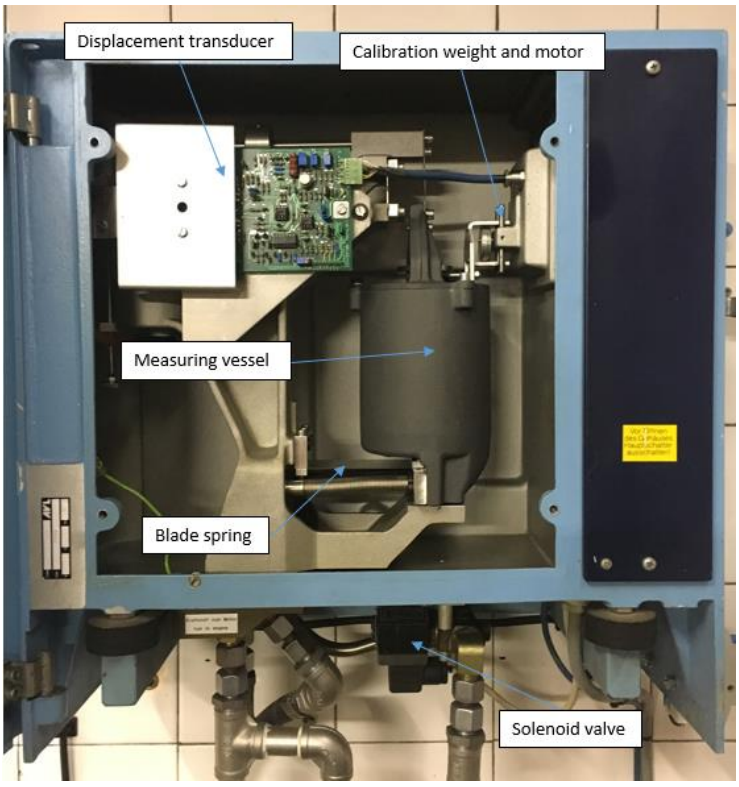

Figure 35: AVL dynamic fuel balance

5.4. Test Cell Ventilation

The test cell used for the project was equipped with an intake air- and extraction duct, assisted with an inlet fan and extraction fan respectively (see Appendix C, Figure 77). The inlet fan helped with airflow over the test setup and aided in keeping the test cell cool during long test periods. An existing extraction pipe connected to the extraction duct was modified and coupled to the test engine's exhaust using flexible tubing, as seen in Figure 36.

Due to the minimal airflow over the test setup and the test engine being air cooled, a centrifugal inlet fan and portable fans were used to cool the test setup. This helped to keep the engine oil cool under high load testing as well as cooling the dynamometer.

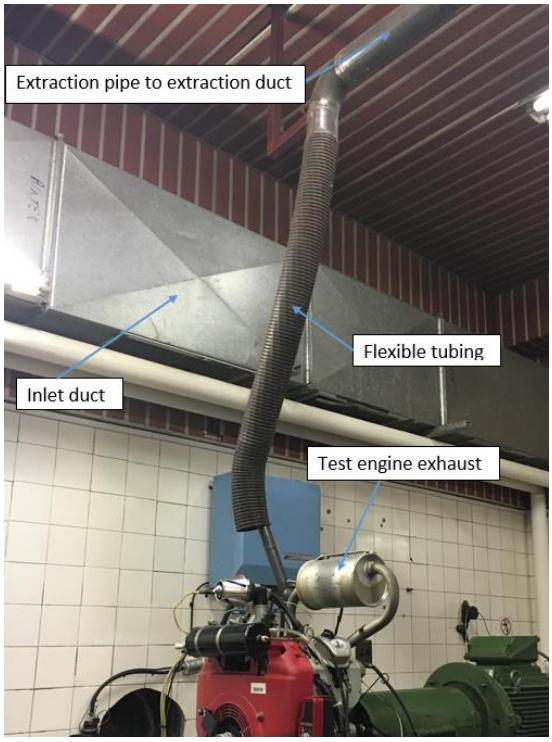

Figure 36: Engine exhaust extraction system

5.5. Test Setup Instrumentation and Control Hardware

To enable full control over the test setup and monitor critical parameters, a range of control hardware was needed. This included sensors, actuators, relays and controllers. The various instrumentation hardware will be discussed in this chapter. For details on the engine management system hardware, please refer to section 3.5.

5.5.1. Sensors

Sensors that were used on the test setup include thermocouples, pressure transducers, oxygen sensors, speed sensors, a load cell and a fuel balance (see section 5.3). Calibration procedures and data for these sensors can be found in Appendix A.

a) Thermocouples

All thermocouples used for the project were Type-K and were installed for the following measurements:

- Inlet air temperature
- Ambient air temperature
- Exhaust gas temperature for both cylinders
- Fuel temperature
- Oil temperature

b) Pressure sensors

Two Wika 5 bar pressure transducers were used for measuring the oil and fuel pressure. A 2 bar transducer was connected to a small damping chamber and used to measure the intake manifold pressure required for in cylinder pressure referencing.

For in-cylinder pressure measurements, an Optrand fibre optic transducer and a spark plug mounted piezoelectric Kistler transducer were used, shown in Figure 37 and Figure 38. Both transducers were calibrated as described in Appendix A.

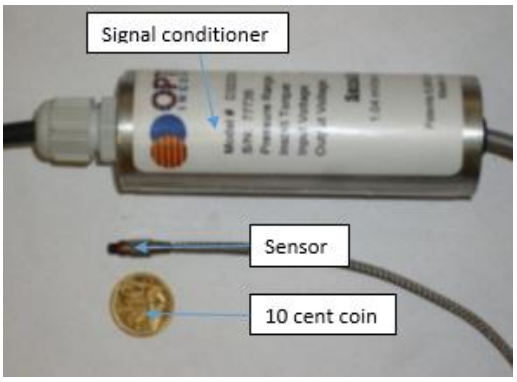

Figure 37: Optrand pressure transducer

Figure 38: Kistler pressure transducer (Spark plug mounted)

In 2012, as part of a Mechanical project 478, J.L. Cuperus (2012) commissioned the test engine with the required components for in-cylinder pressure indicating. A pressure sensor sleeve was added to the second cylinder to allow the fibre optic Optrand sensor to measure in-cylinder pressure. The pressure sensor sleeve and sensor location can be seen in Figure 39.

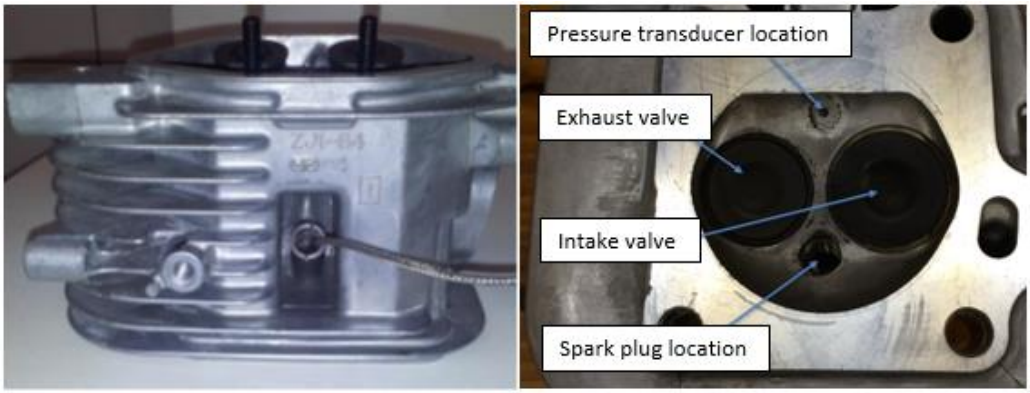

Figure 39: In-cylinder pressure sensor location

The Kistler transducer was used to verify the results obtained by the Optand transducer, see section 6.3.3.

c) Oxygen sensors

Two oxygen sensors were used to individually monitor the air-fuel-mixtures of the two cylinders. The sensors used were Bosch LSU 4.9 sensors and were connected to an Ecotrons ALM-II lambda scanner. The sensors and scanner can be seen in Figure 40. The ALM-II scanner measurements were verified using an ETAS LA2 lambda scanner and both units provided similar results.

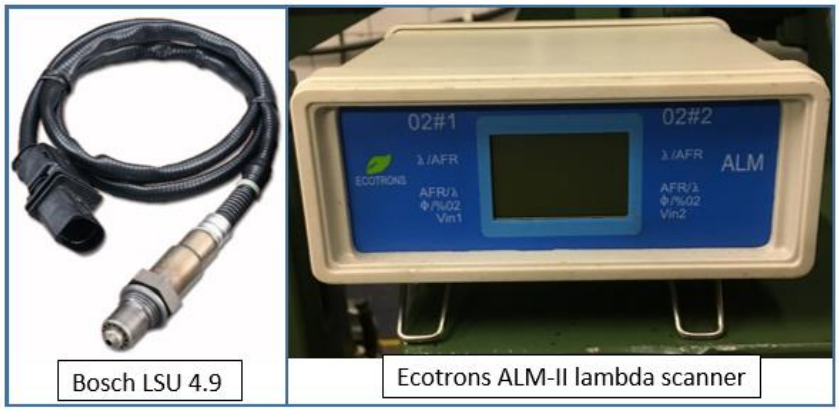

Figure 40: Lambda measuring equipment

d) Speed sensors

The test setup made use of three different speed sensors for both control and data logging purposes. The ECU made use of a magnetic sensor and tooth wheel, as described in section 3.5.1, to measure the engine speed.

A Kübler 5020 incremental encoder with a resolution of 3600 pulses per revolution (ppr) was used for engine indicating measurements. This encoder was

mounted on the front of the engine and connected to the engine fly wheel via a machined spigot with a shaft attachment as seen in Figure 41.

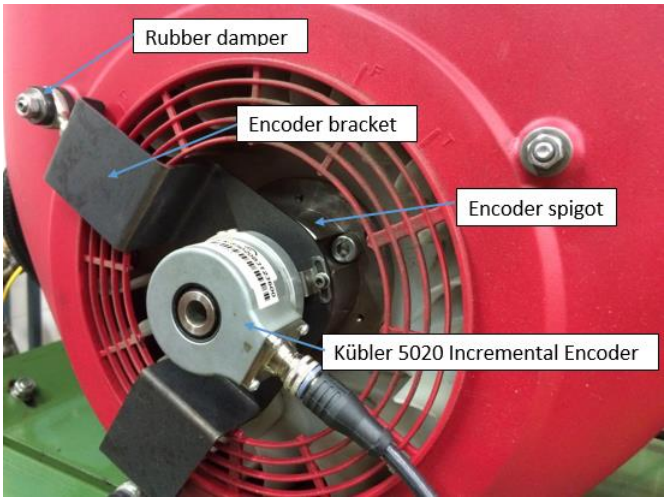

Figure 41: Engine encoder attachment

A Turck RI-12H15E-2B1000-H1181 (1000 ppr) optical encoder, connected to the dynamometer, was used to measure engine speed for the AC drive and control system.

e) Load cell

A HBM U2A (500kg) load cell, placed 0.15m from the dynamometer shaft centre, was used to measure the torque applied by the dynamometer. The load cell produced a low voltage that was amplified using a Loadcell Services LCS/I/0350 load cell transmitter. The load cell transmitter in turn sent a 0-10 V signal to the control PLC that calculated a measured torque value, based on the received voltage signal and calibration values (see Appendix A).

5.5.2. Controllers, actuator and data logging hardware

The controllers used to operate the test setup were installed in a control cabinet located in the control room. Control over the test setup was achieved using these controllers together with an AC drive unit connected to the dynamometer. The installed controllers and modules are shown in Figure 42.

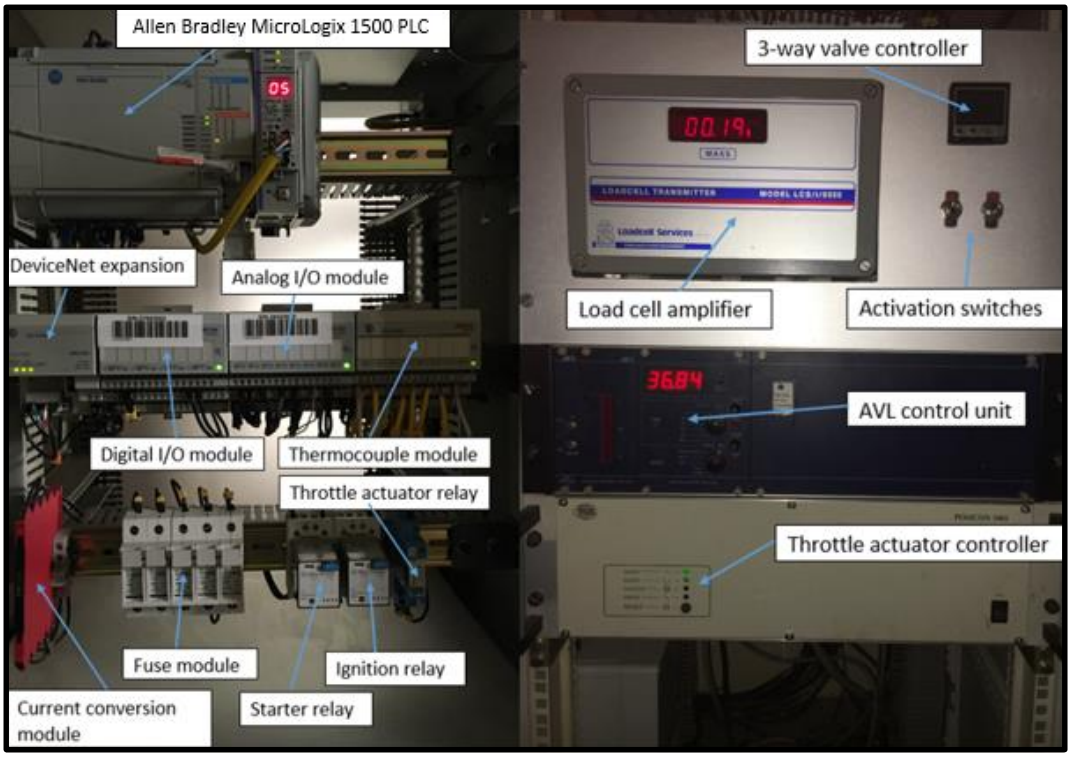

Figure 42: Control cabinet modules

a) PLC

An Allen Bradley MicroLogix 1500 programmable logic controller (PLC) was used to allow control over the dynamometer and throttle actuator and to monitor the measured parameters. The PLC connected to a digital I/O module, an analogue I/O module and a thermocouple module via a device net expansion.

The digital module was used to operate the relays, turn on the drive system, as well as receive an input indicating when the fuel balance was refilling. The relays were supplied with 24 V direct current (DC) from an external power supply located in the control cabinet. These relays were connected to the emergency stops that de-energized once either of the emergency stops were depressed (see section 5.5.3).

The analogue module was used to read inputs measuring oil pressure, fuel pressure, fuel mass in the fuel balance, engine speed, torque and throttle position. Two channels were used as outputs: one sent the speed set-point to the drive system and the other sent a signal to the throttle actuator control module, controlling the throttle position.

All the thermocouples mentioned in section 5.5.1 were connected to the thermocouple module via a junction box on the test bench. This allowed thermocouples to be checked and replaced easily without having to redo wiring to the PLC module.

b) AC dynamometer system

The AC dynamometer system consisted of three major components, a WEG W33 AC motor, an Allen Bradley PowerFlex 753 drive controller and a Penbro Klelnick 18 kW resistive load as shown in Figure 43.

Figure 43: AC dynamometer system

The drive controller was set up by a contracting company to supply power to or absorb energy from the AC motor to control the dynamometer speed. The controller received a speed input from a shaft encoder and controlled the dynamometer speed based on a speed set point received from the main control PLC (set in ETA). The resistive load was used to disperse the energy absorbed by the dynamometer.

c) Throttle actuator and controller

To enable control over the engine throttle, a Technogerma Systems TSG 1003 throttle actuator and a TSG Posicon 1001 control unit were used. The control unit received a 0-10 V signal from the PLC based on the throttle position set-point and in turn controlled the throttle actuator.

d) High speed data acquisition module

To enable accurate engine indicating measurements, in-cylinder pressure had to be captured every 0.1 degrees crank angle (see section 2.6.2.) This resulted in a maximum acquisition rate of 216 kHz, at engine speeds of 3600 rpm. A National Instruments USB-6351 data acquisition (DAQ), as seen in Figure 44, was used to

capture the in-cylinder and manifold pressure based on a trigger signal received from the Kübler 5020 shaft encoder.

Figure 44: Data acquisition device (National Instruments, 2012)

The Optrand and Kistler transducers were interchangeably connected to the DAQ via an 8-pin connector. A similar connector was used for the intake manifold pressure transducer and was interchangeably used with an ignition indication circuit (see section 6.2.1). The circuit diagram for the DAQ can be found in Appendix C.

5.5.3. Emergency stops

To conform to safety requirements, various emergency stops were located in the test facility. Martyr and Plint, 1995, recommend that hardwired emergency stops should be placed both in the test cell and in the control room. An emergency stop was located in the test cell and in the control room, as well as on the AC drive system.

The test cell and control room emergency stops both had normally closed contacts and were integrated into the test setup control system. This enabled them to shut down the ignition and fuel delivery system, when either one was depressed. The drive system emergency stop was connected to an input on the drive controller that triggered a software flag if depressed, disengaging the AC motor.

5.6. Test Setup Control Software and Interface

Various user interface software packages were used to allow control over the test setup. These included supervisory control and data acquisition (SCADA) software, ECU programming software, high speed data acquisition software and a lambda measuring package. The various graphical user interfaces used can be seen in Appendix D.

5.6.1. Supervisory control and data acquisition

For the test setup Engine Test Automation (ETA) software was used as a SCADA interface, using RsLinx to communicate with the PLC. RsLogix was used to program the PLC. ETA enabled the engine to be controlled, parameters to be monitored, alarms and emergency shutoffs to be set, sensor to be calibrated, data to be logged and automated test sequences to be programmed. The user interface developed can be seen in Appendix D, Figure 80.

The program had two main operating modes, torque control and throttle control. In both modes the speed set point had the highest priority as it was directly controlled by the drive system. With the drive activated, the engine would always run at the speed set-point. The dynamometer was able to motor the engine if the engine could not reach the speed set-point. In throttle control mode the user had control over the engine throttle position and engine speed. Depending on the throttle position, the dynamometer would either load or motor the engine to maintain the set engine speed. In torque control mode the user selected the torque set point and speed set point. ETA then used PID control to continuously adjust the throttle position to match the measured torque to the torque set point.

Throttle control mode was mainly used to start the engine and during engine warm-up periods. Torque control mode was used for most tests, including automated tests. The only tests ran in throttle control mode were the timing swing and fuel loop tests, as changes in torque had to be observed (see section 6.2).

5.6.2. High speed data acquisition software

The software package used in conjunction with the DAQ was National Instruments' LabView. The program was used to capture, manipulate and store data. This was done in two parts: a main block diagram program and a user interface panel. The main program was compiled using a block diagram consisting of various interconnected functions. The diagram is shown in Appendix D.3. Figure 91. The program was a further development based on a program used by E. Grobbelaar (2017). The block diagram was then used to create a user interface panel, see Appendix D.2. Figure 81, showing the measured pressure traces for the given cycle.

With the program running, the DAQ read the data from the pressure transducers every 0.1° of crank shaft rotation. The Z-channel pulse of the shaft encoder was used as a reference point to start the program. As each thermodynamic cycle consisted of two crank rotations, two trigger pulses were observed for each cycle. To ensure that the correct pulse was used as the starting point, a "*RESTART"* button was programmed allowing the program to be restarted until the desired starting point was used.

With the correct starting trigger captured, the number of cycles to be logged could be specified and the logging process started by pressing the "*LOG"* button. After the logging procedure was completed, the user was prompted to specify the file to which the data should be stored.

5.6.3. ECU programming software

Together with the ECU, Perfect Power provided its own software package called LetRippII that served as a platform to set up and monitor the ECU (Perfect Power, [S.a.]). For details on the ECU setup and programming, refer to section 4. The software had three major functions namely; ECU programming, real time data

display and data logging. An example of the interface used during testing can be found in Appendix D.1, Figure 82.

The LetRippII software was mainly used to program and set up the ECU. The software provided an easy to use graphical interface to set up and edit ECU maps and set points. With the software connected to the ECU, programming changes could be applied to the ECU while the engine was running, including switching between closed-loop and open-loop control. If required, the software provided a basic help function describing the function of general programming locations.

The software also enabled live data to be viewed while connected to the ECU. These display values could be any of the input, output or active map values and could be logged as well. The logging function featured in the software logged all the channels of the ECU and had a set structure. None of the ECU logs were used for calculations as all the required measurements were obtained by separate systems.

5.6.4. Lambda data acquisition software

The Ecotrons lambda scanner used to capture the lambda measurements was supplied with its own graphical user interface, ALM GUI. The software package had a variety of features including sensor calibration, real time data display, data logging and data playback. Diagnostic tools were also available to indicate faulty sensors.

The software package was used to log the lambda measurements as well as give real time lambda measurements of the individual cylinders. This helped to monitor lambda compared the ECU measurement and indicated any lambda measurement differences between the two cylinders. These measurements were also used to adjust the injection trim of the two cylinders, enabling the lambda measurement for both cylinders to be similar. An illustration of the interface used during testing can be found in Appendix D.1, Figure 83.

6. Test Experiments and Results

One of the main objectives of the project was to further develop the existing test facility to employ an EFI SI engine incorporating a fully controllable engine management system. This allowed control over spark ignition timing, fuel injection duration and closed-loop lambda parameters. Repeatability of the engine and dynamometer setup, in-cylinder pressure measurement as well as the engine's sensitivity to ignition and injection changes were examined.

For all the tests done in this project, 95 octane (RON) ULP was used, as supplied by commercial BP fuel stations. Unless otherwise stated, all test results presented were obtained under closed-loop control at lambda 1.

6.1. Overview

Sodré & Soares (2003) state that a correction factor has to be applied to the measured torque to compensate for ambient conditions other than that specified by the manufacturer. For all the tests done in this project, the SAE J1349 formula was used. This correction required the ambient temperature, atmospheric pressure and relative humidity of the test cell to be known (SAE, 2004). These values were either measured in the test cell or obtained from the local weather institute.

The combustion process was evaluated by analysing the in-cylinder pressure measurements obtained, using both an Optrand and Kistler transducer under various test conditions. It should be noted that in-cylinder pressure measurements are given in bar, to be consistent with curves from the literature.

This chapter gives a description of the tests that were conducted and the data obtained from these tests. All the instrumentation used for the project underwent calibration, before any testing was done. This was done to ensure accuracy of all the measurements. Additional information on the calibration procedure and equipment is given in Appendix A.

6.2. ECU Parameter Testing

Various tests were done to verify that the ECU was set up correctly and that the engine responded to changes in the ECU parameters. These tests include verifying the reference position of ignition timing, correct timing adjustment, the setup's response to spark ignition timing adjustment, the setup's response to fuel injection duration adjustments and the setup's closed-loop control stability. The results obtained from these tests are presented in this chapter and show that full control over the required parameters were achieved.

6.2.1. Ignition timing adjustment

To verify that the actual spark event corresponded to the value set in the ECU, the ignition event had to be captured and accurately phased. This was done by capturing the spark event together with the in-cylinder pressure, all using the National Instruments DAQ. The acquired data was then correctly phased, based on the in-cylinder pressure measurements. The spark event was captured using an inductive clamp and a regulating circuit (see appendix C) to ensure the voltage reading was in range of the acquisition equipment.

Figure 45 shows the results obtained from tests ran at 3600 rpm and 40 N·m. The first test was run with the ignition timing set to 30° before TDC while the second test was run with the ignition timing retarded by 4°. A 0.7-degree error was found between the ECU timing and the actual ignition event while the change in timing was exactly as set in the ECU.

The spark pickup only served as an indication of when the spark event occurred. As the inductive clamp picked up current flow through the ignition lead, the

measurements obtained from it gave an indication of when the spark was formed. The amplitude of the signal was not related to a characteristic of the spark event as all the properties of the inductive clamp were not known. Methods for measuring and characterising the ionisation current are available, but require specialized test equipment not available for this project (Byttner & Holmberg, 2008) (Byttner *et al*, 2001).

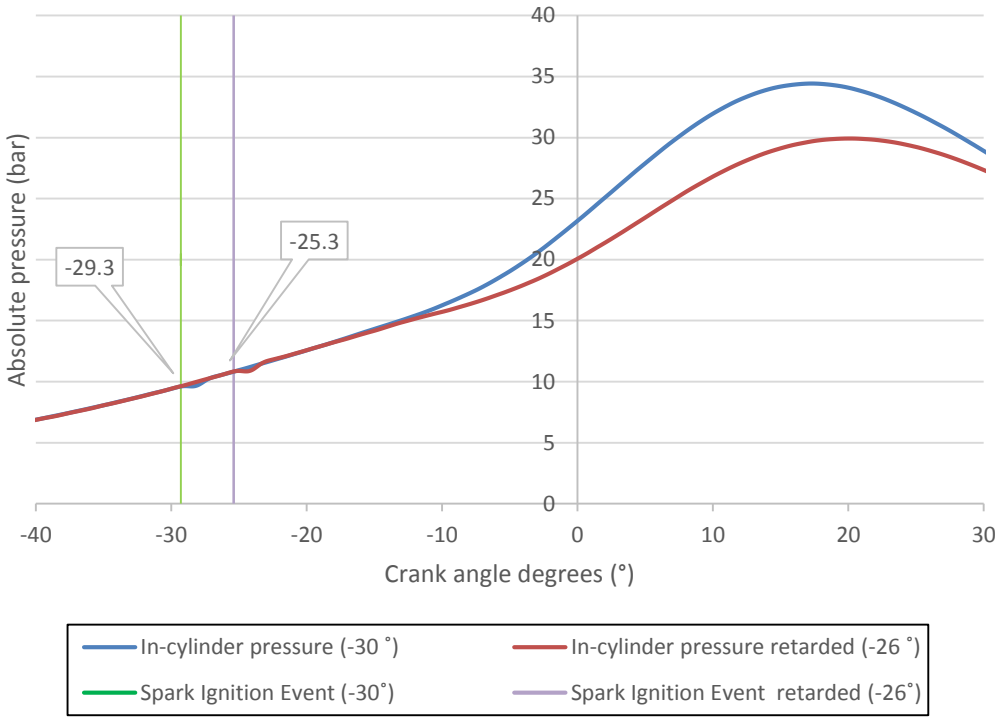

Figure 45: Spark ignition timing verification

6.2.2. Ignition timing sensitivity

To ensure that the test engine responded to changes in the ignition timing, timing swings were done at various partial load test points. These tests were done following the same methodology that had been used to determine MBT for the timing map sites, described in section 4.6. Figure 46 illustrates the results obtained from a timing swing test that was conducted at 3000 rpm and 3600 rpm with the throttle position fixed correlating to a high load condition (between 80% and 90% open). From these tests it was clear that the test engine responded well to changes in ignition timing throughout the operating range of the engine. These results were also used to develop the ignition timing map.

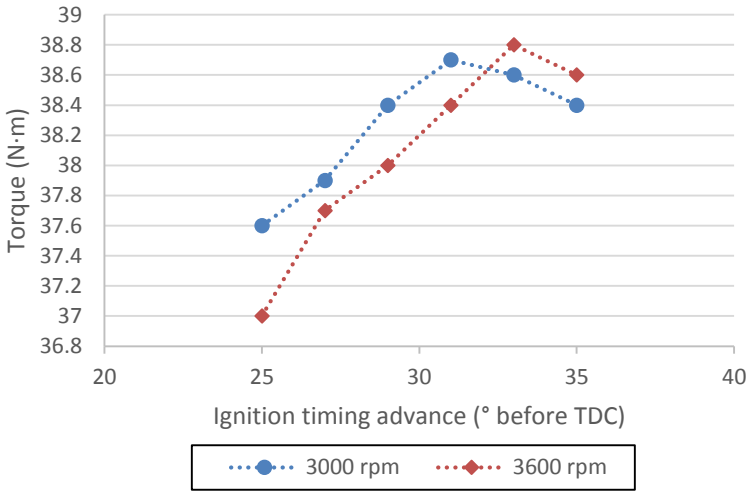

Figure 46: Ignition timing swing

6.2.3. Closed-loop control stability

Tests were done to verify that the engine management system was capable of maintaining a stable lambda under closed-loop conditions. These tests were done with ETA in torque control mode and the ECU set to control at lambda 1. The lambda values for each individual cylinder were captured using the ALM-II scanner together with the individual Bosch oxygen sensors. Figure 47 gives an illustration of the lambda data, obtained from the ALM-II lambda scanner for cylinder-1, for a test run at 3600 rpm and 40 N·m, with ignition timing at 30° CA before TDC.

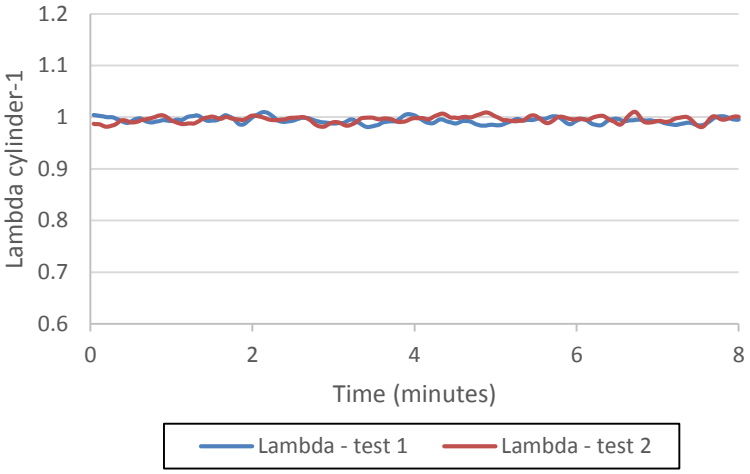

Figure 47: Closed-loop lambda control stability

These results verified that stable closed-loop control was achieved by the test setup.

6.2.4. Fuel adjustment sensitivity

To verify that the test engine responded to changes in fuel injection changes, fuel loop tests were done at various partial load test points. These tests were done with the control system in throttle control mode at a fixed throttle position. The lambda target was then adjusted and the change in engine torque and BSFC was documented. The results obtained from a test run at 3000 rpm and with a throttle position correlating to a high load condition (close to 90% open) is given in Figure 48. These results indicated good response to changes in lambda with maximum power being achieved at a lambda value of around 0.9 as mentioned in section 2.1.5 (Hiller & Coombes, 2004).

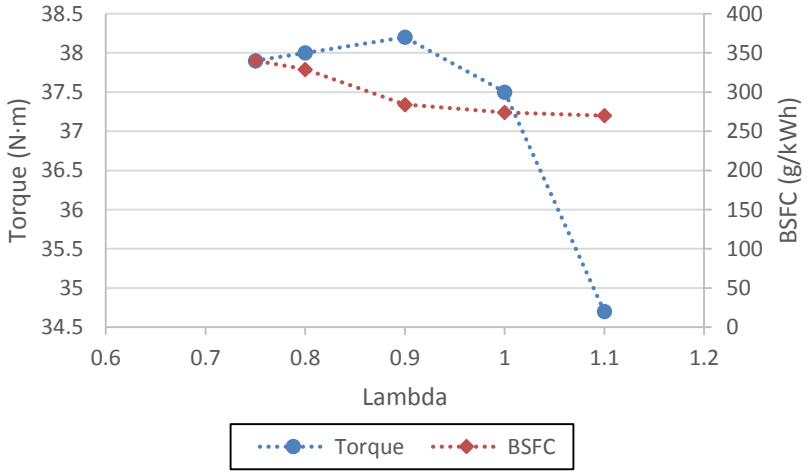

Figure 48: Fuel loop (3000 rpm)

6.3. Repeatability Testing

To establish whether the engine still performed similar to its OEM setup, full load tests were done and the results were compared to that from the manufacturer, as seen in Figure 49. The results obtained were promising and the slight variations were expected as a result of the modification to the intake manifold, changes in the ignition timing and fuel injection. This verified that, after the application of the engine management system, the engine still produced similar results to its OEM setup.

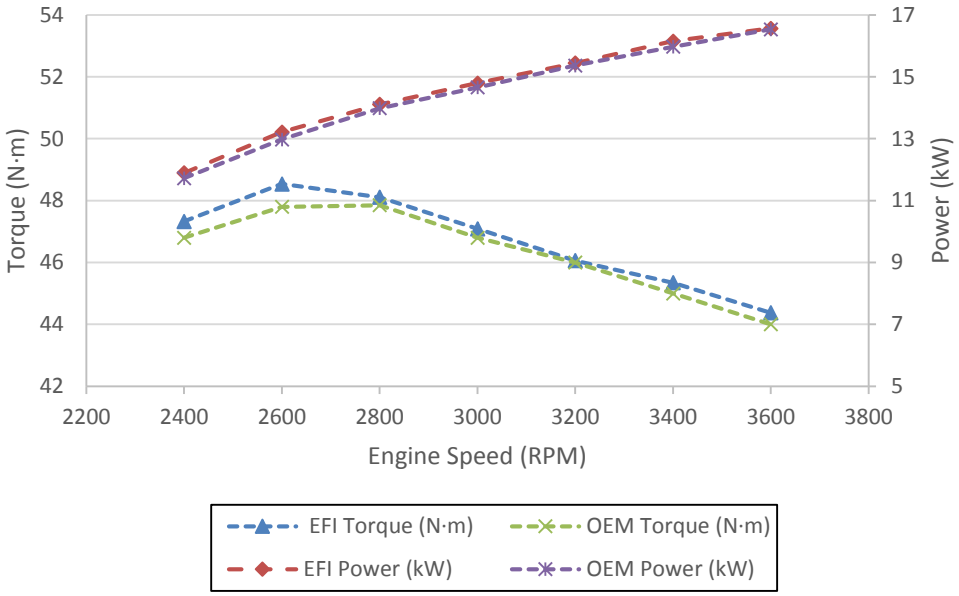

Figure 49: Engine performance curve

By verifying the performance curve of the engine, partial load test points could be selected within the engine operating range. These test points ranged from 2400 rpm to 3600 rpm and from 5 N·m to 40 N·m, as shown in Figure 50. Steady-state tests were done at all partial load test points to provide verification of the test setup's repeatability over the operating range of the engine.

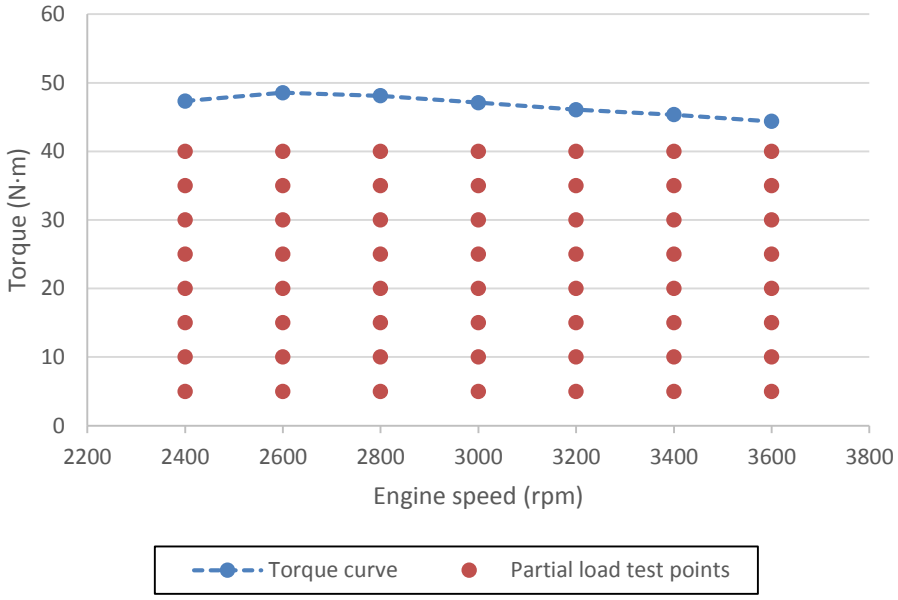

Figure 50: Partial load test points

These steady-state test points were used to program automated test sequences in ETA. Each test point was programmed to run for 8 minutes. These 8 minutes consisted of three stages:

- A 30 second ramp up stage, where the program adjusts the control parameters to run the setup at the given state.
- A 2 minute 30 second steady state stage, that allowed the test setup to achieve steady state stability at the given test point.
- And a 5 minute data logging stage, where the selected channels were logged simultaneously, in 5 second intervals.

This configuration achieved good steady-state results for all the logged test parameters.

The data illustrated and used for analysis only represents the mean value of the data acquired during the logging stage. Figure 51 gives an example of a box-and-whisker diagram for the measured torque at 3600 rpm and gives an indication of what the data represents. The whiskers indicate the data points that deviate most from the mean and the box sections indicate the 2nd and 3rd quartile of the captured data.

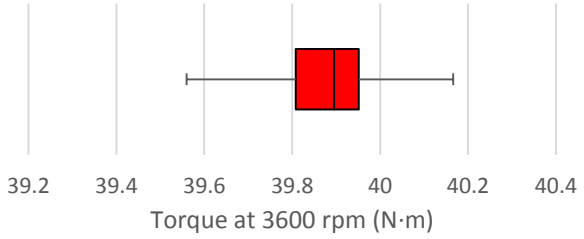

Figure 51: Measured data spread

Prior to the installation of the SI engine on the AC dynamometer test bench, no tests were done exceeding loads of 28 N·m. It was therefore necessary to verify that the test setup was capable of stable control over the operating range of the SI engine. To ensure that the test setup ran steady at the required control points, the dynamometer measurements over the test period were investigated. Figure 52 illustrates the stability of the dynamometer load control as tested at 2400 rpm at 20 N·m and 3600 rpm at 40 N·m, using the torque control mode. This indicated that good load control stability for the test setup was achieved using the torque control function described in section 5.5.2.

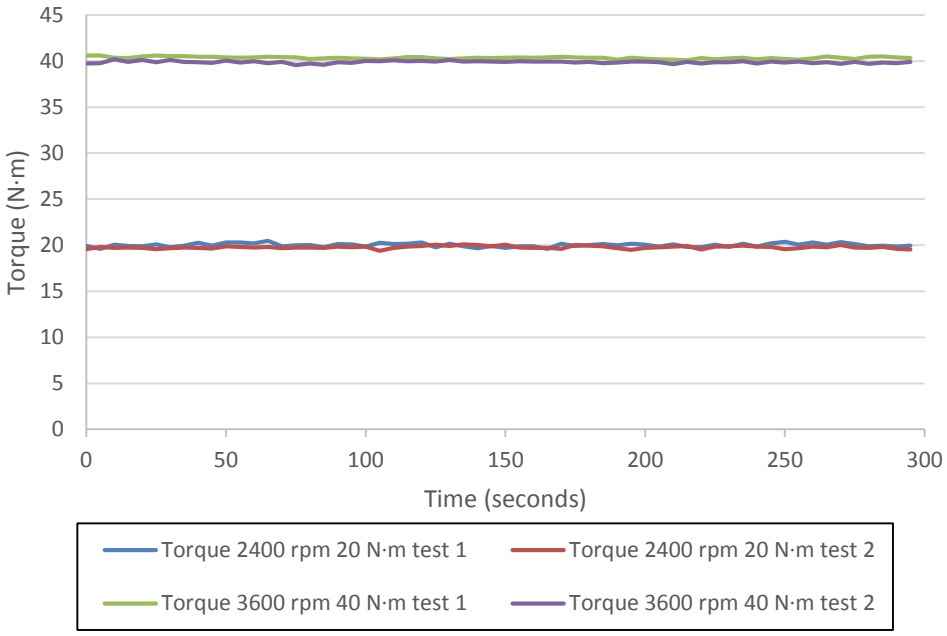

Figure 52: Dynamometer stability

6.3.1. Engine and dynamometer

To establish repeatability of the test setup the BSFC, exhaust gas temperature (EGT) and lambda measurements were evaluated for the test points indicated in Figure 50. These tests were all done in torque control mode under closed-loop control of lambda 1 (apart from the lambda response tests). The repeatability curves for 2400 rpm and 3600 rpm are shown in Figure 54 to Figure 56. Repeatability curves for additional test can be found in Appendix E.

The BSFC obtained from these tests, as seen in Figure 53 and Figure 54, indicated that good repeatability was achieved and it closely matched the values stated by Ferguson & Kirkpatrick (2001).

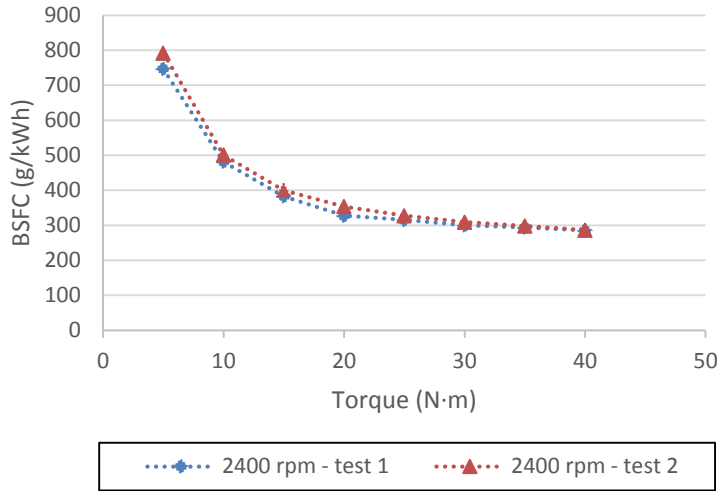

Figure 53: BSFC repeatability (2400 rpm)

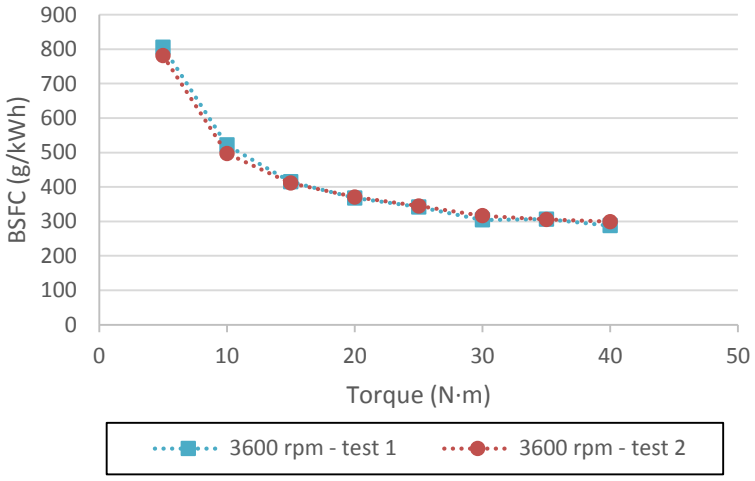

Figure 54: BSFC repeatability (3600 rpm)

It was observed that, for the tests run at 3600 rpm, the EGT did not follow the expected increasing trend as engine load increases. To ensure that these results were accurate, new thermocouples were calibrated and used to run additional tests and produced similar results. According to Heywood (1988), EGT is a maximum at lambda 1 and decreases as the fuel mixture enrichens. He also illustrates that EGT is influenced by ignition timing. As the tests were controlled at lambda 1 and with ignition timing retarded 2° from timing for MBT, it was suspected that the obtained EGT trend was a result of the engine's heat transfer characteristics.

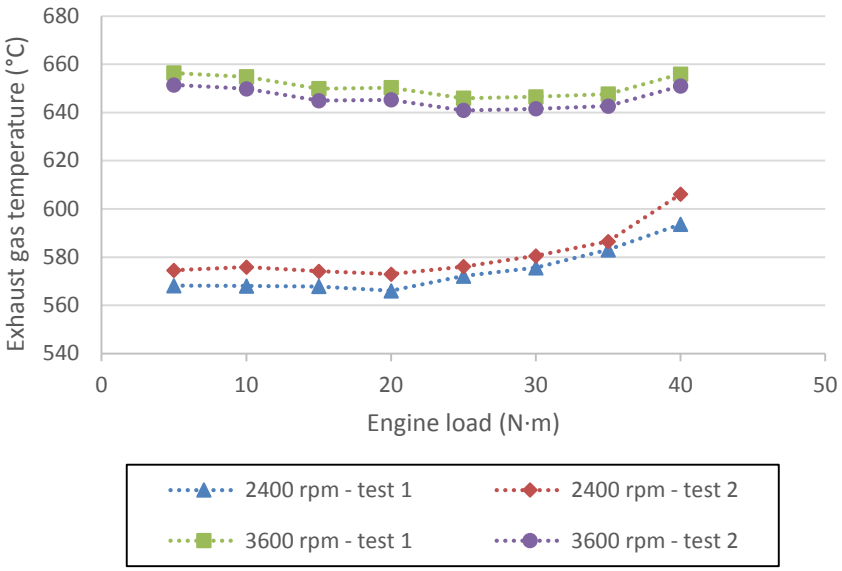

Figure 55: Exhaust gas temperature repeatability

To verify the response of the ECU's closed-loop control, the lambda targets were set to adjust from lambda 1 to lambda 0.95 as load increased from 5 N·m to 40 N·m. These tests were not done at lambda 1, as it was desired to illustrate the lambda response to changes in the lambda set-point. Figure 56 shows that repeatable closed-loop lambda response and stability was achieved. These tests were done over a small lambda range to ensure the lambda measurements did not exceed the limits set in the ECU.

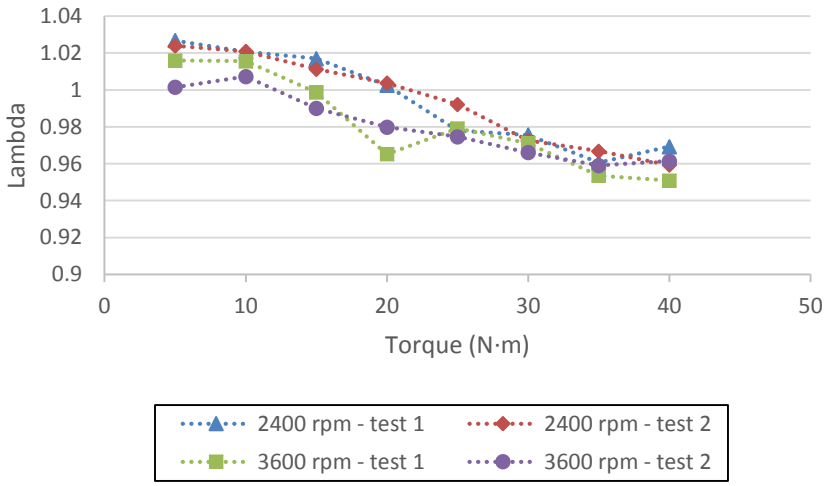

Figure 56: Lambda control repeatability

6.3.2. In-cylinder pressure

All the in-cylinder pressure values were measured as an absolute pressure and were measured from cylinder 1 using an Optrand transducer as well as a Kistler spark plug transducer. To help filter the noise picked up by the transducers, a large number of cycles were captured for each test and an average measurement was used to determine the pressure trace. 500 cycles were captured for each test which produced sufficiently smooth pressure curves without the need for additional filtering.

To enable the pressure curves to be plotted correctly, the corresponding hot motoring curves had to be phased and referenced as described in section 2.6.3. The motoring curves were obtained by running the engine at the required speed with the throttle fixed at the position corresponding to the load. The injectors were then shut off using the ECU, allowing the dynamometer to motor the engine at the set speed and throttle position. Figure 57 shows hot motoring curves for tests ran at 3600 rpm, and throttle positions relating to 20 N·m and 40 N·m operating positions. The results for the tests ran at 3000 rpm can be found in Appendix E.3. No combustion takes place during hot motoring tests resulting in no cycle-to-cycle variations. This led to identical hot-motoring pressure traces for separate tests.

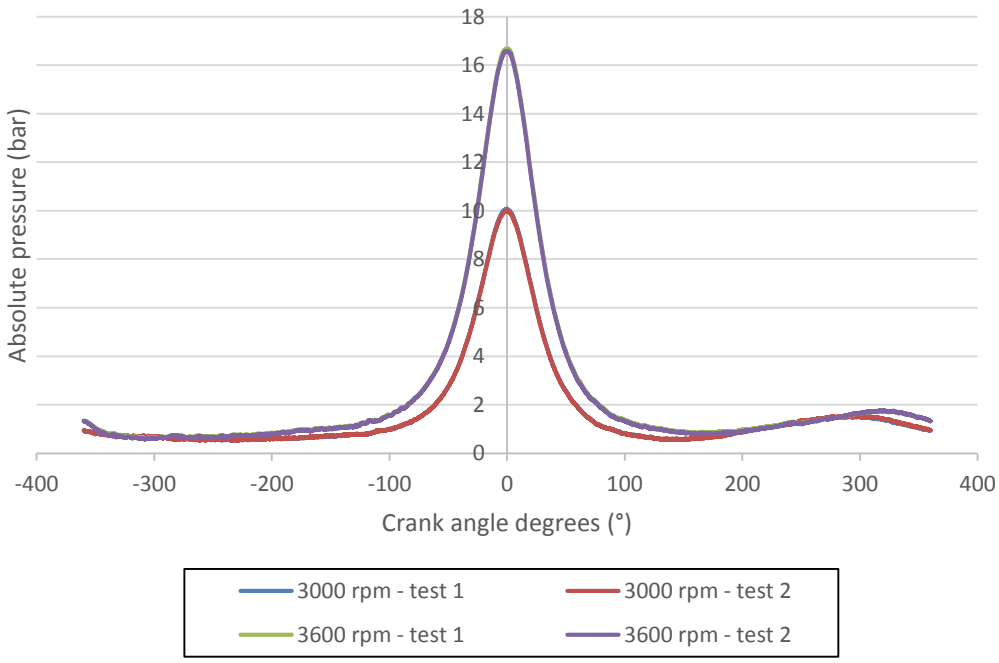

Figure 57: In-cylinder pressure vs. crank angle, hot motoring

Figure 57 shows the resulting log(P)-log(V) curve after phasing, for the 3600 rpm test with a throttle position related to 40 N·m. The reference pressure at BDC, before intake valve closing was pegged at an absolute pressure of 0.96 bar. This

curve had a polytropic exponent of 1.33 during compression and was consistent with values stated in Heywood (1988).

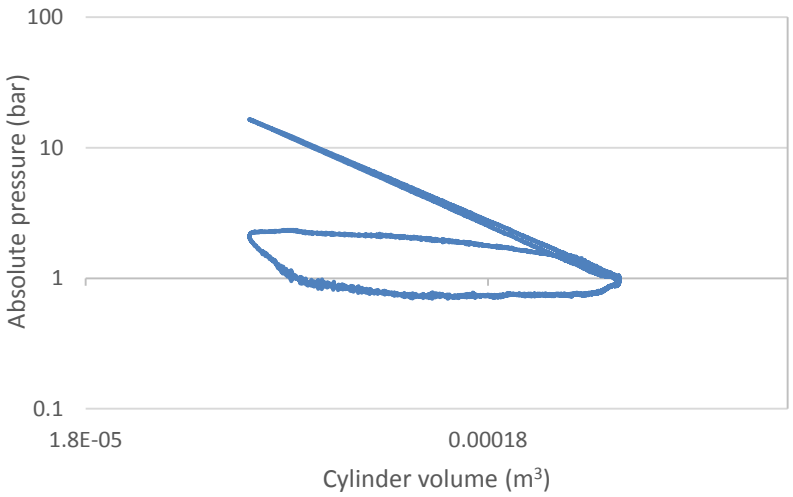

Figure 58: Hot motoring, log(P)-log(V), 3600 rpm WOT

To ensure the test setup operated adequately with the engine running, the cycle-to-cycle variations were investigated. The cycle variations were determined by identifying the peak cylinder pressure for each individual cycle and its corresponding crank angle. Figure 59 gives a graphical representation of the cycle variation based on the peak cylinder pressure for a test run at 3600 rpm and 40 N·m. Together with this method, the $IMEP_n$ for each individual cycle was calculated and the coefficient of variance (COV) was determined based on these $IMEP_n$ values, with the results given in Figure 60.

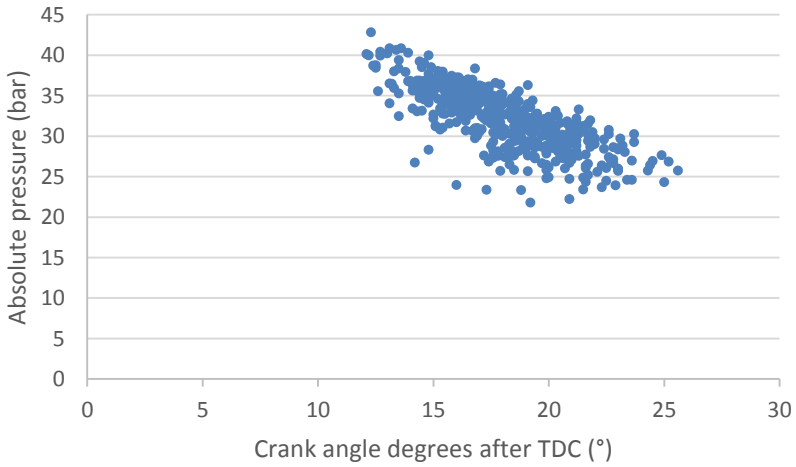

Figure 59: Cycle-to-cycle variation based on peak cylinder pressure

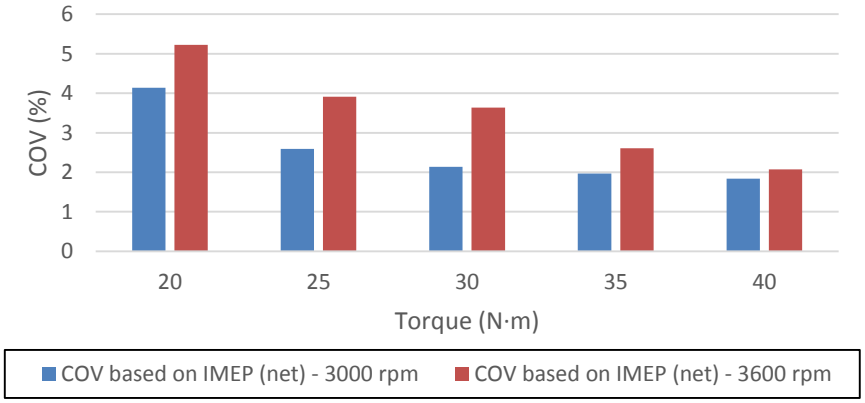

Figure 60: $IMEP_n$ coefficient of variance

Additional tests were run at partial load conditions and from analysing the cycle-to-cycle variations it was clear that the test engine operated at its best under higher loads at 3000 rpm and 3600 rpm. This was to be expected as the engine was originally designed as a generator operating at full load at 3000 rpm or 3600 rpm, depending on the electric frequency required (50 Hz or 60 Hz).

To ensure that accurate and repeatable results were obtained, in-cylinder pressure tests were done at 3000 rpm and 3600 rpm for 20 N·m and 40 N·m load conditions. As the engine experienced greater cycle-to-cycle variations at lower loads, partial load tests were run at 20 N·m as a compromise between lower load and repeatability. Figure 61 illustrates the pressure versus volume graphs for the test done at 3600 rpm. Results for the 3000 rpm test can be found in Appendix E.

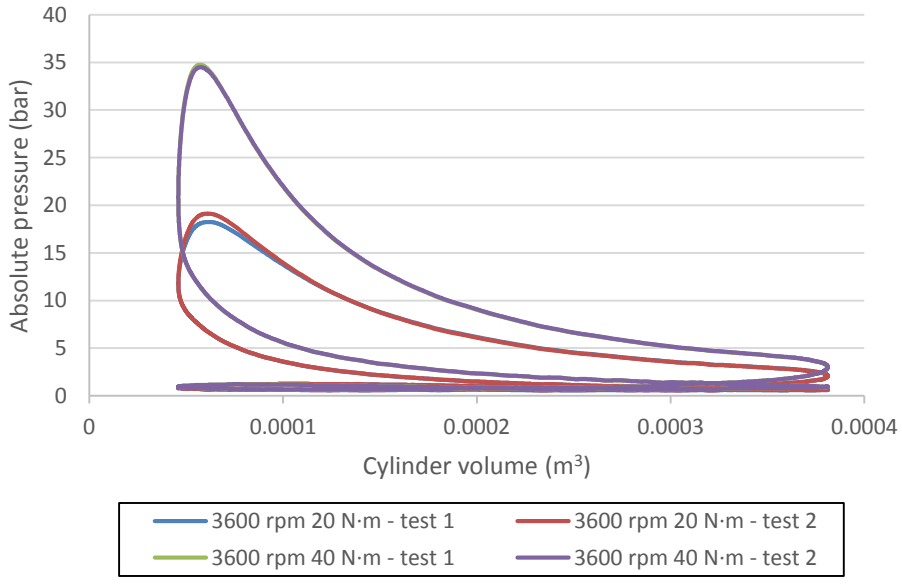

Figure 61: In-cylinder pressure vs. cylinder volume (3600 rpm)

To ensure the phasing and pegging of the fired pressure cycles were accurate, the log(P)-log(V) diagrams were compared to that of the motoring curves. Figure 62 shows the log(P)-log(V) diagram for 3000 rpm at 40 N·m, as this test point produced excellent repeatable results.

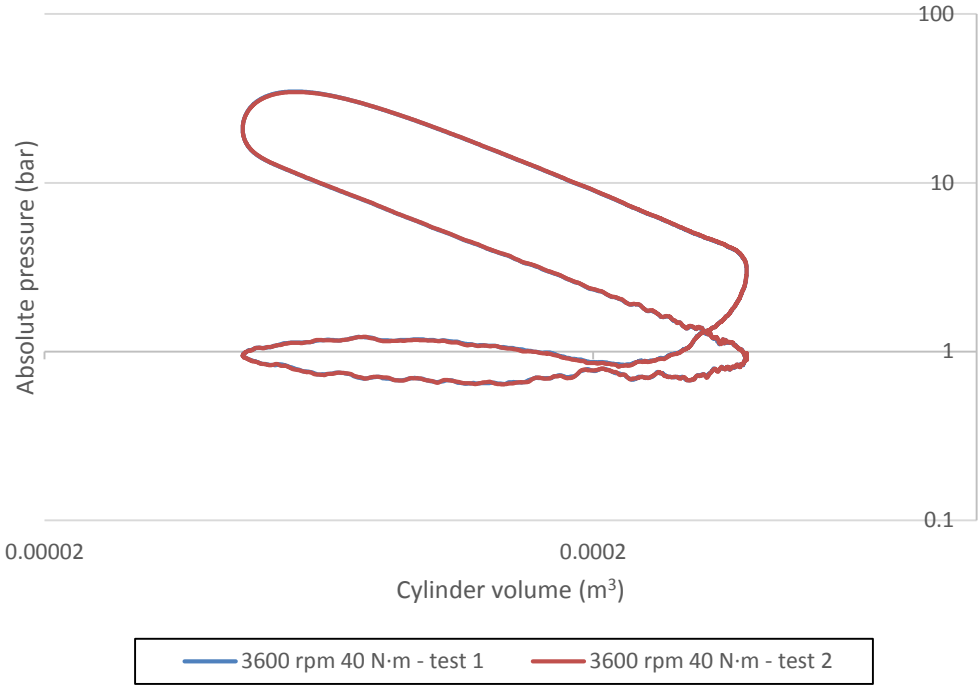

Figure 62: Log(P)-Log(V) (3000 rpm, 40 N·m)

6.3.3. Mean effective pressure analysis

To ensure the test data obtained from the steady state tests and the data obtained from the in-cylinder tests corresponded, the $IMEP_g$, $IMEP_n$, FMEP and BMEP were compared.

The BMEP and FMEP were calculated based on measurements obtained from the dynamometer and drive setup. The FMEP was calculated using results obtained from a Morse test as well as a motoring test. The motoring friction test results were used for further analysis as it produced slightly more stable measurement. The $IMEP_g$, PMEP and $IMEP_n$ were calculated based on the in-cylinder pressure measurements. The results from the tests run at 3000 rpm and 3600 rpm are given in Table 3 and Table 4.

Table 3: Mean effective pressure 3000 rpm (Optrand)

	20 N·m	25 N·m	30 N·m	35 N·m	40 N·m
BMEP (kPa)	374.9	468.6	562.3	656.1	749.8
FMEP (kPa)	170.5	166.8	166.8	163.1	159.3
$IMEP_g$ (kPa)	511.7	588.9	663.5	737.4	823.3
$IMEP_n$ (kPa)	462.5	546.0	626.5	702.2	791.6
PMEP (kPa)	49.2	42.9	37.1	35.2	31.6
BMEP + FMEP - $IMEP_g$ (kPa)	33.8	46.6	65.7	81.8	85.9
Error % ($IMEP_g$ vs. BMEP + FMEP)	6.20	7.33	9.01	9.98	9.45

Table 4: Mean effective pressure 3600 rpm (Optrand)

	20 N·m	25 N·m	30 N·m	35 N·m	40 N·m
BMEP (kPa)	374.9	468.7	562.4	656.1	749.9
FMEP (kPa)	221.2	215.6	211.8	208.1	202.5
$IMEP_g$ (kPa)	541.1	622.0	690.5	769.6	859.3
$IMEP_n$ (kPa)	492.8	581.0	649.7	727.2	817.5
PMEP (kPa)	48.3	41.0	40.8	42.4	41.8
BMEP + FMEP - $IMEP_g$ (kPa)	55.0	62.3	83.7	94.6	93.0
Error % ($IMEP_g$ vs. BMEP + FMEP)	9.23	9.10	10.81	10.94	9.77

To verify these results, similar tests were done using a different Optrand transducer together with a Kistler spark plug transducer. These transducers were calibrated following the same methodology as described in Appendix A. The Kistler transducers also made use of a Kistler charge amplifier that was set up using the manufacturers specification. The new Optrand transducer produced similar results while the Kistler results varied slightly as can be seen in Figure 63. The curve obtained from the Kistler transducer had a polytropic exponent of 1.301 for the compression stroke and 1.282 for the expansion stroke, consistent with values stated in Heywood (1988).

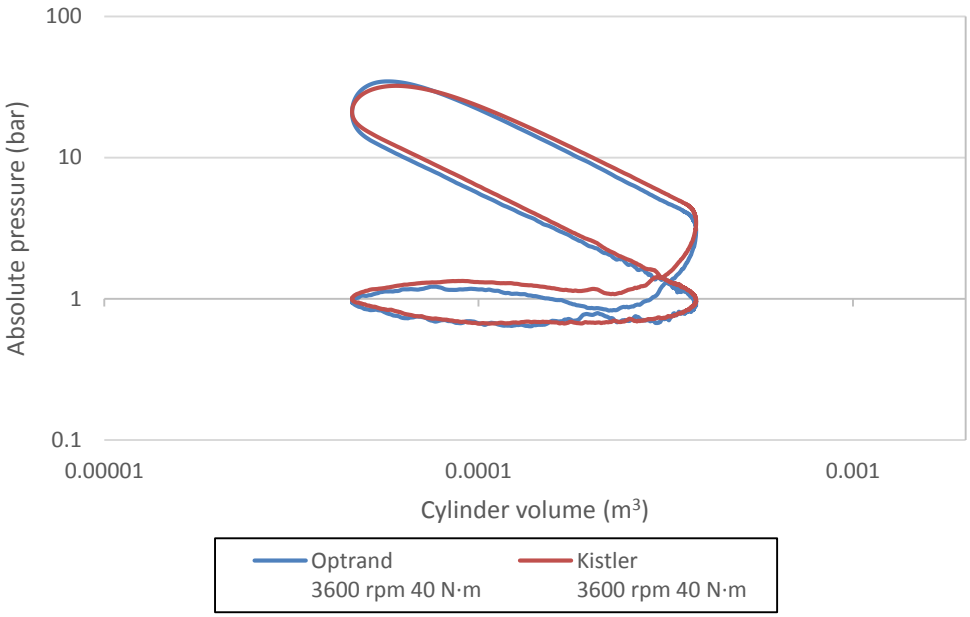

Figure 63: Log(P)-Log(V) Optrand vs Kistler

The slight difference on the pressure trace resulted in a smaller error when comparing the mean effective pressures. Table 5 shows the mean effective pressures calculated for tests at 40 N·m using the Kistler transducer. From these results it was found that the Kistler transducer produced a slightly higher $IMEP_g$ measurement resulting in a smaller error when compared to the BMEP and FMEP. A correlation of 5.3 % between the measured and calculated values was achieved using the Kistler transducer. All in-cylinder pressure measurements used for further calculations were taken using the Kistler transducer. This was as a result of the high errors obtained using the Optrand transducer.

Table 5: Mean effective pressures Kistler 40 N·m tests

	3000 rpm	3600 rpm
BMEP (kPa)	749.8	749.8
FMEP (kPa)	159.3	202.4
$IMEP_g$ (kPa)	860.6	898.9
$IMEP_n$ (kPa)	821.5	838.6
PMEP (kPa)	39.0	48.4
BMEP + FMEP - $IMEP_g$ (kPa)	48.5	52.4
Error % ($IMEP_g$ vs. BMEP + FMEP)	5.33	5.50

The difference between the Optrand and Kistler transducers were as a result of non-linearity, hysteresis and thermal shock errors. Wlodarczyk *et al.* found a 1 % error in the Optrand pressure measurement when compared to a Kistler water

cooled reference transducer. Similar results were found by Kenny (2013) when comparing the Optrand and Kistler transducer as shown in Appendix E.3, Figure 104.

6.4. Heat Release and Mass Fraction Burned

Heat release rate and mass fraction burned curves were used to analyse the combustion process of the test engine. A zero-dimensional, single-zone model, using the heat transfer coefficient proposed by Woschni (1967) was used to model the engine's heat release (refer to section 2.7.2).

The heat release rate results for tests run at 3600 rpm using the Kistler transducer are shown in Figure 64. From these graphs the change in rate of heat release with change in engine load is clearly visible, showing an increase in rate of heat release with an increase in engine torque.

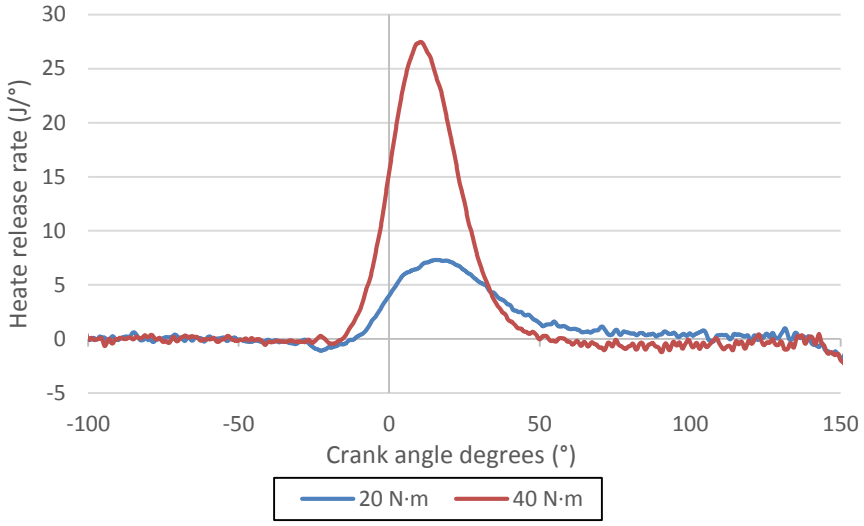

Figure 64: Heat release rate (3600 rpm)

With the heat release rates known, it was possible to calculate the mass fraction burned curves. Figure 65 shows the calculated mass fraction burned curve and its accompanying Vibe function as described in section 2.7.4. The mass fraction burned curves are plotted against degrees after ignition to allow comparison against graphs from the literature. The Vibe coefficients used are given in Table 6. The crank angle after ignition corresponding to 10 %, 50 % and 90 % burned for various tests are given in Table 7.

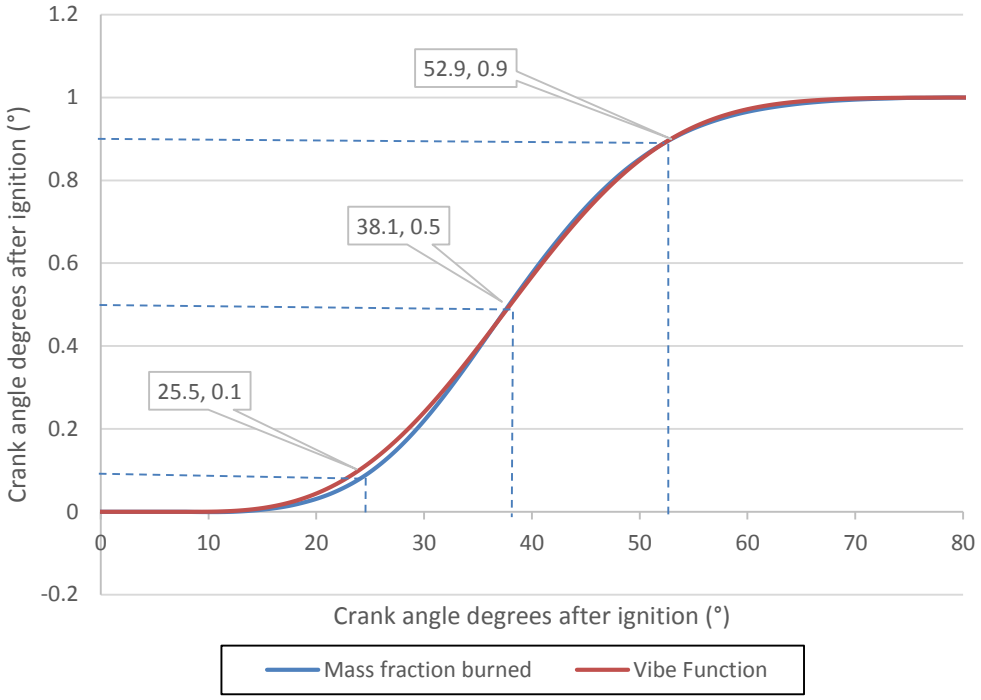

Figure 65: Mass fraction burned (3600 rpm, 40 N·m)

Table 6: Vibe coefficients (3600 rpm, 40 N·m)

Vibe function coefficients	
Constant *m*	1.98
Constant *a*	8.65
combustion start (°)	11.0
combustion duration (°)	70

Table 7: Mass fraction burned angles

	Crank angle after ignition start (°)			
Mass fraction burned	3600 rpm 40 N·m	3600 rpm 20 N·m	3000 rpm 40 N·m	3000 rpm 20 N·m
10 %	25.5	29.6	28.1	35.2
50 %	38.1	42.8	41.5	48.9
90 %	52.9	60.1	53.4	60.5

The mass fraction burned and Vibe curves are the end result of a long sequence of calculations and would therefore contain the cumulative effect of any errors in measurement, calculation or assumptions. Figure 66 and Figure 67 shows a close correlation between the calculated values and that found in the literature, giving a

good indication that there are no significant errors in the measured values or calculations.

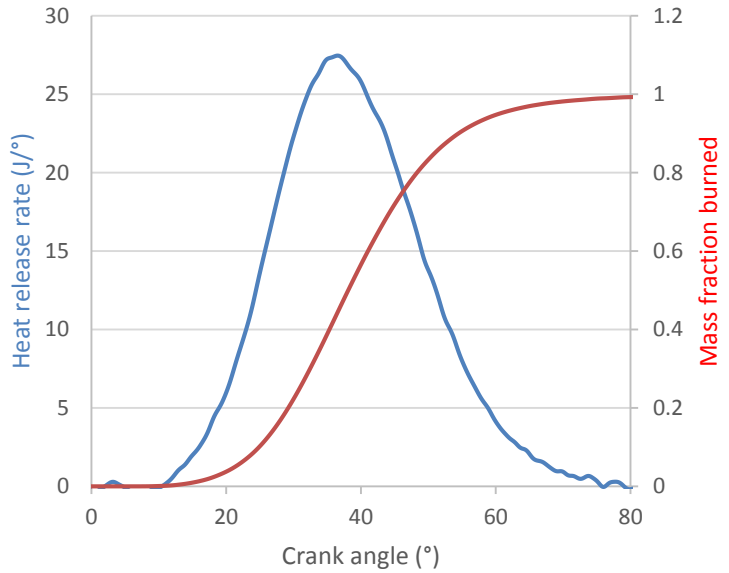

Figure 66: Heat release rate and mass fraction burned profile (3600 rpm, 40 N·m)

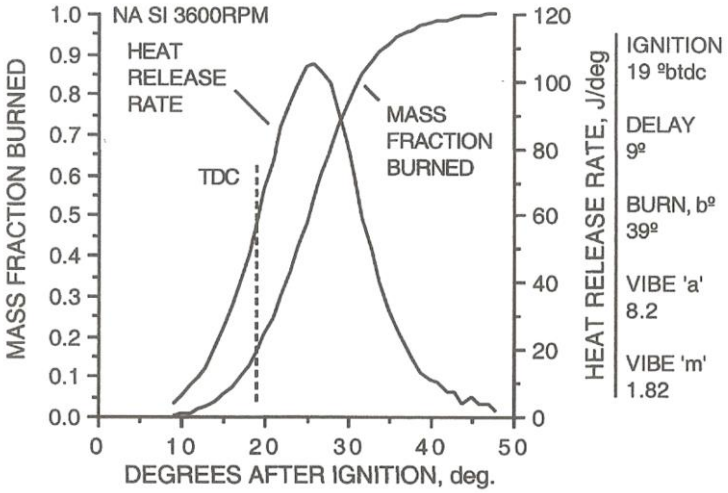

Figure 67: Comparable heat release profile and vibe coefficients (Blair, 1999)

7. Conclusions and Recommendations

During this project, a small capacity SI engine was equipped with an engine management system and was integrated with the test facility's existing small engine test bench. This expanded the Stellenbosch University Engine Test Facility's test capability by enabling full control over engine parameters such as ignition timing, fuel injection duration and mixture concentration.

The engine management system consisted of a Perfect Power XMS5/B ECU, Perfect Power LetRipp software package, 128g/min fuel injectors, a single cable-operated throttle body and the required sensors. This applied engine management system allowed control over ignition timing, fuel injection duration and enabled closed-loop lambda control. In addition, the engine was also equipped with a lambda scanner and separate lambda sensors allowing the mixture concentration of the individual cylinders to be measured.

The ECU was configured and the fuel injection and ignition timing maps were programmed to enable control of the engine over its full operating range. Repeatability tests were done to verify that steady operation of the engine has been achieved over the engine's operating range. The ignition timing was verified using an inductive clamp, regulating circuit, an optical shaft encoder and a high speed DAQ device. Ignition timing swing and fuel loop tests were conducted which confirmed that the engine responded to parameter changes made by the management system.

To investigate the combustion process under different operating conditions, further development on the existing in-cylinder indicating setup was done. This setup included a fibre optic pressure transducer, a spark plug mounted piezoelectric pressure transducer, an optical shaft encoder and a high speed DAQ device. The setup was able to produce repeatable results while measuring in-cylinder pressures at intervals of 0.1° crank shaft rotation.

The indicating tests allowed the cycle-to-cycle variations of the test engine to be determined based on peak in-cylinder pressures or by calculating the IMEP for each cycle. Comparisons of the measured IMEP values to that of calculated theoretical values indicated good accuracy of the indicating setup. A correlation of 5.3 % between the measured and calculated IMEP was achieved using the spark plug mounted piezoelectric transducer. The fibre optic transducer produced similar results during low load tests, but experienced thermal shock at higher loads. This resulted in greater errors when comparing the measured $IMEP_g$, calculated from the engine indicating measurements, to the BMEP and FMEP calculated from the measurements obtained from the dynamometer.

Recommendations for future work are:

- Installation of a water-cooled piezoelectric transducer into the cylinder head of the engine for engine indicating testing. This will enable more accurate IMEP measurements to be recorded as these sensors are less prone to thermal effects.
- Installation of highly accurate emission equipment to enable emission testing.
- Adapt the engine camshaft to enable the use of a camshaft sensor. This will allow the ECU to distinguish between the different engine cycles, and a wasted spark configuration will no longer be required.
- Upgrade to a more sophisticated ECU capable of controlling additional engine parameters. These parameters would include: fuel injection timing, adjustment between set points for TDC of individual cylinders (not only use one as a reference), multiple wide-band sensor inputs and the capability to implement knock sensors. An ECU capable of implementing a flex fuel sensor would be beneficial as it will greatly simplify biofuel testing. Various ECU models are able to use controller area network (CAN bus) modules and connections that greatly simplify sensor and actuator setup.
- Implementation of an engine knock pickup system in the LabView program using the in-cylinder pressure transducer and high-speed the DAQ device.
- Replace the faulty fuel injector (injector for cylinder 1) with the newly acquired injector. Injection tests similar to the tests done in section 3.2.1 should be done to verify that the new injector is fully functional.

Appendix A: Sensor calibration

A.1. Thermocouples

All the thermocouples used during this project, were type K (nickel-chromium/nickel-alumen) thermocouples, because of their wide measuring range (-270 °C – 1260 °C). This ensured accurate measurement of the high EGT. Using the same type thermocouple throughout the setup simplifies fault finding, as the thermocouples could be easily interchanged to check functionality.

A Fluke 9142 calibration field metrology well was used to calibrate the thermocouples used for this project. Together with the fluke calibration well, a calibrated platinum resistance thermometer was used to ensure accuracy of calibration measurements. The Fluke calibration well had a temperature range of -25 °C to 150 °C, significantly lower than the maximum temperature required to calibrate type K thermocouples. The temperatures at which the thermocouples were calibrated, were 0 °C, 20 °C, 40 °C, 60 °C, 80 °C, 100 °C, 120 °C and 140 °C.

The process followed during calibration was as follows: The thermocouples and calibration thermometer were placed in the Fluke calibration well. The desired set point was selected on the Fluke calibration well and the unit controlled the temperature at the given set point. After the calibration well reached the selected set point, the thermocouples were left to stabilise for at least 10 minutes. The measured values were recorded in ETA, based on the measurement indicated by the reference probe. With the values recorded, the set point was increased and the process was repeated. After the 140 °C calibration was completed, the set point was briefly set to 150 °C and then set back to 140 °C. The calibration process was then repeated from 140 °C to 0 °C. This calibration procedure was repeated 3 times and the average values were used to set the calibration in ETA. Table 8 gives the average values of the three calibration cycles, together with the average value for the given sensors.

Table 8: Thermocouple calibration

	0 °C	20 °C	40 °C	60 °C	80 °C	100 °C	120 °C	140 °C
Exhaust 1	0.6	19.7	39.6	59.6	79.2	99.2	120.0	140.2
	0.8	20.0	40.3	60.0	79.8	100.2	120.1	141.1
	0.7	**19.8**	**39.9**	**59.8**	**79.5**	**99.7**	**120.0**	**140.6**
Exhaust 2	0.3	19.4	39.3	59.1	79.0	99.0	119.7	139.9
	0.5	19.8	39.9	59.8	79.5	99.9	120.0	140.7
	0.4	**19.6**	**39.6**	**59.4**	**79.2**	**99.4**	**119.8**	**140.3**
Oil	0.9	19.7	39.4	58.9	78.6	98.2	118.4	139.1
	0.6	19.8	39.4	58.7	78.6	98.5	118.9	139.0
	0.7	**19.7**	**39.4**	**58.8**	**78.6**	**98.3**	**118.6**	**139.0**
Intake air	1.3	20.0	39.5	58.7	78.5	98.1	118.1	138.2
	1.1	19.7	39.3	58.8	78.3	98.2	118.4	138.7
	1.2	**19.8**	**39.4**	**58.7**	**78.4**	**98.1**	**118.2**	**138.4**
Fuel ETA	0.7	19.5	39.0	58.5	78.0	97.7	118.0	138.6
	0.6	19.5	38.7	58.4	78.3	97.9	118.1	138.6
	0.7	**19.5**	**38.9**	**58.4**	**78.1**	**97.8**	**118.0**	**138.6**
Ambient	0.9	19.8	39.0	58.5	78.2	98.0	118.0	138.6
	0.4	19.5	38.7	58.2	78.2	98.0	118.3	138.5
	0.7	**19.6**	**38.8**	**58.4**	**78.2**	**98.0**	**118.1**	**138.5**
Water in	1.2	20.0	39.6	59.3	78.8	98.8	118.9	139.3
	0.8	20.0	39.3	58.8	79.0	98.8	118.9	139.7
	1.0	**20.0**	**39.4**	**59.0**	**78.9**	**98.8**	**118.9**	**139.5**

Additional calibration was needed for the two EGT thermocouples as they measured temperatures exceeding 140 °C. For the high temperature calibration, a Fluke 9150 portable heat furnace was used, and was capable of controlling temperatures ranging from 150 °C to 1200 °C.

The Fluke 9150 used a ceramic core with poor thermal efficiency, resulting in very slow response times. As a result of this slow response time the calibration was only done once while increasing the temperature and once while decreasing the temperature. The following temperature set points were used during calibration: 150 °C, 200 °C, 300 °C, 400 °C, 500 °C, 600 °C, 700 °C, 800 °C, 900 °C and 1000 °C. The temperature was controlled at each set point for at least 45 minutes to ensure the ceramic core and thermocouples settled at the desired temperature.

The platinum resistance thermometer was only used up to 300 °C, as that was the maximum temperature at which it was calibrated. For the higher temperature set points, the measurement value from the Fluke 9150 furnace was used as a reference. This gave consistent results compared to the calibrated thermometer at the lower temperatures. Table 9 shows the calibration data obtained from the high temperature calibration.

Table 9: Thermocouple calibration (high temperature)

		150 °C	200 °C	300 °C	400 °C	500 °C
Exhaust 1	Up	151.9	202.0	300.5	399.2	497.5
	Down	151.9	202.0	303.0	401.1	498.2
	Average	**151.9**	**202.0**	**301.7**	**400.1**	**497.8**
Exhaust 2	Up	152.3	203.1	301.5	399.9	498.0
	Down	152.3	203.1	301.5	399.4	497.8
	Average	**152.3**	**203.1**	**301.5**	**399.6**	**497.9**
		600 °C	700 °C	800 °C	900 °C	1000 °C
Exhaust 1	Up	596.0	695.5	792.1	888.0	983.2
	Down	596.9	697.5	788.0	891.0	983.0
	Average	**596.4**	**696.5**	**790.1**	**892.0**	**983.1**
Exhaust 2	Up	596.5	695.0	791.5	888.5	984.0
	Down	596.4	697.8	788.5	890.1	982.8
	Average	**596.4**	**696.4**	**790.0**	**889.3**	**983.4**

A.2. Pressure Transducers

The pressure transducers used in this project included the following: in-cylinder pressure (Optrand, 0-206 bar and Kistler), oil pressure (Wika, 0-10 bar), fuel pressure (Wika, 0-6 bar) and intake manifold pressure (Wika, -1-3 bar).

The in-cylinder pressure transducer and the intake manifold pressure transducers were connected to a National Instruments high speed DAQ device. This required the sensors to be calibrated using the raw voltages that the sensors sent as inputs

to the DAQ device for the given pressures. The developed LabView program was used to view the sensor voltages as seen by the NI DAQ device, for the calibration pressures.

The oil pressure and fuel pressure transducers were directly connected to the PLC. ETA's in-program calibration function was used to calibrate these two sensors based on the values received from the sensors via the PLC.

For all the calibration above atmospheric pressure a 0-60 bar a Mensor CPB300 deadweight tester (Figure 68) was used. For the calibration below atmospheric pressure a Si Pressure Instruments vacuum pump and calibrated vacuum gauge (Figure 69) were used.

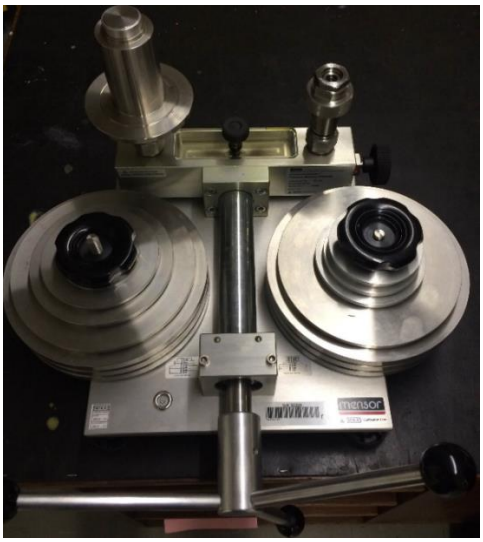

Figure 68: Mensor CPB300 deadweight tester

Figure 69: Si Pressure Instruments vacuum pump

For the calibrations done using the deadweight tester a known force was applied to a small area. This resulted in a pressure being applied to the transducer. To

ensure accuracy, all the components of the deadweight tester were weighed and measured as shown in Table 10.

Table 10: Deadweight tester calibration weights

Type of Mass	True Mass [kg]	Nominal Pressure [bar]
Piston	0.102	0.200
Bell	0.816	1.599
Plate	0.051	0.100
WP 3	4.079	7.993
WP 4	4.079	7.993
WP 5	4.079	7.993
WP 6	4.079	7.993
WP 7	4.079	7.993
WP 8	4.079	7.993
WP 9	2.040	3.996
WP 10	2.040	3.996
WP 11	1.020	1.998
WP 12	0.510	0.999
WP 13	0.204	0.400
WP 14	0.102	0.200
WP 15	0.051	0.100

The true ambient pressure, air density, air temperature and gravitational force in the test cells were taken into account and relevant correction factors were calculated. The results can be seen in Table 11 and were used to calculate the pressure values set in ETA.

Table 11: Pressure calibration constants

Gravitational Force (Standard) [m/s^2]	9.80665
Reference Temperature [°C]	20
Temperature correction	0.000022
Air Density [kg/m^3]	1.2
Weight Density [kg/m^3]	7900
Area [m^2]	0.00004999391
g (Application Site) [m/s^2]	9.796
Ambient Temperature [degrees C]	12
Density Correction Factor	0.999848
Temperature Correction Factor	1.000176

A.2.1. In-cylinder pressure transducer

For the in-cylinder pressure transducer calibration, nine measurements were taken ranging from zero bar to just below 58 bar. The pressure was incrementally increased and thereafter decreased, while acquiring the calibration data. This process was repeated three times to ensure repeatability. The average values were used to determine the transducer sensitivity and zero offset, and were used to construct the calibration curve to determine the sensor's linearity. The calibration measurements and results are shown in Table 12 and Table 13 and the calibration curve is shown in Figure 70.

The sensitivity and zero offset values were used in the LabView program to capture the in-cylinder pressure trace. From the calibration curve R^2 was calculated to be 1, which indicated a perfectly linear curve.

Table 12: In-cylinder pressure transducer calibration data (Optrand)

True Pressure [bar]	Voltage [V] UP 1	Voltage [V] DOWN 1	Voltage [V] UP 2	Voltage [V] DOWN 2	Voltage [V] UP 3	Voltage [V] DOWN 3	Voltage Average [V]
0	0.60	0.61	0.60	0.60	0.60	0.61	0.60
9.79	0.75	0.75	0.75	0.75	0.75	0.75	0.75
17.78	0.87	0.87	0.87	0.87	0.87	0.87	0.87
25.77	0.99	0.99	0.99	0.99	0.99	0.99	0.99
33.76	1.11	1.12	1.11	1.11	1.11	1.11	1.11
41.75	1.23	1.23	1.23	1.23	1.23	1.23	1.23
49.75	1.35	1.35	1.35	1.35	1.35	1.35	1.35
53.74	1.41	1.41	1.41	1.41	1.41	1.41	1.41
57.74	1.47	1.47	1.47	1.47	1.47	1.47	1.47

Table 13: In-cylinder pressure transducer calibration results

Sensitivity [mV/bar]	15.02
Sensitivity [mV/psi]	1.03
Zero offset [mV]	604.43

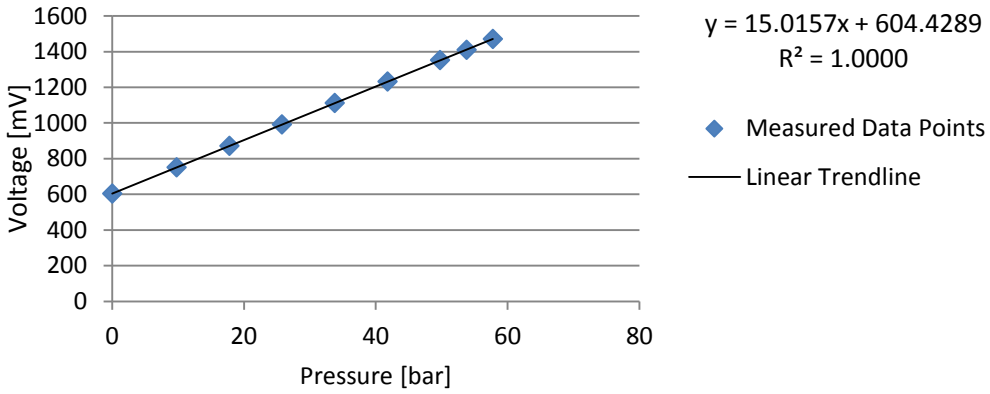

Figure 70: In-cylinder pressure transducer calibration curve

A.2.2. Intake manifold pressure transducer

The intake manifold pressure transducer was calibrated both below and above atmospheric pressure using the Si instruments vacuum pump. The pressure pump can pull a vacuum as well as apply a positive pressure depending on the bypass valve orientation. As the manifold pressure is unlikely to be above atmospheric pressure, most of the calibration points were taken under vacuum conditions. Atmospheric pressure was calibrated after a vacuum was pulled and also after a positive pressure was applied. The calibration was done three times while increasing the pressure as well as decreasing the pressure, and the average of the results were used to calibrate the sensor and plot the calibration curve. Figure 71 shows the calibration curve obtained from these calibration tests.

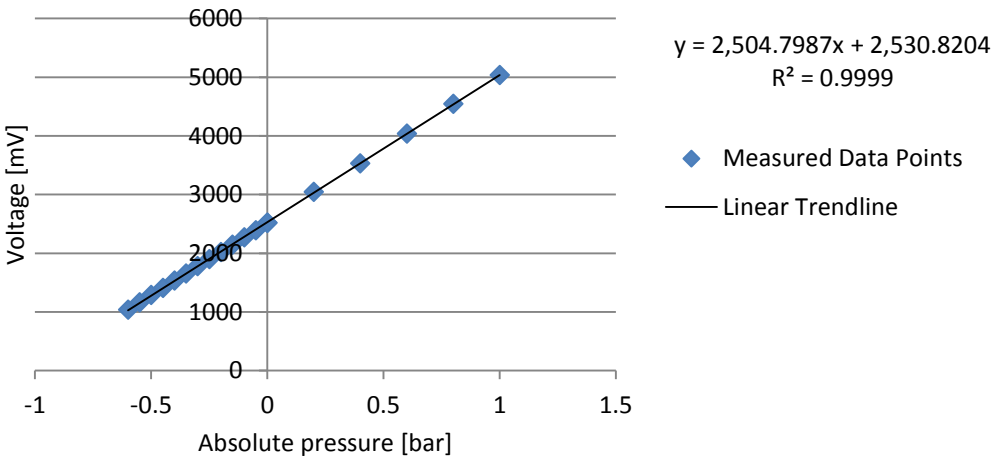

Figure 71: Intake manifold pressure calibration curve

Table 14 shows the calibration results for the intake manifold pressure transducer.

Table 14: Intake manifold pressure transducer calibration results

Sensitivity [mV/bar]	2 504
Zero offset [mV]	2 530

A.2.3. Oil pressure and fuel pressure transducers

These transducers were calibrated using ETA's internal calibration function. The calibration function in ETA used the sensor values received from the PLC and from it derived a calibration curve. Both sensors were calibrated by increasing and then decreasing the applied values in intervals. This process was repeated three times to ensure that accurate calibrations were made

A.3. Load Cell

During calibration of the load cell, two calibration arms were attached to the dynamometer, one with a weight tray (0.459m from the dynamometer centre) and the other with a counterweight to offset the weight tray. The load cell's range far exceeded the required range, as the test engine had a maximum torque of 45 N·m (Manufacturer claimed torque before EFI conversion).

The load cell was calibrated within the operating conditions of the test engine (0-36 N·m, 9 calibration points). This calibration process made use of ETA's calibration function and a sample of the results is shown in Table 15 and

Figure 72. The calibration process was done before testing (cold engine) and also after the engine had been warmed up.

Table 15: Load cell calibration operating range

	UP	UP	DOWN	DOWN
Torque [N·m]	Voltage [V]	AMP Torque [N·m]	Voltage [V]	AMP Torque [N·m]
0	0.01	0.00	0.04	0.26
4.496	0.61	4.22	0.65	4.48
8.992	1.26	8.74	1.30	9.03
13.489	1.91	13.29	1.96	13.61
17.985	2.56	17.84	2.60	18.15
22.481	3.21	22.41	3.25	22.67
26.978	3.87	27.01	3.90	27.21
31.483	4.53	31.61	4.55	31.75
36.038	5.19	36.28	5.19	36.28

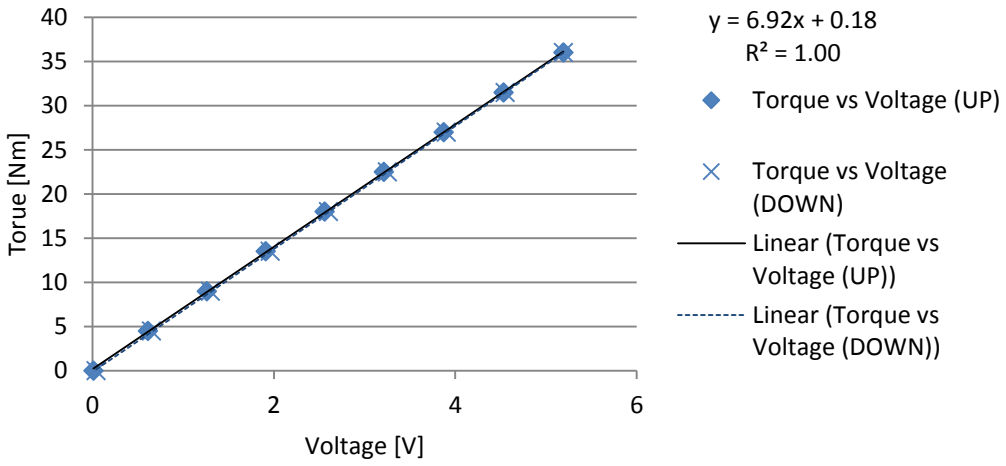

Figure 72: Load cell calibration operating range

A.4. ETA Speed Set-point

The drive which controls the AC dynamometer was equipped with a shaft encoder used to measure the dynamometer speed and thereby the engine speed. The shaft encoder was checked and calibrated upon installation by Rockwell Automation, as the speed input was required for the dynamometer PID control. ETA then used a voltage received from the drive which represented the engine speed. The speed value, as seen by ETA, was calibrated by motoring the engine (spark plugs removed) at a set speed point. These values were also checked by using a tachometer and a marker on the dynamometer shaft. A sample of the results is shown in Figure 73:

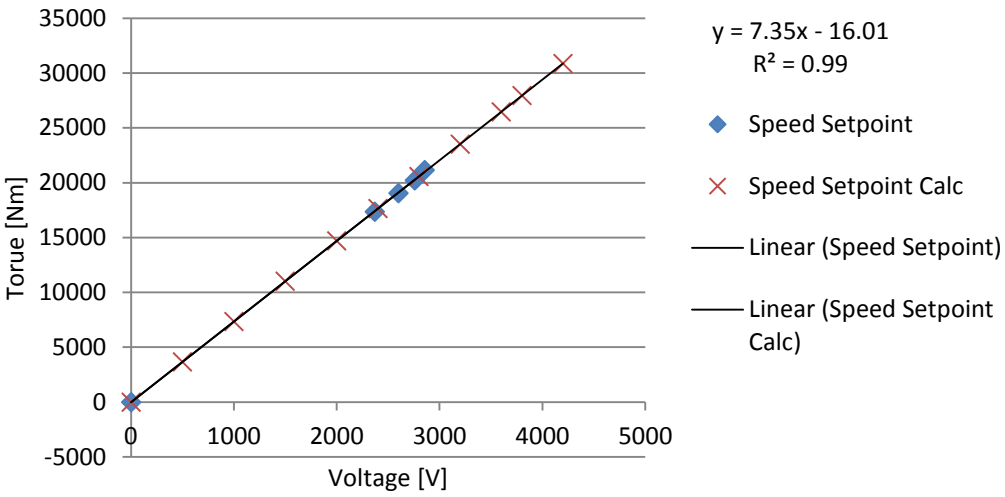

Figure 73: ETA speed set-point calibration

Appendix B: Calculations and Derivations

The procedure followed to derive the zero-dimensional, single-zone heat release model along is given in this appendix.

B.1. Derivation of a Heat Release Model

Klein (2004) states that the combustion process can be modelled purely as a heat addition process. By employing the first law of thermodynamics the heat release can be written as:

$$dQ = dU + dW + dQ_w \tag{B.1}$$

Where *U* represents the sensible internal energy of the charge and *W* represents the boundary work done. The heat conduction through the cylinder walls are also taken into account and is represented by the dQ_w term in equation B.1. This energy balance equation is then expanded as follows:

Set,

$$U = mc_vT \tag{B.2}$$

Taking the derivative of equation B.2 yields:

$$dU = mc_vdT + c_vTdm \tag{B.3}$$

The boundary work can be written as:

$$dW = PdV \tag{B.4}$$

The ideal gas law states:

$$T = \frac{PV}{mR} \tag{B.5}$$

With *R* constant, *T* can be derived as:

$$dT = \frac{1}{mR}(VdP + PdV - RTdm) \tag{B.6}$$

The constant volume specific heat can be written as follows:

$$c_v = \frac{R}{\gamma - 1} \tag{B.7}$$

Substituting equations B.3, B.4, B.6, and B.7 into equation B.1 yields:

$$dQ = \frac{1}{\gamma-1}VdP + \frac{\gamma}{\gamma-1}PdV + dQ_w \tag{B.8}$$

B.2. Heat Release Calculation Methodology

The filtered and correctly phased pressure traces was used in the heat release calculations.

As illustrated in 2.6.2 using Figure 19 the piston position at a specific crank angle can be calculates as follows:

$$H_t = L_{cr} + L_{ct} - \sqrt{L_{cr}^2 - (L_{ct}\sin\theta)^2} \tag{2.19}$$

The cylinder volume for the given crank angle is then given by:

$$V = \frac{2A_P L_{ct}}{CR-1} + H_t A_P \tag{2.20}$$

With the instantaneous cylinder volume know, it is possible to follow a numerical approach to determine the rate of change in cylinder volume:

$$\left(\frac{dV}{d\theta}\right)_i = \frac{V_{i+1}-V_{i-1}}{\theta_{i+1}-\theta_{i-1}} \tag{B.9}$$

This can also be calculated analytically by taking the derivative of the piston position to crank angle and multiplying it by the piston crown area.

$$\frac{dV}{d\theta} = A_P\left[\frac{L_{ct}^2\sin\theta\cos\theta}{\sqrt{L_{cr}^2-(L_{ct}\sin\theta)^2}} + L_{ct}\sin\theta\right] \tag{B.10}$$

From section 2.7 the mean gas temperature can be calculated as:

$$T_i = T_{ref}\left(\frac{P_i}{P_{ref}}\right)\left(\frac{V_i}{V_{ref}}\right) \tag{2.21}$$

With the reference values take at bottom-dead-centre prior to the compression stroke.

The mean piston velocity is calculated as follows:

$$S_P = \frac{4L_{ct}N}{60} \tag{B.11}$$

The heat transfer area (including the piston crown and combustion chamber ceiling) to the cylinder walls is calculated with:

$$A_w = 2\pi \left(\frac{D}{2}\right)^2 + \pi D H_t \tag{B.12}$$

Appendix C: Diagrams

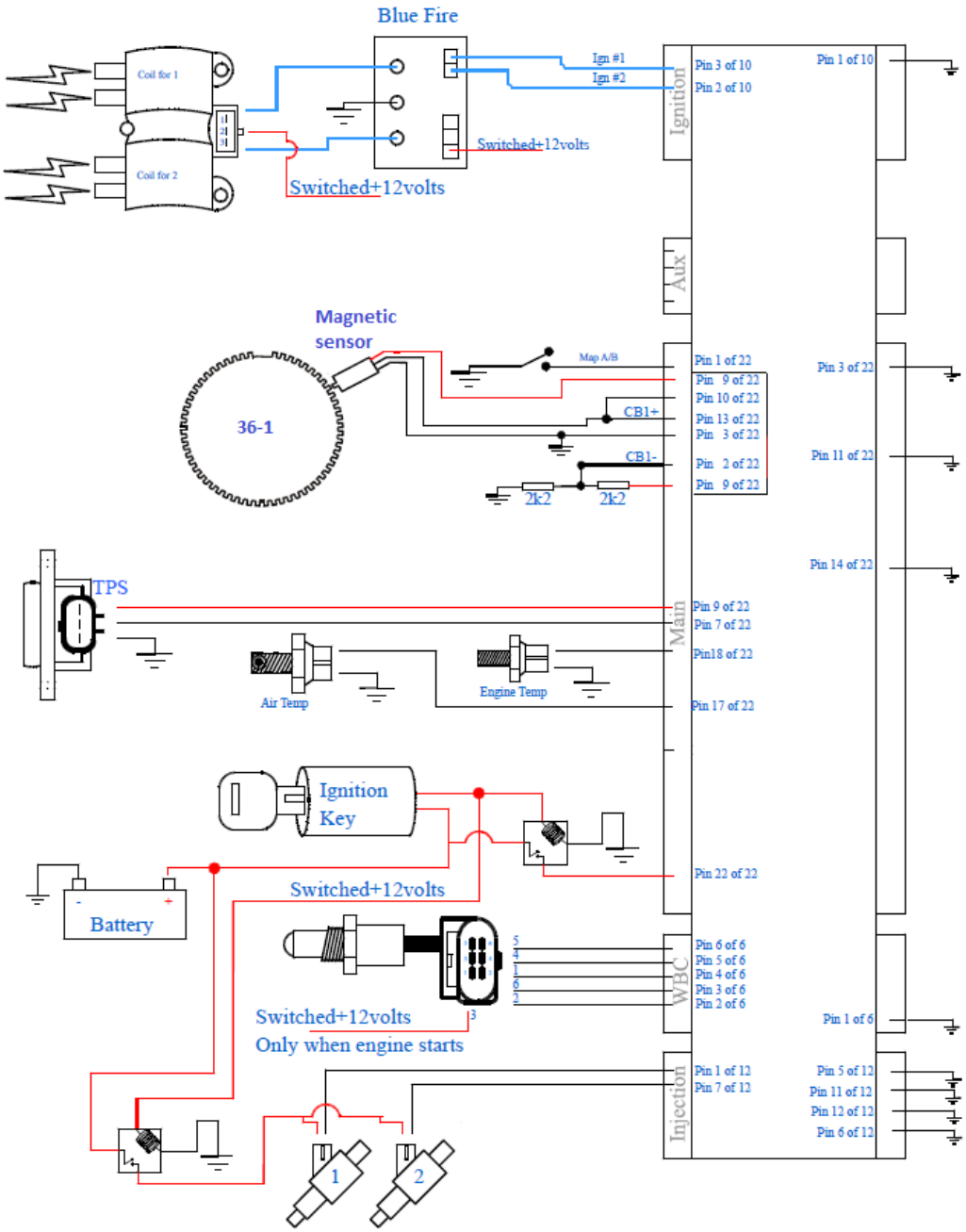

Figure 74: Perfect Power XMS5B ECU wiring diagram (adapted from, Perfect Power, [S.a.])

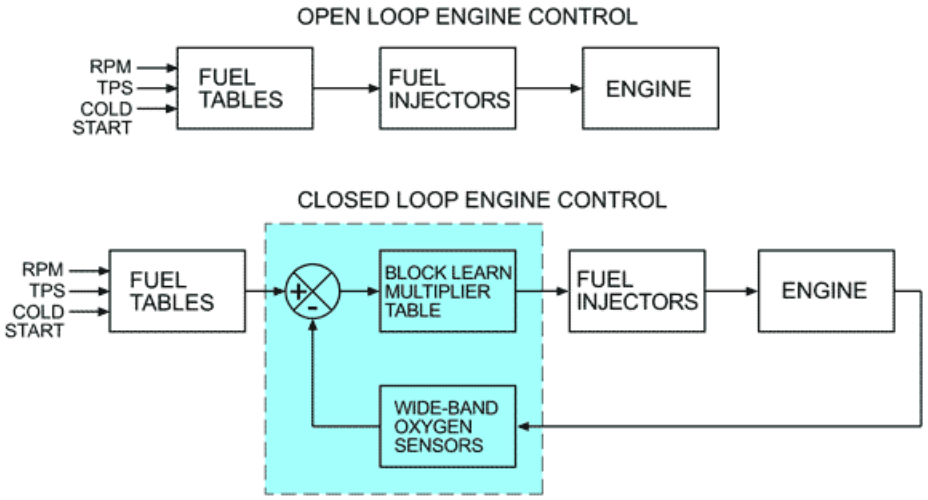

Figure 75: Engine control modes (Twintec, [S.a.])

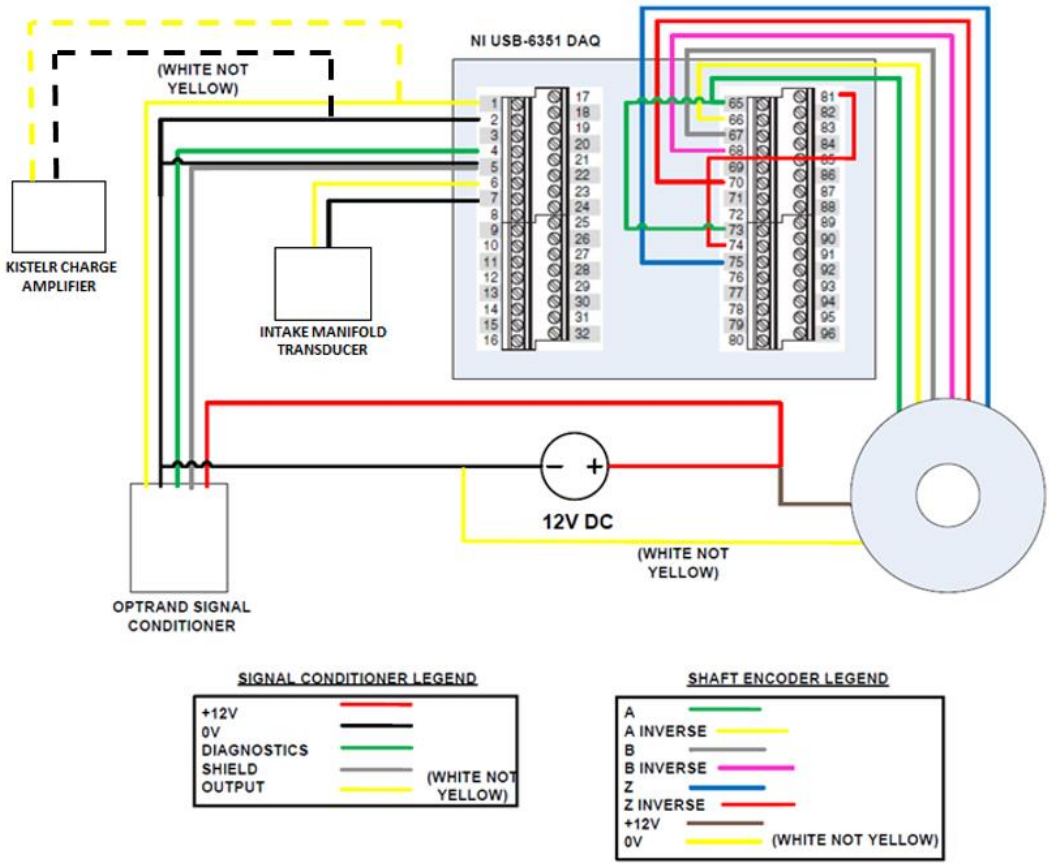

Figure 76: National Instruments USB-6351 wiring (adapted from, Kenny, 2013)

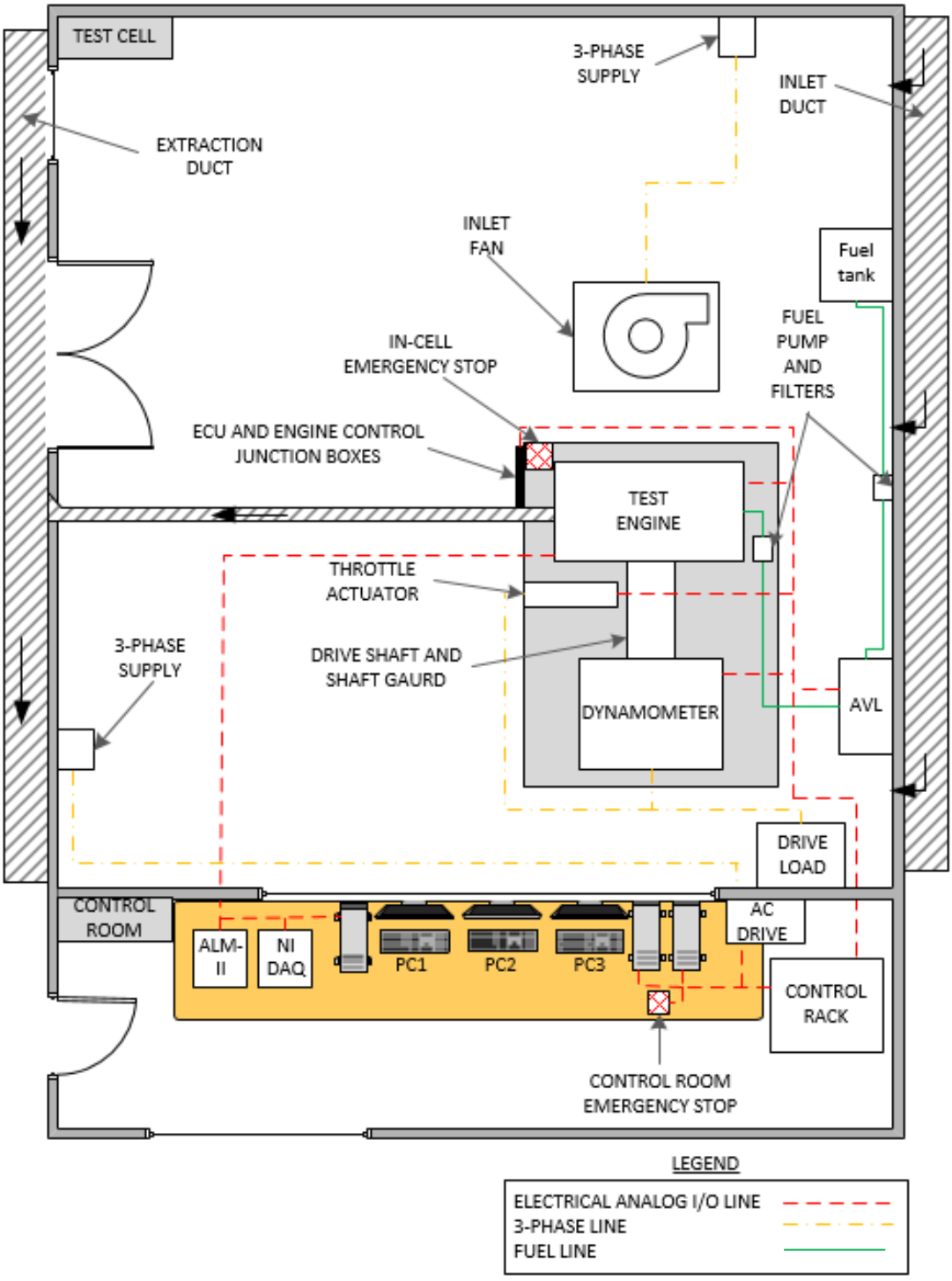

Figure 77: Test cell layout

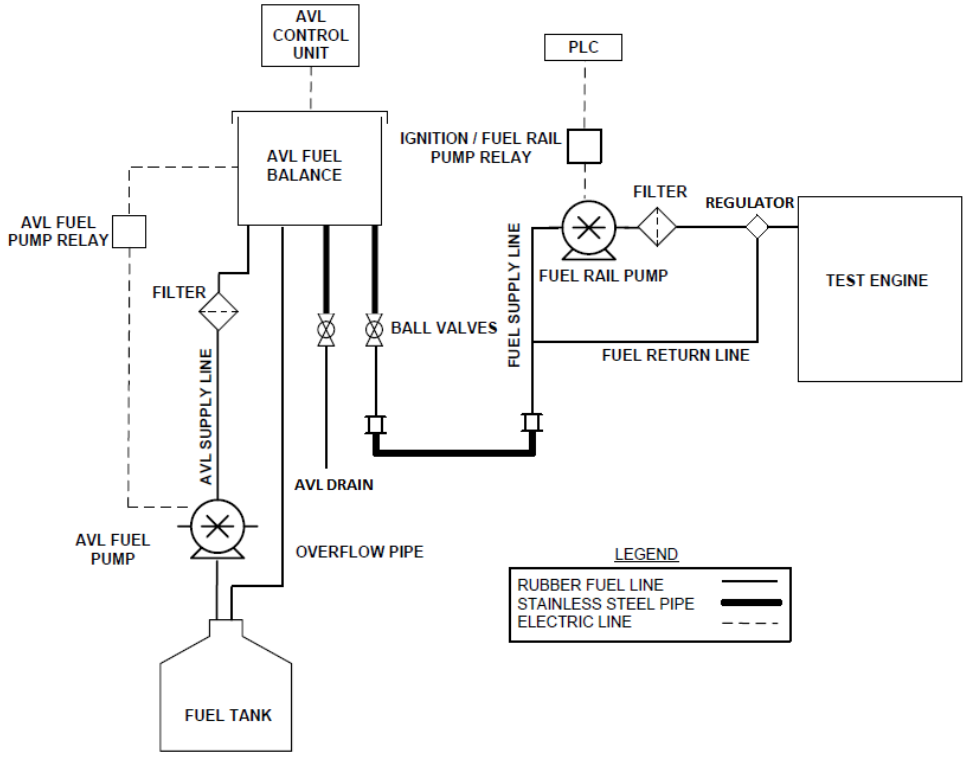

Figure 78: Fuel system layout

As seen in Figure 78, a drain line was added to the fuel system to simplify the calibration procedure as the vessel had to be drained prior to calibration.

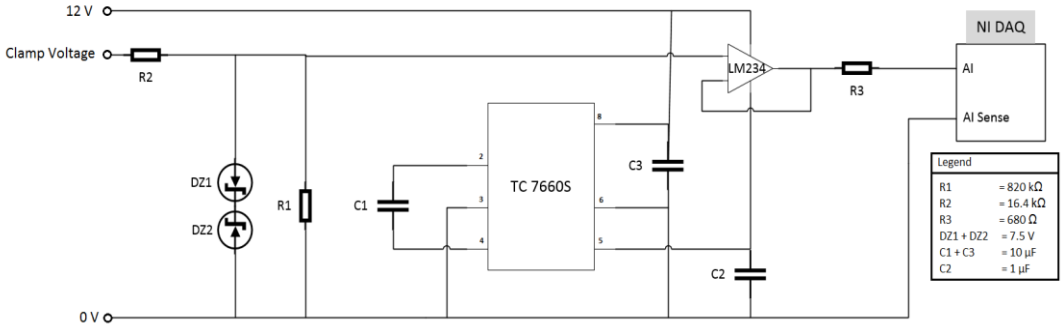

Figure 79: Ignition capture circuit

Appendix D: Software Programs

D.1. User Interface Software

Illustrations of the different graphical user interfaces that were used for the project are given in this appendix subsection.

The ETA, SCADA package used during this project was supplied by Cape Advanced Engineering (CAE)

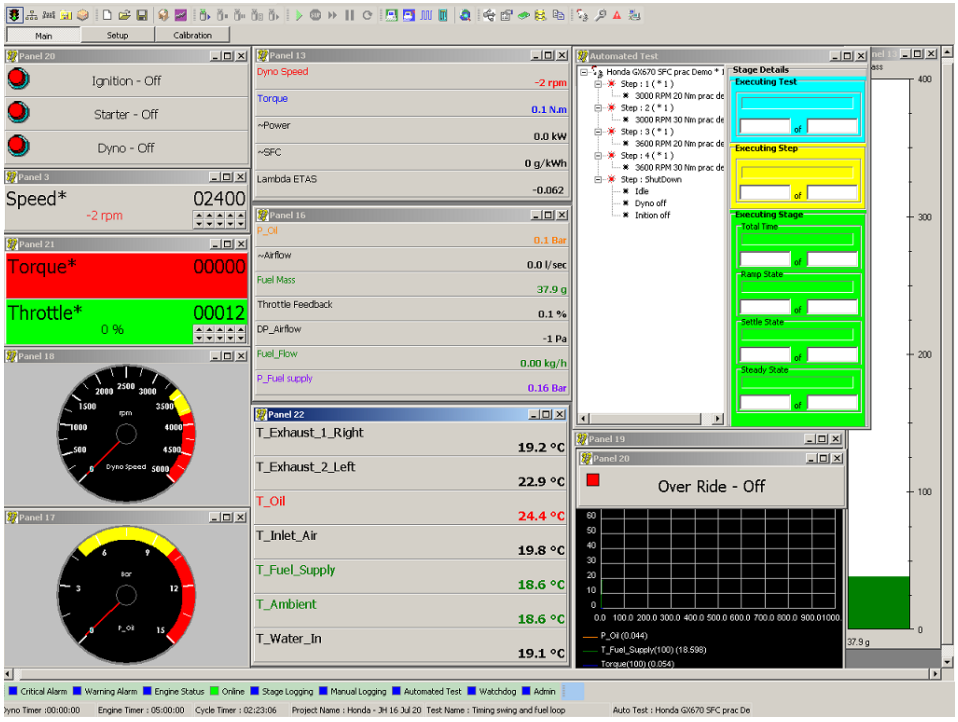

Figure 80: ETA interface

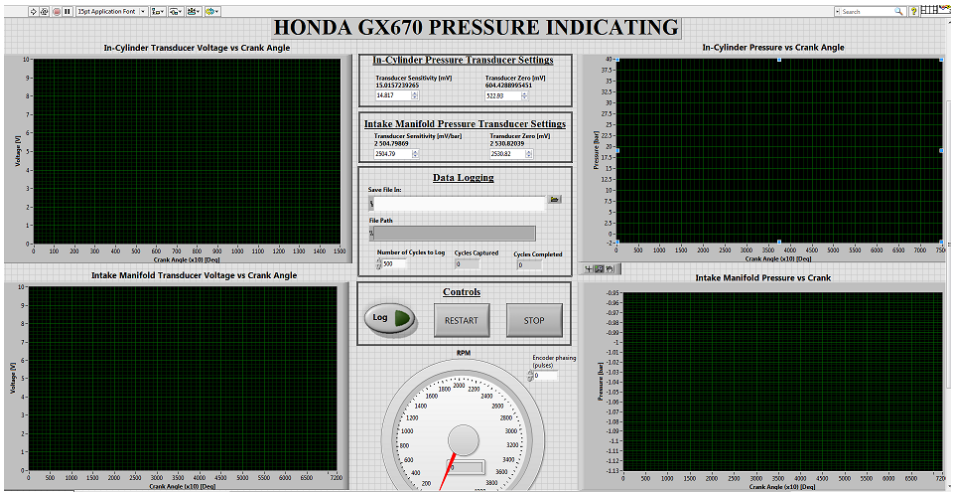

Figure 81: LabView interface

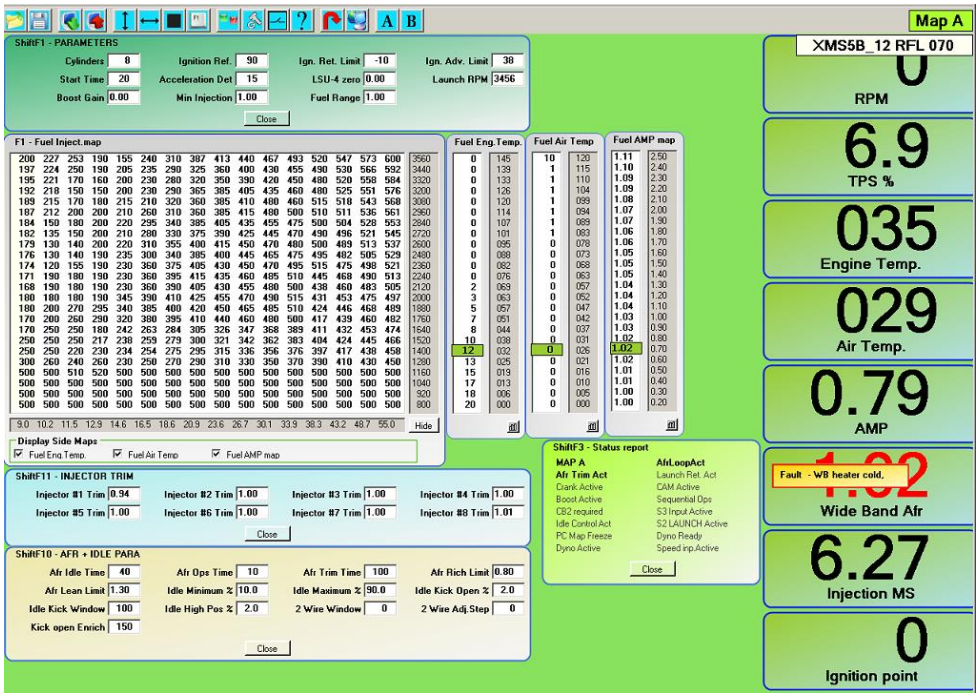

Figure 82: ECU programming interface

Figure 83: ALM GUI lambda interface

D.2. ECU Parameters and Maps

Examples of the ECU's programmed maps and set points are given in this section. The ECU setup parameters are shown, to an extent, in Figure 84 and the ECU calibration points are shown in Figure 85. The fuel injection map is illustrated in

Figure 86 and shows the injection parameters used during open-loop conditions. The timing map illustrated in Figure 87 shows the ignition timing parameters that were used for all tests, except the timing swing tests.

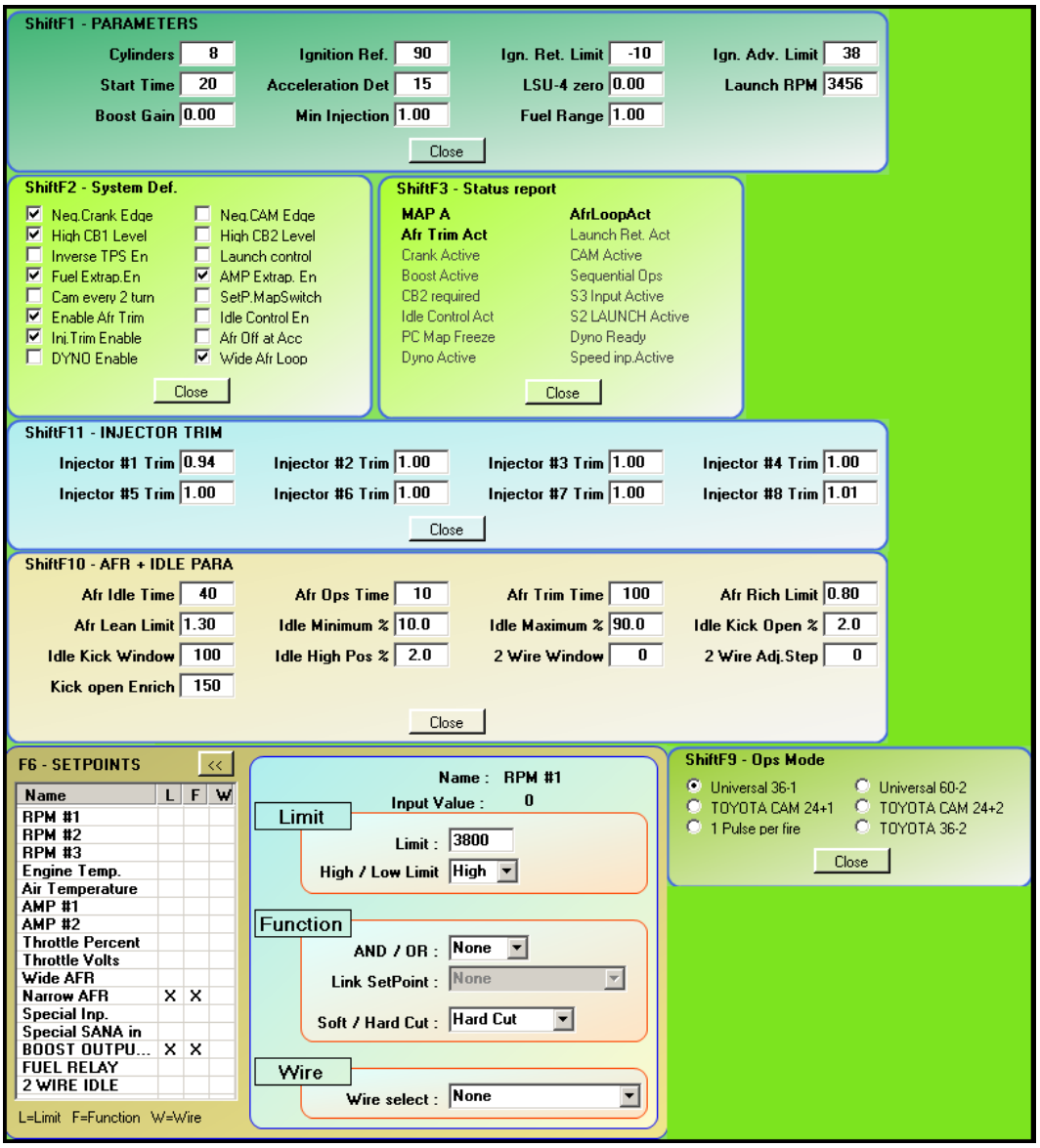

Figure 84: ECU setup parameters

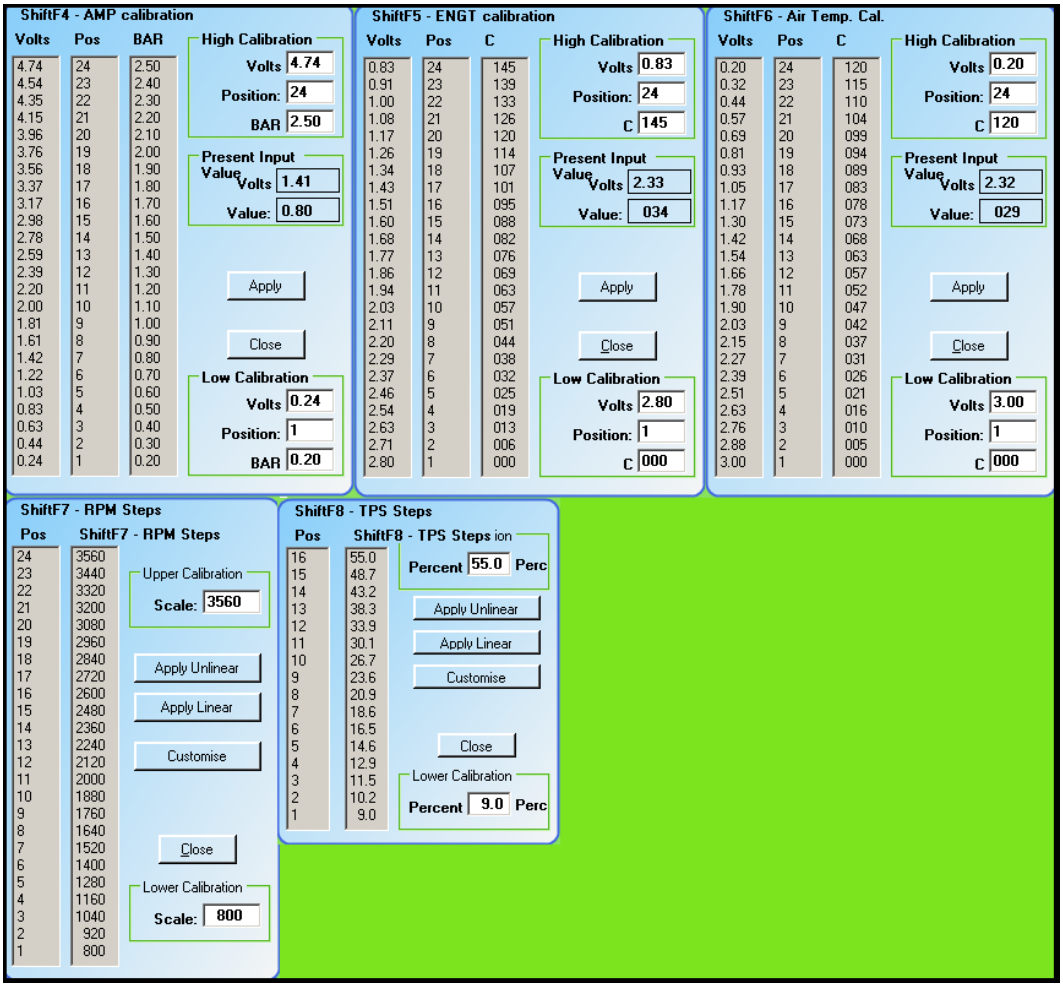

Figure 85: ECU calibration

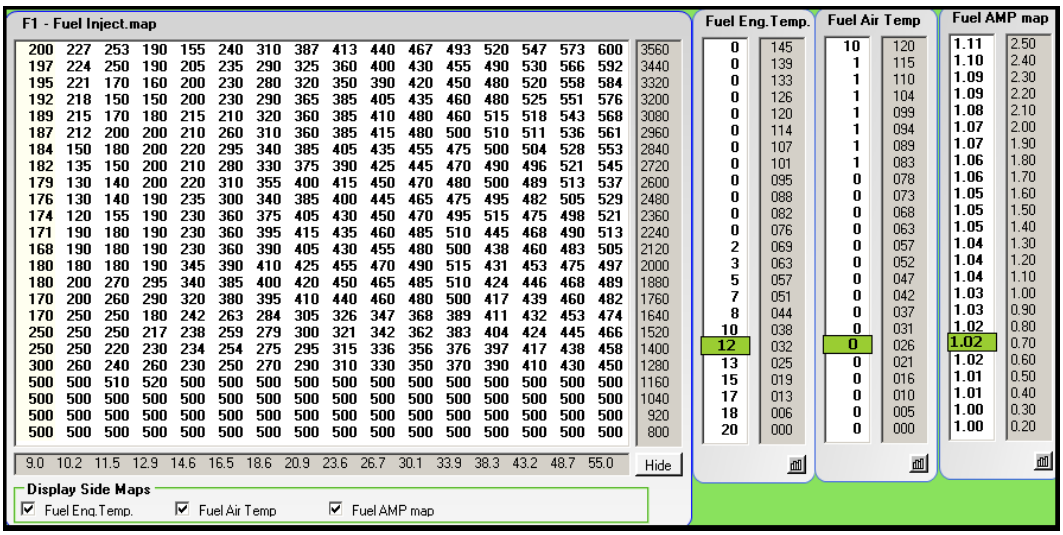

Figure 86: ECU fuel injection map

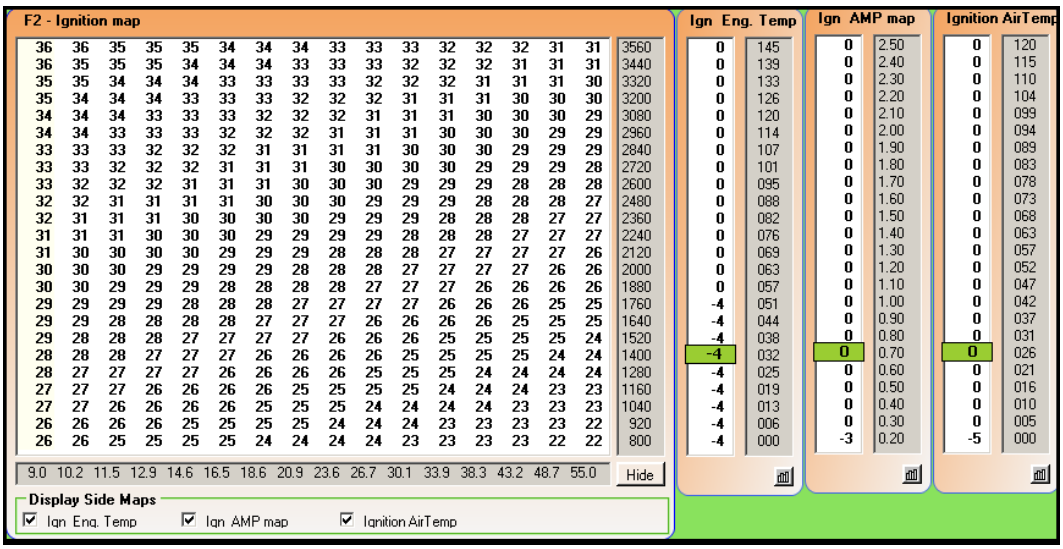

Figure 87: Ignition timing map

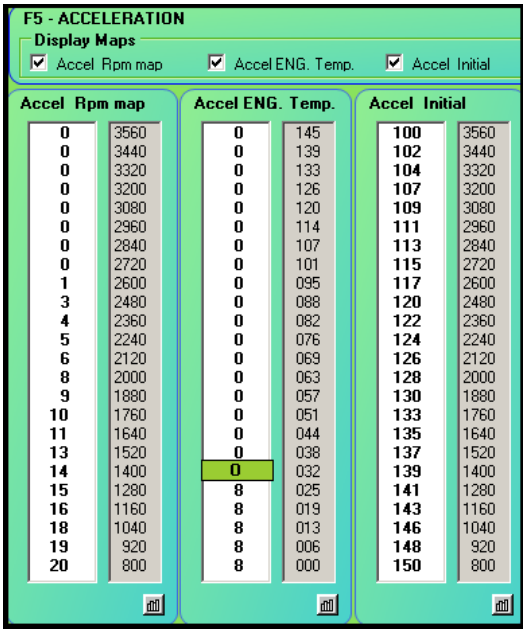

Figure 88: ECU acceleration map

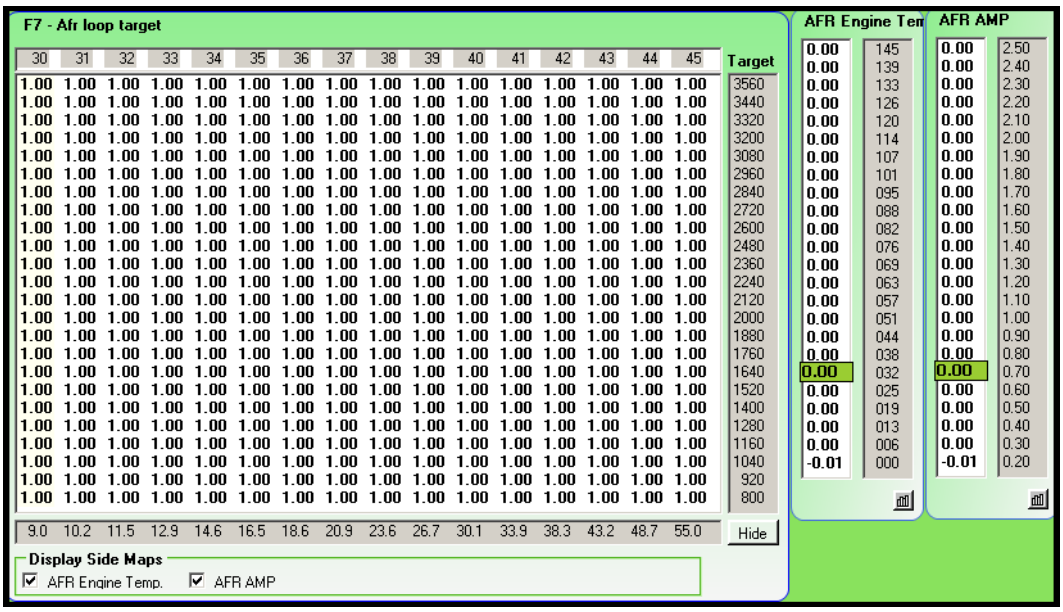

Figure 89: ECU closed-loop target map

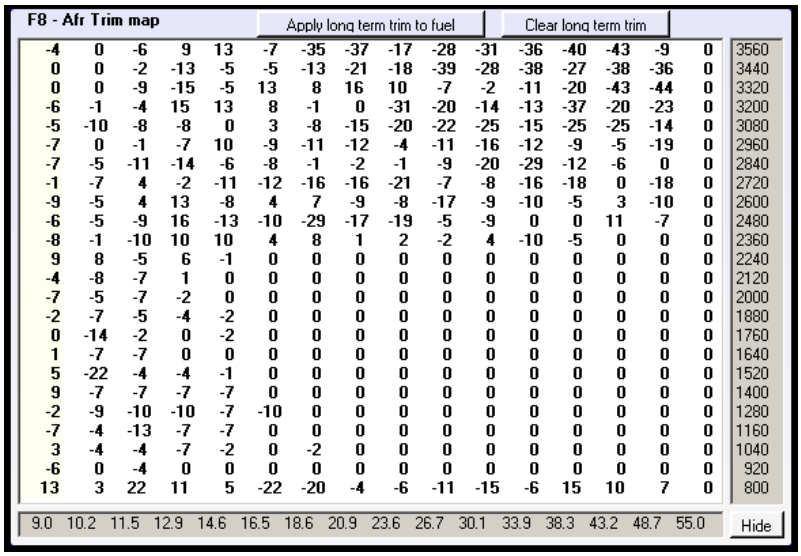

Figure 90: ECU long term fuel trim map

D.3. LabView Block Diagram

The LabView block diagram used for indicating measurements is shown in Figure 91. This only serves as an illustration of the structure of the program.

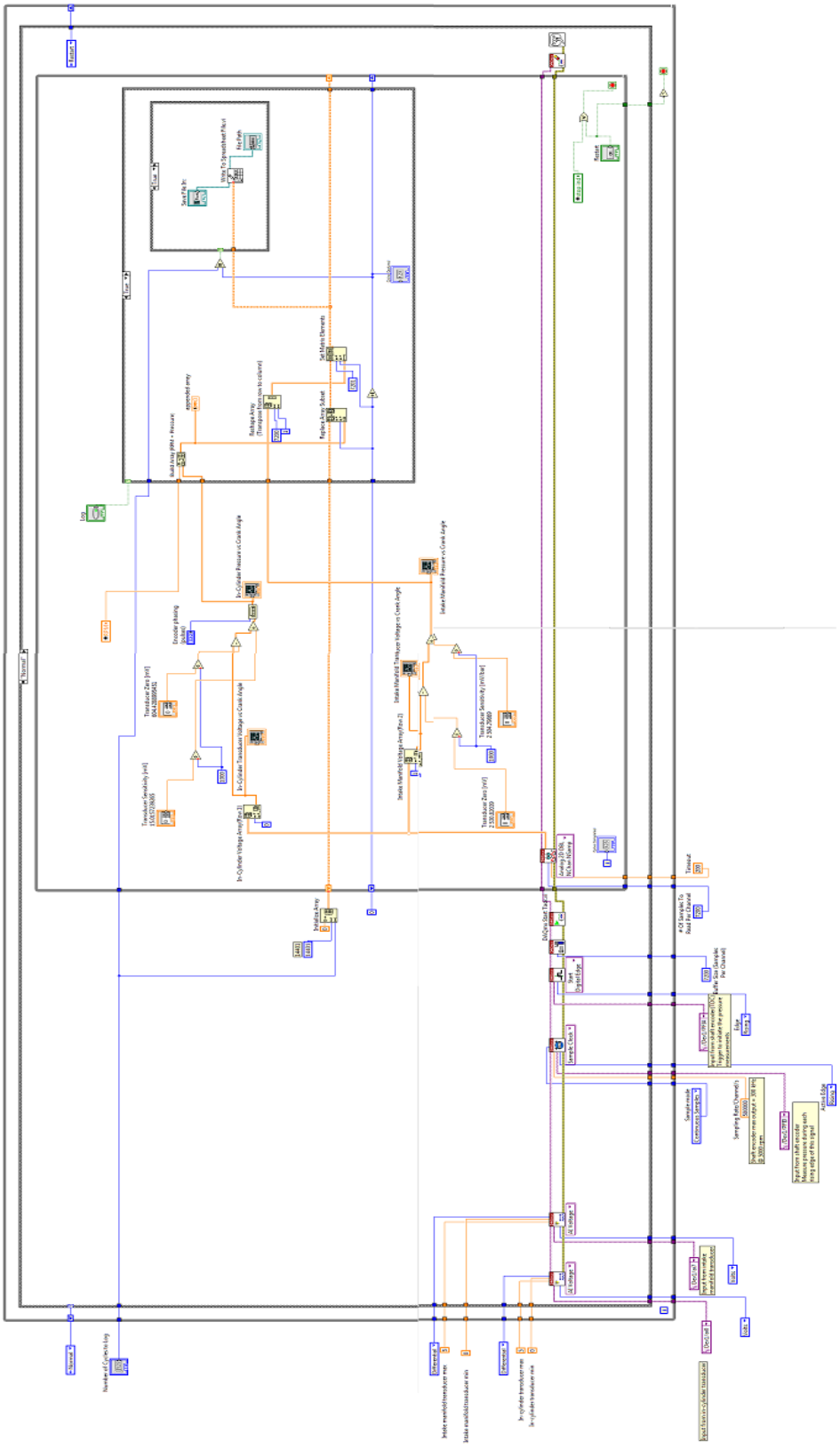

Figure 91: LabView block diagram

Appendix E: Additional Data

This section illustrates the additional data that was obtained as mentioned in Chapter 6.

E.1. BSFC

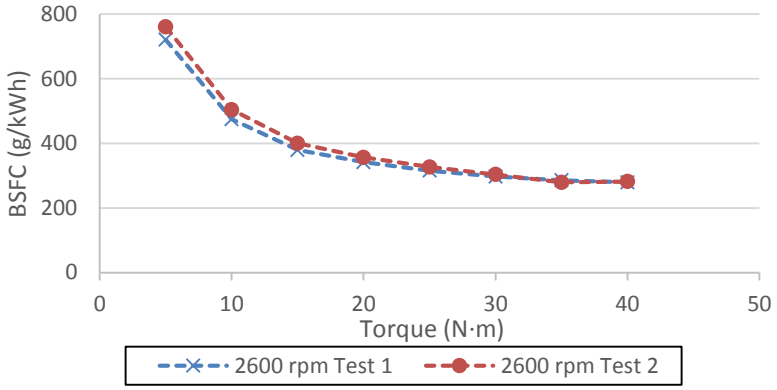

Figure 92: BSFC repeatability (2600 rpm)

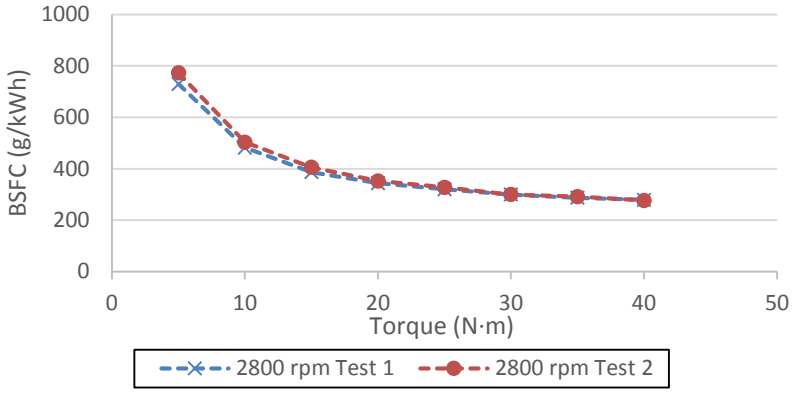

Figure 93: BSFC repeatability (2800 rpm)

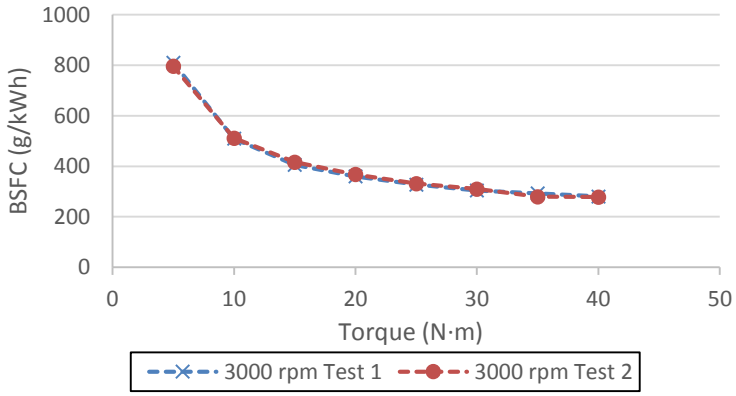

Figure 94: BSFC repeatability (3000 rpm)

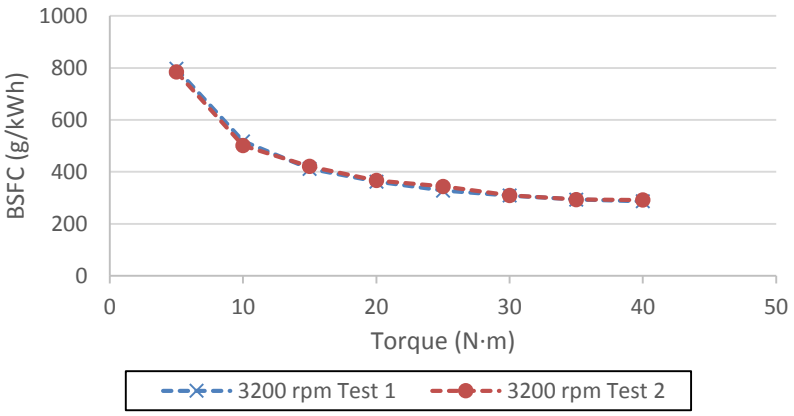

Figure 95: BSFC repeatability (3200 rpm)

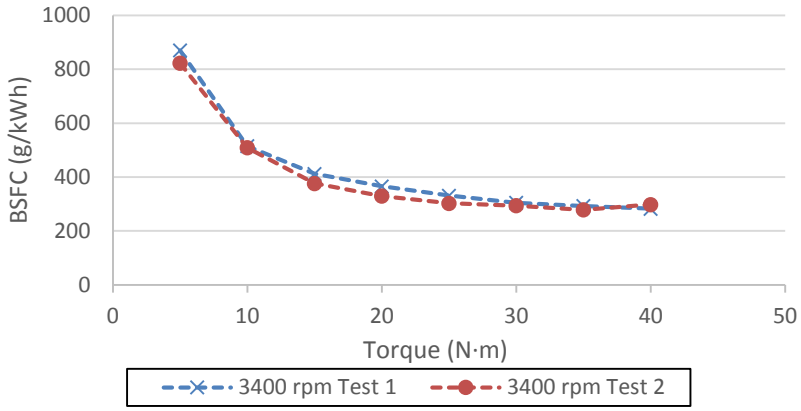

Figure 96: BSFC repeatability (3400 rpm)

E.2. Exhaust Gas Temperature

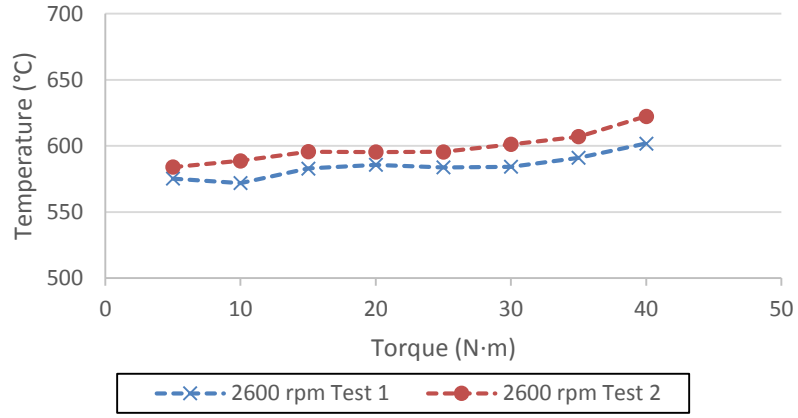

Figure 97: Exhaust gas temperature repeatability (2600 rpm)

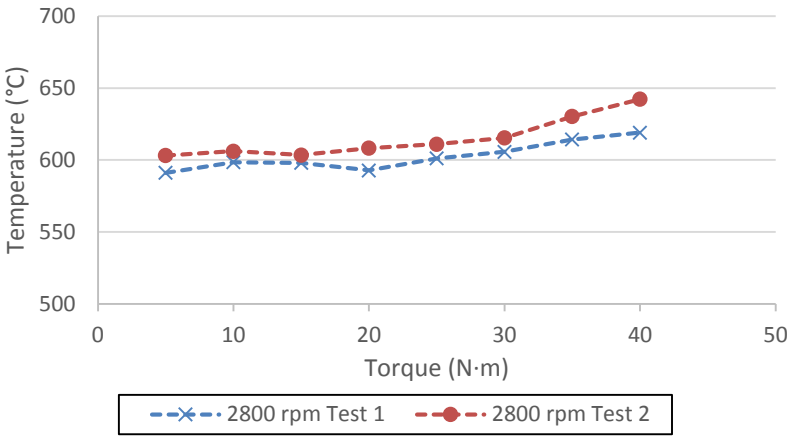

Figure 98: Exhaust gas temperature repeatability (2800 rpm)

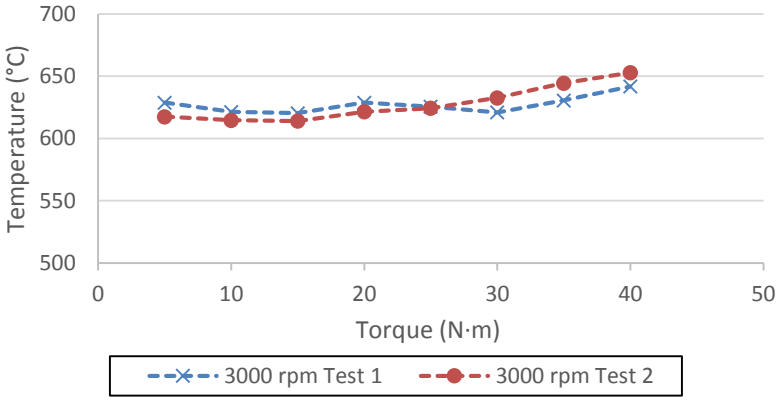

Figure 99: Exhaust gas temperature repeatability (3000 rpm)

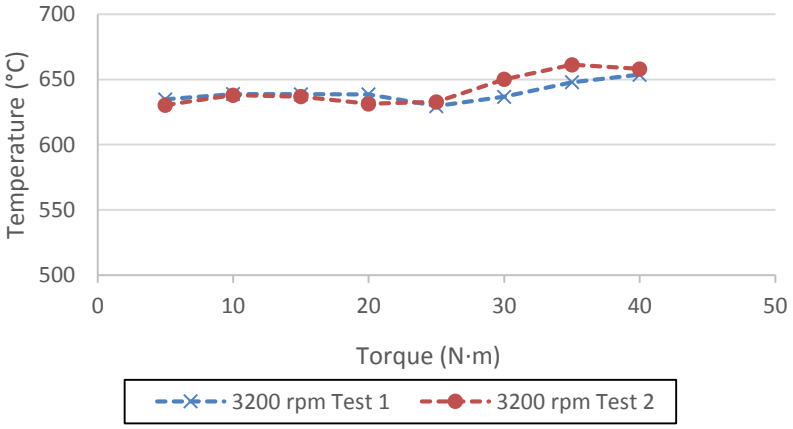

Figure 100: Exhaust gas temperature repeatability (3200 rpm)

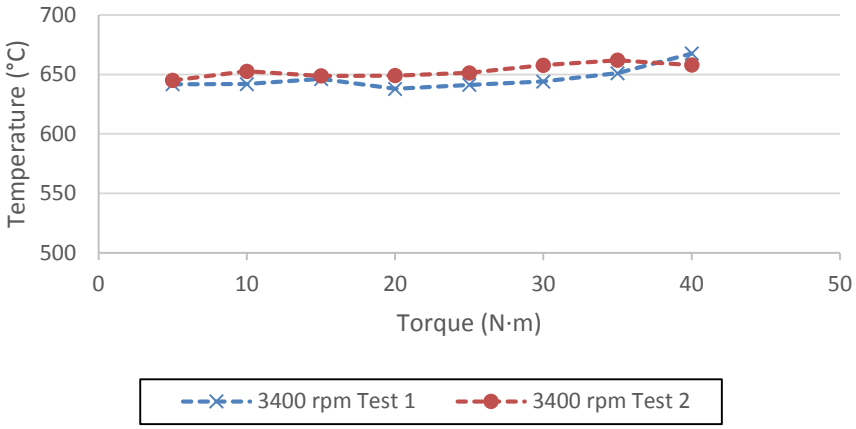

Figure 101: Exhaust gas temperature repeatability (3400 rpm)

E.3. In-Cylinder Pressure Measurements

Figure 102 illustrates the pressure curves obtained from motoring tests run at 3000 rpm. These tests were run at throttle body positions correlating to 20 N·m and 40 N·m.

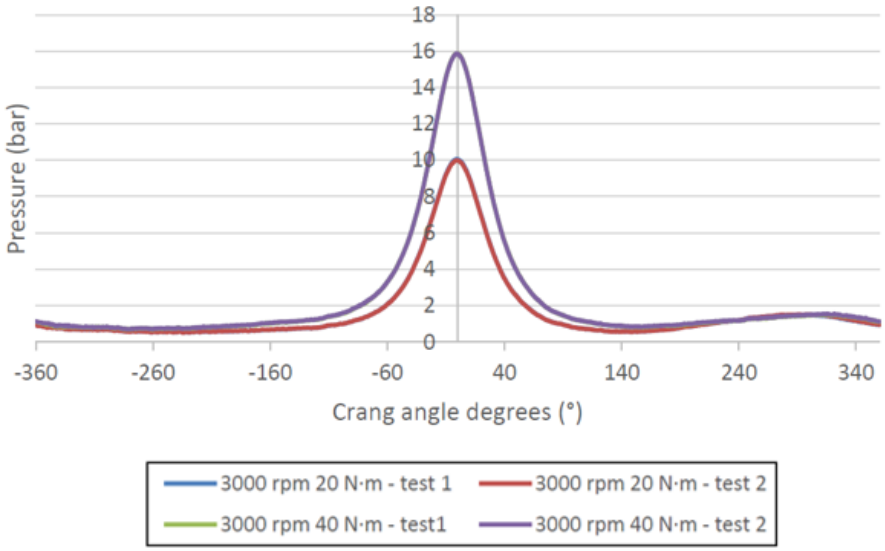

Figure 102: In-cylinder pressure vs. crank angle, hot motoring (3000 rpm)

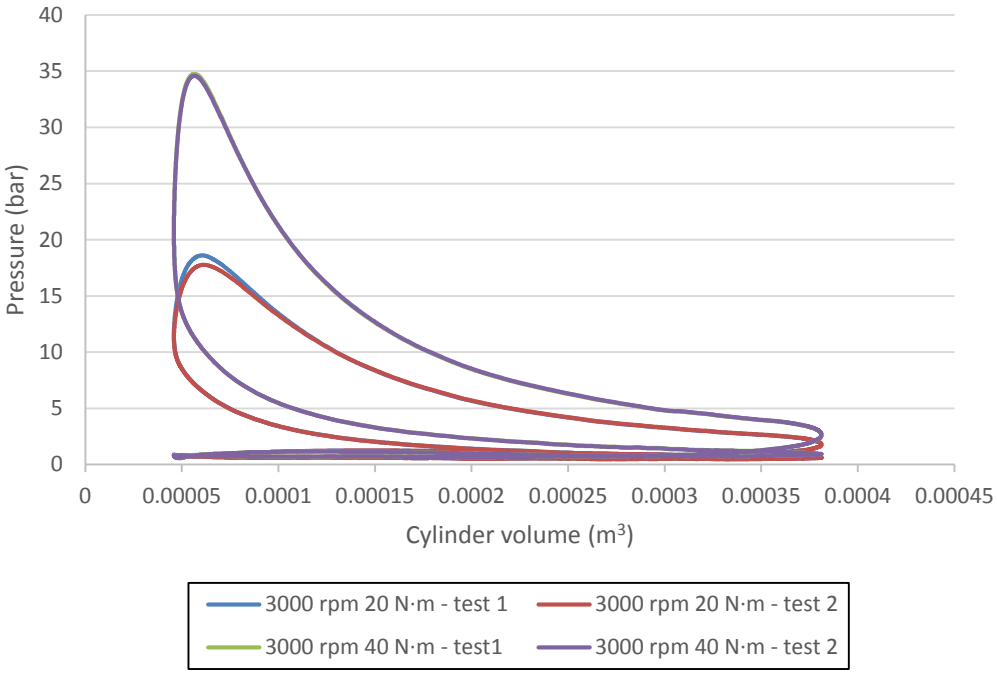

Figure 103: In-cylinder pressure vs. cylinder volume (3000 rpm tests)

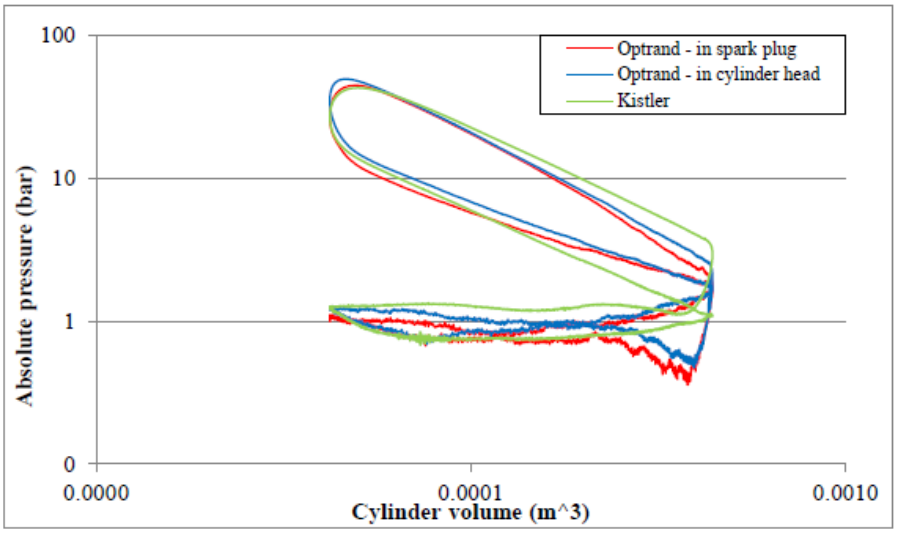

Figure 104: Transducer comparison: log P - log V (3600 rpm @ 90 N·m) (Kenny, 2013)

E.4. Heat Release Curves

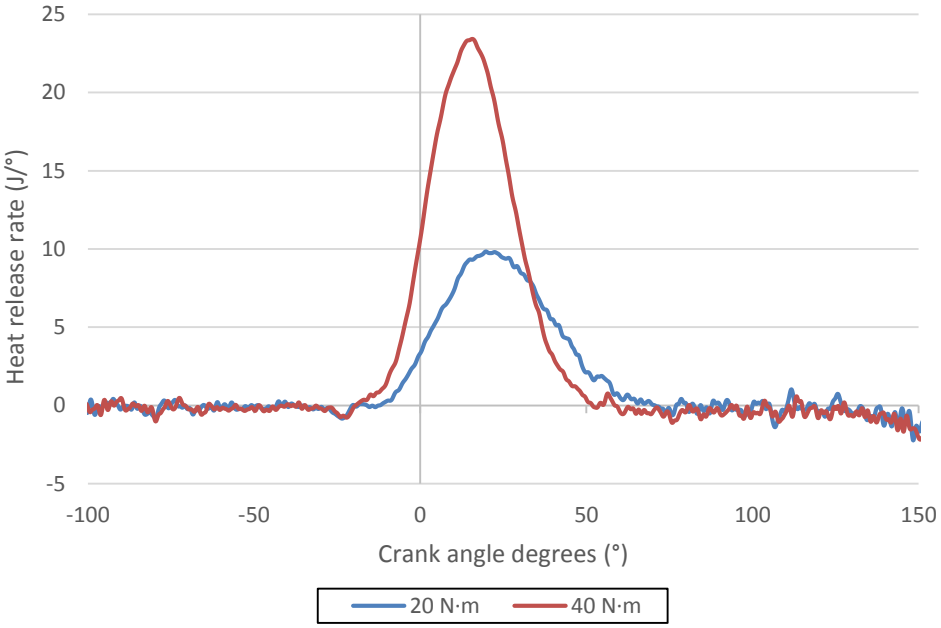

Figure 105: Heat release rate (3000 rpm)

Appendix F. Honda GX670 Starting Procedure

Before proceeding with the starting procedure it is important that you familiarize yourself with the safety document for the engine test facility. Thereafter please read though the instructions below before operating the Honda GX670 and electric dynamometer test setup. In order to avoid any injury to the personnel or damage to the equipment used, the instructions listed below must be followed very carefully and where applicable the tasks must be executed in the order they are listed.

1. Inspect the engine test setup for any damage to the structure and ensure that there are no fluid leaks from the test setup
2. Ensure that all the equipment is securely fastened, before starting the test setup.
3. Check that the engine oil level is correct. Remove the dipstick and clean off any oil on the dipstick. Re-insert the dipstick completely. Remove the dipstick and check that the engine oil level is at the correct level, as indicated on the dipstick.
4. Check the driveshaft and ensure that all the bolts are securely fastened.
5. Ensure that the fuel container has an adequate amount of fuel for the tests.
6. Remove the plugs from the ends of the fuel hoses. Insert the fuel supply hose (to the AVL dynamic fuel balance) into the petrol fuel container and ensure the end of the hose is completely submerged in the fuel and as close to the bottom of the container as possible. Insert the second fuel hose into the same container. In the event that the AVL dynamic fuel balance is overfilled, this hose will transport the excess fuel back to the container supplying the fuel.
7. Fully open the fuel supply valve (underneath the AVL, to the left) to the engine.
8. Connect the battery to the engine and ensure the battery leads are connected using the correct polarity (connect the positive terminal first then the negative terminal).
9. Connect the battery charger to the battery (now also connected to the engine) and activate the charger. The test engine recharges the battery, but this is not sufficient considering all the additional electronics that run off the battery.
10. Plug in and power on the 3-phase power to the drive, by moving the switch to the “1” position (on position).
11. Enter the control room and switch on the computers that will be used to control and monitor the test setup (PC1, PC2 and PC3, see Figure 77 for clarification). PC1 is used to monitor the oxygen content as seen by the wide band lambda scanner and is also used for the in-cylinder pressure

measurements. PC2 is used to communicate with the Perfect Power XMS5B ECU using LetRipp software. PC3 uses ETA to control the engine test setup as well as capture relevant data inputs.

12. Plug the white lead that powers the 19" rack into the wall socket and switch it on. Flip the red switch on the white plug, located in the bottom left of the 19" rack, to the on position. This plug supplies power to the multi-plugs in the 19" rack.
13. All controllers, including the PLC will now be on. The only controller that will still be off is the throttle actuator controller which has an additional switch on its front panel. Leave this controller off for the time being.
14. Open ETA on PC3, but don't go online. You can only edit channel properties when in offline mode. Right click the P_Oil tab and select properties. Click on the expression tab and enter the following in the empty block: X * 0 + Torque. Click apply and click OK. This should set the oil pressure channel to display the current measured torque as soon as the engine is running. Leave ETA open for now.
15. Switch on the throttle actuator controller, using the switch on its front panel. The electromagnetic clutch of the actuator will engage inside the test cell and can be heard from the control room.
16. You will now have to verify that you have throttle control. In order to do this, the ignition will have to be set to the "ON" position in ETA. NOTE: As soon as the ignition is switched on, the fuel pump on the test bench will start pumping fuel to the engine which is not running at the moment and the fuel supply line to the engine will be pressurized. Although there is a bypass line for the fuel, do not keep the ignition switched on for extended periods without having the engine running as this will cause the fuel pump to heat up. In the event that the ignition has to stay on for longer periods of time (e.g. when performing throttle calibration), remove the negative terminal from the battery to ensure no power is supplied to the fuel pump.
17. Proceed to verify that you have throttle control over the entire throttle range (closed throttle to wide open throttle). Go online with ETA using the traffic light icon located in the top left hand corner of the graphic user interface. Switch the ignition to the "ON" position and change the throttle set point. The throttle controller's hand held unit can be used to verify throttle response, but it is recommended to verify throttle response by physically identifying change in throttle position. If the throttle is not responding, push the reset button on the front panel of the throttle actuator controller. If the throttle remains unresponsive, re-calibration will be required. Once you have throttle response, switch off the ignition in ETA, but leave the throttle actuator controller on.

18. Open the LetRipp software on PC2 and ensure the software establishes a connection with the ECU. Communication to the ECU is occasionally disrupted as a result of the long USB cable used to connect the ECU to the computer. If a connection cannot be established, disconnect and reconnect the blue USB cable located at the back of PC2. Open the injection trim MAP in the LetRipp software (shortcut: “shift+F11”). This will be used to control the injector trim of Injector1 as it is slightly over fuelling. NOTE: If the LetRipp software freezes while the engine is running, disconnect and reconnect the blue USB communications cable. This will not affect the engine as the ECU is designed to run the engine without a computer connected to it.
19. Open the GUI software on PC1, but remain offline for the time being as the lambda scanner is still switched off.
20. Enter the test cell and switch on the two portable fans that aid in the airflow over the engine and dynamometer. Switch on the ALM-II lambda scanner and ensure that both lambda probes are heating up. Switch on the extraction fan in the test cell and close the test cell door after leaving the test cell. Once the extraction fan is running, proceed to the control room of the first test cell and switch on the inlet fan. Return to the Honda GX670 control room and go online in ETA and the GUI software. Start running the GUI software by pushing the play button and select to display only the lambda values for the two sensors.
21. Turn the red switch on the drive to the on position to switch on the drive. This is needed, even with the dynamometer off, as it powers the shaft encoder that measures the engine speed. Switch on the ignition in ETA and set the speed to 2500 rpm. Depending on throttle calibration, set the throttle position to more or less 6 %. You should now be in throttle control mode (throttle icon highlighted green).
22. Start the engine by clicking the “Starter” button in ETA, but DO NOT SWITCH ON THE DYNO AT THIS STAGE. If needed, increase the throttle instantaneously by 10 % and immediately return it to its previous value. This will engage the acceleration map that briefly enrichens the fuel mixture helping the engine speed up, and aids in the response of the closed-loop lambda control at start-up.
23. Monitor the lambda reading on the GUI software to establish if the wide band lambda control of the ECU is controlling the fuelling. Monitor the reading of the first lambda probe to correctly trim the first injector. The injector trim for the first cylinder is around 88 % (value of 0.88 in the LetRipp software) at low speed and low load, and increases to around

98 % as the speed and load increases. This would be rectified by installing a new injector.

24. Once the engine is running, increase the throttle position to ensure the engine idles smoothly around 1500 rpm. Visually inspect the test setup for any leakage of fuel or oil and ensure that no components are vibrating excessively. With the drive switched on the engine speed will be displayed in ETA. P_Oil will now display the torque measured by the dynamometer, which at this moment should only be the drag on the dynamometer (<2Nm).
25. Allow the engine to heat up sufficiently before starting the actual engine test. Monitor T_Oil in order to determine the temperature of the engine.
26. With the engine running smoothly, set the speed to at least 2500 rpm. Increase the throttle slowly while carefully monitoring the indicated engine speed. As soon as the engine speed just exceeds the speed set point, switch on the dynamometer by clicking the "Dyno" button in ETA. **NOTE: Engine speed should NOT exceed speed set point by more than 50 rpm when the dynamometer is switched on, otherwise the dynamometer will clamp the engine which can lead to failure of the driveshaft.** Monitor the torque applied to the engine as the dyno comes online and decrease the throttle setting if necessary to prevent the torque from spiking.

    Some torque and speed guidelines when running the test setup:

    - Max engine rated speed is 3600 rpm.
    - Max rated torque is 46 N·m, but be very cautious when applying torque values exceeding 35 N·m.
    - The setup runs smoothly at speeds above 2800 rpm and load ranging from 5 – 40 N·m.
    - Be cautious at loads below 10 N·m, as ECU closed-loop control and the torque PID control in ETA battle each other to maintain a steady lambda and torque set point.
    - If the speed set point is adjusted too fast (without increasing the throttle set point), the torque will drop to 0 and the dynamometer will start motoring the engine. The dynamometer will load the engine again once you increase the throttle set point enough, but be careful not to use to large increments when changing set point values as this will cause the dynamometer to cycle between motoring and loading the engine. A sudden increase in the throttle setting (or decrease in the speed set point) will force the dynamometer to very suddenly apply a very large amount of torque

to the engine. Any of the above situations may cause the drive shaft to fail.

27. In order to switch off the test setup after the test is completed:
    Reduce the load on the engine by decreasing the throttle setting. You may also want to reduce the speed at which the engine is running by reducing the speed set point, but be very careful when doing so. As soon as the speed set point is reduced, the dynamometer will load the engine and the throttle will have to be reduced first (to reduce the load on the engine) before the speed set point can be reduced further. DO NOT allow the load on the engine to cycle more than 10 N·m to 15 N·m when following this procedure. NOTE: Pay attention to the lambda measurements as the trim on the first injector will have to be altered as the load and speed is reduced. When, at the desired lower speed, reduce the load on the engine by reducing the throttle setting. As soon as the load drops below 3 N·m (before the dynamometer starts to motor the engine) click the "Dyno" button to disengage and switch off the dynamometer. Now only the engine is running and you can reduce the speed to and let the engine cool down by running at about 2500 – 2800 rpm until the oil temperature has dropped sufficiently. With the engine running at 2500 rpm you can switch off the "Ignition" to shut the engine down.
28. Go offline in the GUI software as well as in ETA. If not intending to run again, switch off the throttle actuator along with the rest of the controllers in the 19" rack, otherwise leave it on.
29. Switch off the inlet fan, extraction fan, portable fans and the ALM-II lambda scanner. Switch off and unplug the 3-phase power inside the test cell. Close the fuel supply valve to the engine. Remove the fuel hoses from the fuel supply canister and wipe off any excess fuel on the hoses before sealing them with the plugs. Switch off and disconnect the battery charger and disconnect the battery from the engine. Ensure that all the computers, controllers and other electronic devices have been switched off and that the drive enclosure has been closed.
30. Finally do a general inspection of the test setup: Ensure the drive shaft bolts are still tight. Check for any fluid leaks around the test setup. Ensure the test setup is clean as it will allow easier identification of leaks in the future.

References

AIP, 2013. *Refining of Petroleum*. [Online]. Available at: http://www.aip.com.au/industry/fact_refine.htm [Accessed 07 October 2015].

Alimin, A. J., Chamari, M. F., Hushim, M. F. & Rashid, L.A. [S.a.]. *Influence of Fuel Injector Position of Port-Fuel Injection Retrofit-Kit to the Performance of Small Gasoline Engine.* Malaysia: Faculty of Mechanical and Manufacturing Engineering.

Annand, W. J., 1963. Heat Transfer in the Cylinders of Reciprocating Internal Combustion Engines. *Proc. I. Mech. E, 177*: 973-990.

Atkins, R. D., 2009. *An Introduction to Engine Testing and Development*. Warrendale: SAE International.

Arcoumanis, C. & Kamimoto, T. 2009. *Flow and Combustion in Reciprocating Engines*. Berlin: Stringer

AVL, 1984. *Operating manual: Dynamic fuel consumption measuring equipment 730*. Graz: AVL.

AVL, 2002. *Engine indicating: User handbook*. Graz: AVL.

Balich, G. W. & Aschenbach C. W., 2004. *The Gasoline 4-Stroke Engine for Automobiles.* [Online]. Available at: http://www3.nd.edu/~msen/Teaching/DirStudies/Gas4Stroke.pdf [Accessed 07 October 2015].

Blair, G. P. 1999. *Design and Simulation of Four Stroke Engines.* Warrendale: Society of Automotive Engineers.

Bohacs, R. T., 2001. *How to Tune with Demon Carburettors.* Surrey: Brooklands Books LTD

Bosch, 1995. *Automotive electric/electronic systems*. Stuttgart: Robert Bosch GmbH.

Bosch, 2013. *Bosch Port Injection* [Online]. Available at: http://www.bosch-mobility-solutions.com/media/en/ubk_europe/db_application/downloads/pdf/antrieb/de_5/pfi_full_de.pdf [Accessed 10 March 2015].

Bosch, 2013. *Gasoline direct injection, Key technology for greater efficiency and dynamics.* Stuttgart: Robert Bosch GmbH.

Bosch Auto Parts, 2015. *Oxygen Sensors* [Online]. Available at: https://www.boschautoparts.com/commercial/oxygen-sensors {Accessed 07 October 2015].

Bosch, [S.a.]. *Original Equipment Information: Lambda Sensors* [Online]. Available at: http://www.eccmec.it/wp-content/uploads/2012/05/Catalogo-lambda-sensors.pdf [Accessed 07 October 2015].

Brown, B. R., [S.a.]. *Combustion Data Acquisition and Analysis*. Loughborough: Loughborough University.

Byrne, K., Skeen, M. & Kessissoglou, N., 2006. *Measurements of the sound transmission loss of a small expansion chamber muffler to consider the effect of mean flow and wall compliance.* Australia: The University of New South Wales, School of Mechanical and Manufacturing Engineering.

Byttner, S., Rögnvoaldsson, T. & Wicström, N., 2001. *Estimation of combustion variability using in-cylinder ionization measurements.* Sweden: Halmstad University.

Byttner, S., Holberg, U., 2008. *Closed loop control of EGR using ion currents.* Sweden: Halmstad University

Callahan, T. J., Yost, D. M. & Ryan, T. W. 1985. Acquisition and Interpretation of Diesel Engine Heat Release Data, in *SAE Technical Paper Series.* Warrendale: Society of Automotive Engineers.

Castaing, B. M., Cowart, J. S. & Cheng, W. K., 2000. Fuel Metering Effects on Hydrocarbon Emissions and Engine Stability During Cranking and Start-up in a Port Fuel Injected Spark Ignition Engine. SAE Paper: 2000-01-2836.

Çengel, Y. A. & Boles, M. A., 2007. *Thermodynamics: An Engineering Approach Sixth Edition.* Singapore: McGraw-Hill Higher Education

Charles, O. P., 1991. *Bosch Fuel Injection & Engine Management: Theory of Operation, Troubleshooting and Service.* Massachusetts: R. Bentley

Chevron, 2009. *Motor gasolines technical review* [Online]. Available at: http://www.chevronwithtechron.com/products/documents/69083_MotorGas_Tech_Review.pdf [Accessed 13 February 2015].

Classen, T. & Shanner, K., 2011. *Trend in Automotive Exhaust Gas Sensing*. Stuttgart: Robert Bosch GmbH.

Cuperus, J. L., 2012. Development of an In-Cylinder Pressure Measurement System for Heat Release Analysis of a Spark Ignition Engine. BIng final year project. Stellenbosch: Stellenbosch University

Dapper, P., 2013. *Fuel Delivery: BMW F10 M5.* [Online]. Available at: http://m5carblog.blogspot.co.za/2013/02/fuel-delivery.html [Accessed 07 October 2015].

Drake, M., Fransler, T. D. & French, D. T., 1995. Crevice Flow and Combustion Visualization in a Direct-Injection Spark-Ignition Engine Using Laser Imaging Techniques. SAE paper: 952454.

Eckert, P., Kong, S. & Reitz, R. D. 2003. Modelling Autoignition and Engine Knock Under Spark Ignition Conditions. SAE paper: 2003-01-0011.

EUBIA, [S.a.]. *Bioethanol production and use*. [Online] Available at: http://www.erec.org/fileadmin/erec_docs/Projcet_Documents/RESTMAC/Brochure5_Bioethanol_low_res.pdf [Accessed 24 March 2015].

Enright, N., 2015. *Basic principles of operation and application of fuel injection systems in petrol-powered cars* [Online]. Available at: http://lit.ie/News/News%20Documents/ETTA-ENGINEERING-TOPIC-2015-student.pdf [Accessed 07 October 2015].

Ferguson, C.R. & Kirkpatrick, A.T., 2001. *Internal combustion engines applied thermosciences*. 2nd ed. New York: John Wiley & Sons.

Flynn, P. F., Hunter, G. L., Durret, R. P., Farrel, L. A. & Akinyemi, W. C., 2000. *Minimum Engine Flame Temperature Impacts on Diesel and Spark Ignition Engine NOx Production*. SAE Paper: 2000-01-1177.

Goering, C.E., 1998. *Engine heat release via spread sheet*. [Online]. Available at: http://www3.abe.iastate.edu/ae342/AE342_2008/labs/lab3_IMEP/Lab%203_IMEP.pdf [Accessed 01 August 2015].

Grobbelaar, E. (2017). *The Development of a Small Diesel Engine Test Bench Employing an Electric Dynamometer*. Unpublished MScEng thesis. Stellenbosch: University of Stellenbosch

Heywood, J.B., 1988. *Internal combustion engine fundamentals*. New York: McGraw-Hill.

Hiller, V.A.W. & Coombes, P., 2004. *Hiller's fundamentals of motor vehicle technology*, 5th ed. Cheltenham: Nelson Thomas Ltd

Jenvey Dynamics. 2015. *Throttle Body Selection.* [Online]. Available at: http://www.jenvey.co.uk/faq/general-faq [Accessed 07 October 2015]

Kim, Y., Sun, J., Kolmanovsky, I. & Konscol J., 2003. A Phenomenological Control Orientated Lean NOx Trap Model. SAE paper: 2003-01-1164.

Lambda Power, [S.a.]. *Tech Notes: Closed-Loop and Open-Loop.* [Online]. Available at: http://www.lambdapower.co.uk/TechNotes/Tech-3.asp [Accessed 07 October 2015].

Lilly, L.R.C., 1984. *Diesel engine reference book*. Cornwall: Butterworth

Kenny, W. J., 2013. *Development of a Testing Facility for Spark Ignition Engine Fuels*. MScEng thesis. Stellenbosch: Stellenbosch University

Klein, M. 2004. A Specific Heat Ratio Model and Compression Ratio Estimation. Thesis. Linköping: Linköping University.

Kotzé, J. 2010. A Comparative Study on the Performance of Biodiesel in a Modern 1.9 Litre Turbo Diesel Engine. MScEng thesis. Stellenbosch: Stellenbosch University

Krishnan, S. 2004. *ME 418 – Combustion Engines* [Online]. Available: http://www.me.ua.edu/me418/ [Accessed 28 September 2015]

Kumar, J.S., Ganesan, V., Mallikarjuna, J.M. & Govindrajan, S., 2013. Design and optimization of throttle body assembly by CFD analysis. *Indian Journal of Engineering & Material Sciences, 20: 350-360.*

Martyr, A. & Plint, M., 1995. *Engine testing theory and practice*. Tottenham: Hartnolls Limited.

National Instruments, 2016. *NI USB-6351 X series data acquisition*. [Online] Available at: http://sine.ni.com/nips/cds/view/p/lang/en/nid/209071 [Accessed 16 Oktober 2016].

Noyori, T., Inoue. H., 2007. *Effect of Fuel Spray Charactaristics on Smoke Emissions in a Small-Displacement Spark-Ignition Direct-Injection*. SAE Paper: 2007-01-3492

Optrand. 2001. *High Temperature Miniature Pressure Sensors*. Plymouth: Optrand. [Online]. Available: http://www.optrand.com/catalog/opcat2001large.pdf [Accessed 03 September 2015]

Perfect Power. [S.a.]. *LetRipp II Software manual*. [Online]. Available: https://www.perfectpower.com/index.php/95-support-manuals/513-letripp-ii-software-user-guide-content-index [Accessed 11 September 2016]

Perfect Power. [S.a.]. *XMS5A/B LetRipp II Engine Management System DIY manual*. [Online]. Available: https://www.perfectpower.com/index.php/95-support-manuals/606-xms5a-b-technical-manual-content-index [Accessed 11 September 2016]

Probst, C., 1989. *Bosch Fuel Injection and Engine Management: How to Understand, Service and Modify.* Cambridge: Bentley Publishers

Reif, K., 2015. *Automotive Mechatronics.* Wiesbaden: Springer Vieweg.

Reif, K., 2015. *Gasoline Engine Management*. Wiesbaden: Springer Vieweg.

Richards, P., 2014. *Automotive Fuels Reference Book: Third Edition*. Warrendale: SAE International

Rogers, D.R., 2010. *Engine Combustion: Pressure Measurement and Analysis.* Warrendale: SAE International.

SAE. 1987. *Procedure for mapping engine performance – Diesel and Spark Ignition Engines.* SAE J1312

SAE. 2004. *Surface Vehicle Standard.* SAE J1394

SAPIA, 2008. *Petrol and diesel in South Africa*. [Online] Available at: www.sapia.co.za [Accessed 15 February 2015].

Sodré, J.R. & Soares, S.M.C., 2003. *Comparison of engine power correction factors for varying atmospheric conditions*. [Online] Available at: www.scielo.br/pdf/jbsms/v25n3/a10v25n3.pdf [Accessed 11 November 2015].

Stone, R., 1992. *Introduction to Internal Combustion Engines.* Houndmills: MacMillan.

Van Basshuysen, R. & Schäfer, F., 2004. *Internal combustion engine handbook: basics, components, systems and perspectives*. Wiesbaden: Vieweg Verlag.

Worret, R., Bernhardt, S., Schwarz, F. & Spicher, U. 2002. *Application of Different Cylinder Pressure Based Knock Detection Methods in Spark Ignition Engines*. SAE paper: 2002-01-1668.

Wlodarczyk, M.T., Poorman, T., Xia, L., Arnold, J. & Coleman, T. 1998. *Embedded Fiber-Optic Combustion Pressure Sensor for Automotive Engine Controls.* [Online] Available at: http://www.optrand.com/ [Accessed 22 September 2016]

Wlodarczyk, M.T., Poorman, T., Arnold, J. & Coleman, T., 1999. *Long-life fibre-optic pressure sensors for harsh environment applications*. [Online] Available at: http://www.optrand.com/ [Accessed 28 September 2016]

Woschni, G. 1967. *A Universally Applicable Equation for the Instantaneous Heat Transfer Coefficient in the Internal Combustion Engine*. SAE paper: 670931.

WWFC, 2009. *Ethanol guidelines*. Worldwide Fuel Charter.

Zhao, F. & Lai, M., [S.a.]. *The Spray Characteristics of Automotive Port Fuel Injection – A Critical Review.* SAE Paper: 950506.